UNIVERSITY OF OKLAHOMA

GRADUATE COLLEGE

EXPLORING PARE TOXIN DYNAMICS: FROM IMPACT TO QUANTIFICATION IN BACTERIAL CELLS

A DISSERTATION

SUBMITTED TO THE GRADUATE FACULTY

in partial fulfillment of the requirements for the

Degree of

DOCTOR OF PHILOSOPHY

By

SHENGFENG RUAN
Norman, Oklahoma
2024

EXPLORING PARE TOXIN DYNAMICS: FROM IMPACT TO QUANTIFICATION IN BACTERIAL CELLS

A DISSERTATION APPROVED FOR THE

DEPARTMENT OF CHEMISTRY AND BIOCHEMISTRY

BY THE COMMITTEE CONSISTING OF

Dr. Christina R. Bourne, Chair

Dr. Ann H. West

Dr. Rakhi Rajan

Dr. John P. Masly

Table of Contents

List of Figures

List of Tables

List of Abbreviations

AMR	antimicrobial resistance
BLI	bio-layer interferometry
CFU	colony-forming unit
Ct	threshold cycle
DSB	double-strand break
EV	empty vector
LB	Luria-Bertani broth
MIC	minimum inhibitory concentration
MtParDE	*Mycobacterium tuberculosis* ParDE
NSB	non-specific binding
OD_{600}	optical density at 600 nm
PaParDE	*Pseudomonas aeruginosa* ParDE
PCN	plasmid copy number
PCR	polymerase chain reaction
PSK	post-segregational killing
P/C	plasmid to chromosome
qPCR	quantitative polymerase chain reaction
RT-qPCR	reverse-transcription quantitative polymerase chain reaction

SDS-PAGE sodium dodecyl-sulfate polyacrylamide gel electrophoresis

TA toxin-antitoxin

Abstract

The increasing prevalence of antimicrobial resistance (AMR) in pathogenic bacteria has brought significant challenges to global public health. However, it has been decades since the discovery of the last antibiotic, making it essential to explore novel therapeutic targets and mechanisms to combat bacterial infections. Bacterial toxin-antitoxin (TA) systems, which exist widely among bacterial species, have been attracting attention in the field for their potential to be co-opted for health purposes. These non-secreted TA systems typically consist of a stable toxin that inhibits essential cellular processes, leading to cell growth inhibition or cell death, and a labile antitoxin (RNA or protein) that neutralizes the cognate toxin under normal growth conditions. In the case of Type-II ParDE TA system, the ParE toxin protein is neutralized by the ParD antitoxin protein through direct protein-protein interactions. Under stress conditions, degradation of the ParD antitoxin releases the ParE toxin. Similar to quinolone antibiotics, this liberated ParE toxin interacts with and inhibits DNA gyrase, causing the accumulation of double-strand breaks (DSBs) in DNA in the bacterial cell, which could lead to cell death. The detrimental DNA gyrase inhibition mediated by ParE toxins and their widespread presence in Gram-negative bacteria of concern make them a potential, potent agent for antibacterial drug development.

The idea of co-opting TA systems as a strategic tool to control bacterial growth is still in its early stage due to the lack of knowledge on how to artificially activate the toxins *in vivo*. This dissertation focuses on ParE subfamily members from *Pseudomonas aeruginosa* and *Mycobacterium tuberculosis* and aims to provide new insights for the proof of concept of co-opting the ParE toxins as a novel therapeutic agent. By exploring the effects of ParE toxin-mediated DNA damage on bacterial growth, genetic resistance, and antibiotic susceptibility, this work addresses a key gap in our understanding of the role of the ParE toxin in bacterial physiology and therapeutic development. This dissertation comprises three key research chapters:

The work in Chapter II investigated the phenotypic impacts of induced ParE toxin expression on bacterial growth, genetic mutation, and antibiotic susceptibility. The expression of ParE toxins—originating from *P. aeruginosa* and *M. tuberculosis*—was induced in *P. aeruginosa* cells and *Escherichia coli* surrogate cells. Differential toxicity profiles were noted, with the PaParE1 toxin exhibiting essentially no toxicity and the other ParE toxins exhibiting dose-dependent toxicity. ParE toxin-mediated DSBs in DNA trigger error-prone DNA repair pathways, such as the SOS response, which could lead to the accumulation of genetic mutations potentially contributing to the emergence of antibiotic resistance. Results indicated that the expression of potent ParE toxins led to an increased mutation frequency, except for the case of the attenuated ParE toxin. However, this increase in mutation frequency did not translate into significant resistance against a broad spectrum of common clinical antibiotics within the observation period. These findings support the concept of co-opting TA systems as an antibacterial approach.

The work in Chapter III uncovered a survival mechanism that *E. coli* cells use to evade the lethal effects of plasmid-mediated ParE toxin expression. In the work of Chapter II, we observed an interesting phenotype where *E. coli* cells, after exposure to the plasmid-mediated inducible expression of the ParE1 toxin from *M. tuberculosis*, became "insensitive" to subsequent induction of the ParE1 toxin. Moreover, the proportion of these insensitive cells increased with continued passages in the presence of the inducer. This phenotype was not correlated with changes in the plasmid sequence and could not be rescued by increasing the inducer uptake. Instead, it was associated with a marked reduction in plasmid copy number (PCN). This reduction in PCN was reproducible across various *E. coli* strains and ParE toxins, indicating a generalized response mechanism. Furthermore, bacterial whole genome sequencing revealed a N845S residue substitution in DNA polymerase I, which is known to participate in the replication of the type of plasmid used in our experiments. This observed survival strategy of reducing PCN highlights the adaptability of bacterial cells to stress conditions and provides valuable insights into microbial adaptation and genetic engineering methods.

The work in Chapter IV validated the feasibility of using a novel bio-layer interferometry (BLI)-based method to quantify low-abundance ParE protein molecules in cell lysate. In the work of Chapter II, we noticed that despite sharing a conserved three-dimensional structure, the ParE toxins exhibited varying toxicity profiles. This differential potency may stem from variations in protein sequence or expression levels. Traditional detection methods like Western blot and mass spectrometry failed to detect those potent ParE toxins due to their toxic nature and resulting low abundance in cell lysate. To overcome the limitation, we employed the highly sensitive BLI technique. Using the attenuated ParE1 toxin from *P. aeruginosa*, which allows for robust expression and purification, we optimized the specific binding of ParE1 toxin molecules to biosensors by adjusting the number of dips and cell lysate concentration in the running buffer. We established linear relationships between the specific binding signals and ParE1 toxin concentrations using different types of biosensors, demonstrating the feasibility of using BLI-based method for the quantification of ParE protein molecules in cell lysate.

Overall, this dissertation not only provides a comprehensive view on the phenotype impacts of ParE toxins on bacterial growth, genetic mutation, DNA stability, and antibacterial response, laying the foundation for co-opting TA systems as an antibacterial strategy, but also introduces a novel methodological approach. This approach will enhance our understanding of the molecular dynamics of toxin proteins, which facilitates future studies on TA system biology.

Chapter I: Introduction

In 1928, Alexander Fleming accidentally discovered the antibiotic penicillin at St Mary's Hospital in London. During World War II, the demand for penicillin sharply increased, saving the lives of thousands of soldiers from infections. Since then, the discovery of penicillin marked the beginning of the "golden age" of antibiotics from natural products [1], and antibiotics have been a powerful weapon against bacterial infections. However, with the uncontrolled use of antibiotics, many human pathogens have gradually evolved and developed drug resistance. Exposure to antibiotics selectively kills susceptible bacteria, while resistant cells survive and can spread their antimicrobial resistance (AMR) genes through mechanisms such as horizontal gene transfer [2–5], contributing to the growing AMR crisis.

To date, AMR has been increasingly threatening global public health with more than 2.8 million infections and more than 35,000 deaths reported in the United States each year [6]. However, the development of new antibiotics failed to catch up with the rapid emergence of AMR [1]. Alarmingly, it has been predicted that without immediate action, AMR infections could cause the deaths of 10 million people worldwide every year by 2050 [7]. Traditional methods of antibiotic discovery, which primarily relies on screening natural products, have become less and less productive as the same or similar compounds have been discovered repeatedly over time [8,9]. Hence, people are indeed looking for alternative approaches to develop antibiotics. Among those, the toxin-antitoxin (TA) systems have been identified as particularly promising, with research focusing on co-opting the toxin component as a strategic tool to control bacterial growth [10].

1. Toxin-Antitoxin Systems

TA systems are small genetic loci that are widely found on chromosomes and plasmids in a broad range of bacteria and archaea (**Fig. 1.1**) [11,12]. These systems typically comprise two small genes

that encode non-secreted products: a toxin and an antitoxin. The toxin is typically a stable protein that targets various cellular processes to affect cell growth, while the antitoxin is either a protein or an RNA that binds to and neutralizes its cognate toxin. The antitoxin is generally less stable than the toxin and is readily degraded by proteases or ribonucleases; however, it is typically expressed at a higher level than the toxin under normal growth conditions to keep neutralizing the toxic effects of the toxin [13].

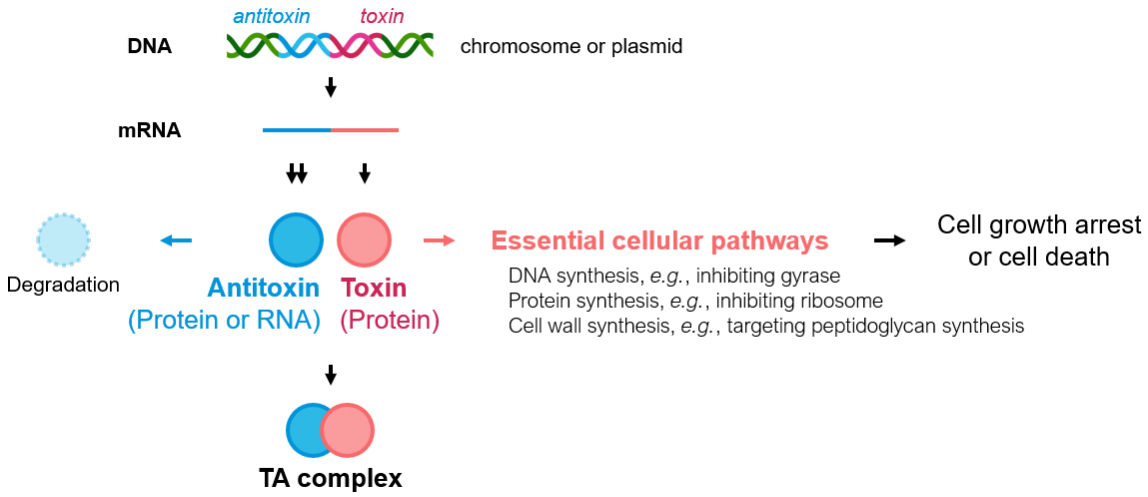

Figure 1.1. Schematic illustration of toxin-antitoxin (TA) systems.

Based on the nature and mechanism of action of the antitoxin, TA systems have been classified into eight types, designated types I through VIII [12–14]. In type I, III and VIII TA systems, antitoxins are RNAs that neutralize toxin RNAs (type I) or proteins (type III), or that repress toxin transcription (type VIII), thereby inhibiting toxicity [13]. While in type II and IV to VII TA systems, antitoxins are proteins that neutralize toxin proteins by direct protein-protein interactions (type II) or post-translational modification (type VII), that bind to cellular targets of toxins (type IV), or that facilitate toxin degradation (type V and VI) [13]. Among them, the type II TA systems are the most well studied TA systems, where both the toxin and the antitoxin are

proteins and the antitoxin binds to the toxin, forming a stable TA complex through strong protein-protein interactions [10,15–17].

According to the toxin-antitoxin database (TADB) 3.0 [12], 403 TA loci of type II were experimentally validated, which is the highest number among all types. These type II TA systems are categorized into several families based on the structural similarities of their toxin and antitoxin components and mechanisms of action [15,16,18]. For example, the RelE toxin from the RelBE family and the MazE toxin from the MazEF family are endoribonucleases that cleaves mRNA, inhibiting protein translation [19–21]. The HipA toxin from the HipBA family is a serine/threonine kinase that phosphorylates and inactivates the glutamyl-tRNA synthesis, leading to cell growth arrest [22]. Additionally, the CcdB toxin from the CcdAB family and the ParE toxin from the ParDE family target DNA gyrase, inhibiting DNA replication and transcriptions [23–26]. Under normal growth conditions, the toxins are neutralized by the antitoxin; however, the potential toxicity conferred by the toxins makes it seems to be contradictory to their widespread presence in bacterial chromosomes and plasmids, which implies that they would provide benefits to the hosts.

2. Biological Functions of TA systems

When the first TA system, CcdAB, was discovered on an F plasmid, an “addiction model” was proposed to explain how plasmid-encoded TA systems help the plasmid to persist in a bacterial population [27–29]. According to this model (**Fig. 1.2A**), when the CcdAB-encoding plasmid is lost after cell division, the liberated CcdB toxin from the CcdAB TA complex kills the plasmid-free daughter cell through a mechanism called post-segregational killing (PSK) [30–32], which ensures that cells lacking the plasmid-encoded CcdAB TA system are selectively eliminated, thus maintaining the presence of the plasmid in the population. It was later found that the release of the CcdB toxin, *i.e.*, the activation of the toxin, relied on Lon protease-mediated degradation of the CcdA antitoxin [33,34]. Additionally, a recent study demonstrated single-cell evidence of PSK

mediated by multiple type II TA systems [30], suggesting a conserved mechanism for plasmid stabilization mediated by TA systems.

On the other hand, abundant homologues of plasmid-encoded TA systems have subsequently been discovered on bacterial chromosomes, which may be acquired through horizontal gene transfer. While the physiological functions of these chromosomally encoded TA systems are still debated, research has suggested that in some specialized cases they may prevent chromosome loss through the same PSK mechanism [35]. Additionally, they may protect cells from PSK mediated by plasmid-encoded TA systems through an "anti-addiction model" (**Fig. 1.2B**) [36]. In this model, it is hypothesized that when the plasmid-encoded antitoxin is not replenished due to plasmid loss, the chromosomally encoded TA system could compensate by replenishing a compatible antitoxin to keep neutralizing the toxin, preventing its release [32]. This model reflects an evolutionary adaptation of bacteria to counter the threat posed by plasmid addiction.

In addition to maintaining genetic elements through PSK, it has been suggested that TA systems may provide other physiological benefits to bacteria, such as stress response, phage defense, virulence, and antibiotic resistance [15,37–42]. For example, the overexpression of the PemK toxin from the type II PemIK TA system was shown to inhibit the early-stage phage infection in *Klebsiella pneumoniae* [43]. The RelE toxin from the RelBE TA system and the MazF toxin from the MazEF TA system are endoribonucleases that can mediate cell survival in response to stress by cleaving mRNA to remodel the proteome [29,44]. Low-level expression of the ParE toxin from the ParDE TA system was shown to offer protection to bacteria against quinolone antibiotics [45]. However, higher concentrations of ParE toxin were still toxic to the cells [45]. This reflects the dual effects of the TA systems.

Under normal growth conditions, an excessive amount of antitoxin keeps neutralizing the toxin [32,46]. However, under environmental or other stress, the degradation of antitoxin will lead to excessive free toxins, which subsequently lead the fate of bacteria to survive or die [32,37,47]. This stoichiometric balance between toxin and antitoxin under different conditions reveals the "time

bomb" mechanism in bacterial cells, in which toxin remains inactive until the degradation of antitoxin. It leads to the hypothesis that intentionally activating these "time bombs" by manipulating the TA system can be used as a new means to control bacterial proliferation. The concept of co-opting toxin molecules as antibacterial agents provides an innovative way to develop new antibacterial strategies.

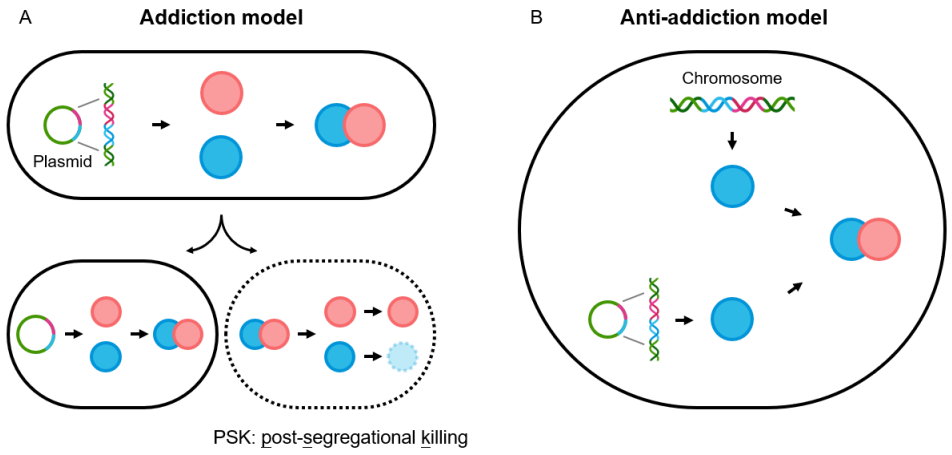

Figure 1.2. Schematic illustration of addiction and anti-addiction models. (A) In the addiction model, plasmid-free cells are killed by the released toxin from the TA complex due to the degradation of the antitoxin. (B) In the anti-addiction model, the replenished antitoxin from the chromosome prevents the cell from PSK even when the TA-encoding plasmid is lost.

3. Gyrase Inhibition of ParE toxins

The ParDE TA family is one the well-studied type II TA systems that is widely found in pathogenic bacteria such as *Mycobacterium tuberculosis*, *Vibrio cholerae*, and *Pseudomonas aeruginosa* [12,48]. This system is composed of the ParE toxin protein and the ParD antitoxin protein. The names were derived from initial observations of partitioning defects when they were deleted from the low copy number RK2 plasmid [49,50]. The subsequent research indicated that

similar to the quinolone antibiotics, the ParE toxin has the inhibition activity on DNA gyrase, although through an unknown molecular mechanism [23,26,45,51].

DNA gyrase is an essential type II topoisomerase in bacteria and responsible for introducing negative supercoils into DNA, which is very important for bacterial DNA replication, transcription and chromosome segregation [26,52]. It is a tetrameric enzyme that is composed of four subunits: two GyrA subunits and two GyrB subunits. The GyrA subunits are primarily responsible for the binding of one segment of DNA ("G" segment) using the C-terminal domains (CTDs), cleaving the DNA and passing another segment of DNA ("T" segment) through the break, while the GyrB subunits hydrolyze ATP to provide the necessary energy [26,53,54]. After the T segment passes through the cleavage site, the cleaved G segment is ligated. This reduces the linking number by two, introducing negative supercoils [26]. The resulting change of the topology of the DNA helps in maintaining the underwound state of the DNA, which is favorable for processes like transcription and replication.

The re-ligation of the cleaved DNA is critical to DNA integrity. If the cleavage is not properly sealed, it can lead to persistent breaks that promote chromosomal rearrangements, disruption of genes, and ultimately cell death [55]. Quinolones are antibiotics that target DNA gyrase [51]. Quinolones intercalate into cleaved DNA and also bind to residues Ser83 and Asp87 of the GyrA subunits, which are near the cleavage site [56,57]. This interaction of quinolone and DNA Gyrase leads to the stabilization of the DNA cleaved state, preventing the re-ligation of the DNA breaks. The failure to re-ligate the DNA breaks leads to the accumulation of double-stranded breaks (DSBs) in DNA, triggering cellular repair pathways, such as SOS response, which in turn up-regulate error-prone polymerases and other repair proteins [58,59]. Because the lack of repair fidelity is inherent in these rescue processes, SOS response has been identified as a driving factor of adaptive gene mutation [60,61], potentially producing AMR mutants under drug treatment pressures.

Similar to quinolones, ParE toxin has been characterized as a DNA gyrase inhibitor but with a

distinct mechanism [23]. It is reasonable that low-levels of ParE-triggered DNA damage and repair events may produce a group of mutant bacteria, which are selected as AMR mutants after being treated with antibiotics; however, high-levels of ParE-triggered DNA damage and repair may be too much for cells to repair, which eventually leads to cell death. The dual effect of ParE toxin provides a therapeutic window for using these "time bombs" to control bacterial growth.

4. Plasmid Stability

Plasmids are circular, double-stranded DNA molecules that are naturally present in the microbial world, including bacteria and archaea [62]. The TA systems are found to function as "addiction modules" that mediate selection to enforce retention of plasmids via PSK, which is achieved by killing the plasmid-free cells by the free toxin due to the degradation of the shorter-lived antitoxin after cell division [30,31,63]. Most AMR plasmids carry one or more TA systems, hence the function of "addiction modules" of TA systems promotes the inheritance and spread of AMR genes [15,64].

However, under natural conditions, a plasmid is more likely to be lost over time if it does not provide survival advantages for the host, such as encoding useful AMR genes, such that the maintenance of the plasmid will become a burden on the host metabolism [65,66]. In genetic engineering procedures, the stability of plasmids in the host cells is important for gene cloning and recombinant protein expression. Therefore, laboratory-based plasmids often carry a selection maker, such as AMR genes, to force the host cells to maintain the plasmids. However, their stability is both a boon and a bane for the survival of bacteria, especially under the pressure of toxin expression. Our research demonstrates an interesting phenotype that, under the double pressure of plasmid selection and ParE toxin expression, bacteria escaped the fate of being killed by either through a mechanism of reducing the plasmid copy number (PCN). This finding emphasizes the potential fragility of plasmid-based bacterial defense mechanisms that may be used for therapeutic purposes.

The background outlined in Chapter I of this dissertation sets up the rational for the importance of the research presented in the following chapters. The main gaps in the field of TA system to be solved in this work include: (1) Can the toxicity of ParE toxin on cells be used as an antibacterial strategy? (2) Whether ParE toxin toxicity has other side effects? (3) Why ParE toxins have differential toxicity? Chapter II in this dissertation aims to prove the new concept of antibacterial methodology by leveraging the ParE toxins as a tool but avoiding the mutagenic potential to cause the emergency of AMR. Chapter III reveals a survival mechanism of cells evading ParE toxin expression from plasmids. Chapter IV demonstrates a new methodology to quantify ParE toxin molecules in cell lysate to support studies on the contributors to differences in ParE toxicity.

Chapter II: Phenotypic Impacts of ParE Toxin Expression on Bacterial Hosts Reveal Variable Toxicity that Increases Mutation Frequency and Improves Antibacterial Responses

Shengfeng Ruan and Christina R. Bourne

Department of Chemistry and Biochemistry, University of Oklahoma, Norman OK USA

This chapter represents unpublished research conducted in the Bourne lab, located within the Department of Chemistry and Biochemistry at the University of Oklahoma. The manuscript is in preparation for submission.

Experiments were initially designed by Dr. Christina Bourne; however, I provided technical expertise to this design and developed improved data collection and processing protocols. I built all the reagents, and collected and processed all the data for this chapter. All figures were produced by me. Writing of the manuscript was performed by me with assistance from Dr. Christina Bourne. Editing and feedback on all writing was provided by Dr. Christina Bourne.

1. Abstract

This chapter investigated the phenotypic impacts of induced ParE toxin expression in bacterial hosts, with a particular focus on the differential toxic potencies of ParE toxins via gyrase inhibition and possible contribution to improve antibacterial responses. By studying the effects of four ParE toxins, which were derived from *Pseudomonas aeruginosa* and *Mycobacterium tuberculosis*, within the native hosts and an *Escherichia coli* surrogate, this study reveals a subtle link between induced toxin activity and bacterial survival responses. Consistent with previous studies, the results showed an evident contrast in the toxicity levels of different ParE toxins: PaParE1 toxin showed essentially no toxicity, while other ParE toxins showed significant dose-

dependent toxicity profiles. Furthermore, a dose-dependent increase in mutation frequency was observed, which interestingly did not lead to antibiotic resistance within the observation period. In contrast, in the presence of ParE toxin expression, increased cell susceptibility to a broad spectrum of antibiotics was observed. This observation suggests a potential direction for therapeutic development by co-opting toxin components of TA systems. In summary, this chapter contributes to a broader understanding of the role of ParE toxins in bacterial physiology and indicates a new direction for the development of innovative antibacterial strategies.

2. Introduction

Antibiotic resistance is a pressing issue significantly threatening global public health, promoting ongoing efforts to find novel and effective ways to treat bacterial infections [6]. Although modifying existing antibiotics to improve their efficiency offer a temporary solution; however, given that emerging resistance outpaces the discovery of new antibiotics, alternative research directions are urgently needed to develop long-term reliable drugs [66,67]. In this context, leveraging bacterial toxin-antitoxin (TA) systems has been considered a particularly promising approach to explore [10].

TA systems are widely present in bacterial chromosomes and plasmids, and more than 500 TA loci have been experimentally validated in over 6000 species [11,12]. TA systems typically consist of two small, non-secreted components: a toxin that affects cell growth and an antitoxin that neutralizes the effect of cognate toxin [13]. Most toxins are stable proteins (except type VIII, in which the toxin is an RNA) that target a variety of essential cellular pathways, such as DNA replication, translation and cell wall synthesis [37,42]. In contrast, the antitoxin is more labile and can be either a protein or an RNA that is readily degraded by proteases or ribonucleases [13]. Under normal growth conditions, the antitoxin is expressed more than the toxin and binds to the toxin, forming a stable TA complex, which not only prevents the antitoxin from degradation but also prevents the toxin from killing cells [32,46].

According to the nature and mechanism of action of the antitoxin, TA systems have been classified into eight types, designated types I through VIII [12–14], exhibiting varying mechanisms of action. Among them, the type II TA systems, distinguished by their protein-based pairs, are the most well studied [15,16,68]. In type II TA systems, the antitoxin binds to and neutralizes the toxin through strong protein-protein interactions [17]. Although it is unclear how the toxin is released from the stable complex, it was assumed that when bacteria are challenged with environmental stresses, the selective degradation of antitoxin leads to excessive free toxins, which exert their effects to bacterial growth [46,47]. This stoichiometric balance between toxin and antitoxin under normal and stress conditions reveals the potential "time bomb" mechanism within bacterial cells, where toxin is dormant until antitoxin is degraded. This leads to a hypothesis that intentionally triggering these "time bombs" by manipulating the TA system could provide a novel means for bacterial growth control. The concept of using toxin molecules as innovative agents to inhibit bacterial growth provides a promising way to develop new antibacterial strategies. However, due to the current limitations in understanding how to artificially disrupt the toxin-antitoxin interactions, this potential has not been largely developed.

This chapter focuses on the type II ParDE TA system, aiming to provide new insights into the proof-of-concept of controlling bacterial growth by co-opting TA systems. The ParDE TA system is one example of those widely studied TA systems, in which the toxin protein inhibits DNA gyrase, an essential enzyme for fundamental bacterial processes such as DNA replication and transcription [26,51]. Although the molecular mechanism remains to be fully understood, the ParE-mediated gyrase inhibition, similarly to the action of quinolone antibiotics, can impact cell growth and potentially result in cell death by triggering double-stranded breaks (DSBs) in DNA [23,26,45]. These DNA damages trigger the SOS response, and eventually lead to rescue of cells via genetic repairs, frequently with introduced mutations [69,70]. Such a mechanism suggests that low levels of DNA damage induced by ParE activity could promote genetic mutations, potentially producing antibiotic-resistant mutants under drug treatment pressures. On the contrary, at higher concentrations, the ParE toxin overwhelms cell's repair ability and leads to cell death. This dual

effects of ParE toxin, promoting survival at low concentrations and causing cell death at high concentrations, opens a therapeutic window. By using this window, this chapter aims to define each endpoint of that window and in so doing to demonstrate the potential of co-opting ParE toxins as a targeted strategy for the development of novel treatments, harnessing what can be described as bacterial "time bombs" for therapeutic benefit.

3. Experimental Details

3.1. Bacterial Strains and Plasmids

The bacterial strains and plasmids used in this study are listed in **Table 2.1**. Standard protocols or manufacturer instructions were followed for PCR cloning, DNA manipulation and DNA transformation. DNA sequences of ParE toxins were obtained from the toxin-antitoxin database (TADB) [12]. Primers were designed for amplification of *parE* genes from chromosomal DNAs with overlaps to allow the ligation of genes into appropriate plasmids by Gibson assembly (NEB). Where noted, 6× histidine or Strep affinity tag were fused to *parE* genes. Resulting plasmid constructs were purified using Zyppy™ Plasmid Miniprep Kit (Zymo Research) and verified by DNA sequencing from GENEWIZ (USA). The chemically competent cells of experimental strains were prepared according to standard protocols. Plasmids were transformed into competent cells by heat shock (for *Escherichia coli*) or electroporation (for *Pseudomonas aeruginosa*) method according to standard protocols.

3.2. Viability Assays

Overnight cultures of experimental strains were inoculated from -80°C frozen 20%-glycerol stocks in M9 minimal medium (for *P. aeruginosa*) or Luria-Bertani (LB) broth medium (for *E. coli*), supplemented with appropriate antibiotics and 1% glucose, and grown overnight (18-20 h) at 37°C with shaking at 200 rpm. The overnight cultures were subsequently back-diluted at a

ratio of 1:20 in fresh media supplemented with appropriate antibiotics and, where appropriate, arabinose within a specified concentration range, and grown at 37°C with shaking at 200 rpm. Aliquots of cultures were collected at the defined time intervals and 10-fold serial dilutions in sterile 0.9% saline solution or test medium were performed. Aliquots of these dilutions were spotted onto LB or M9 agar plates supplemented with appropriate antibiotics and 1% glucose for the determination of colony-forming units (CFUs). The CFUs were subsequently converted to CFU/mL based on the initial spotting volumes. The limit of detection for CFU/mL measurements was calculated using the formula: 1 CFU divided by the initial spotting volume (μL), multiplied by 1000 μL/mL. M9 minimal medium was prepared by diluting 5× M9 salts to 1× in sterile Milli-Q water with supplements of 0.1 mM calcium chloride, 2 mM magnesium sulfate, and 0.2% casamino acid. 5× M9 salts were prepared by dissolving 64 g of disodium hydrogen phosphate heptahydrate, 15 g of potassium dihydrogen phosphate, 2.5 g of sodium chloride and 5 g of ammonium chloride in final 1 L of Milli-Q water. Carbenicillin was added at 100 μg/mL and kanamycin was added at 50 μg/mL. Figures were generated using GraphPad Prism 8.01.

Table 2.1

Bacterial strains and plasmids used in this study.

Strains or plasmids	Description	Source of reference
Strain		
Escherichia coli K-12 MG1655	F- lambda- *ilvG*- *rfb*-50 *rph*-1, experimental strain.	Dr. Tyrrell Conway (Oklahoma State University)
Pseudomonas aeruginosa PA14	Experimental strain.	Dr. Erike Lutter (Oklahoma State University)
Pseudomonas aeruginosa PAO1	Genomic DNA source, experimental strain.	Dr. Erike Lutter (Oklahoma State University) and Dr. Helen Zgurskaya (University of Oklahoma)
Mycobacterium tuberculosis Rv1960c	Genomic DNA source.	DNA directly purchased from ATCC
Plasmids		

pHerd20T	ColE1/pMB1/pBR322/pUC origin of replication, pBAD promoter, acceptor of PaParDE genes, Amp^r, donor of *araC*-P_{BAD} fragment.	Hongwei Yu (Marshall University)
pMind	ColE1/pMB1/pBR322/pUC origin of replication, tetRO promoter, Neo^r Kan^r.	pMind was a gift from Brian Robertson (Addgene plasmid # 24730; http://n2t.net/addgene:24730; RRID:Addgene_24730)
pMindBAD	pMind tetRO promoter replaced with a 1.216-kb fragment of *araC*-P_{BAD} from pHerd20T, acceptor of MtParDE genes.	This study

3.3. Minimum Inhibitory Concentration

Minimum inhibitory concentrations (MICs) of ciprofloxacin (CIP), trimethoprim (TMP), and rifampicin (RIF) were determined in 96-well microtiter plates essentially as described (**Fig. 2.1**) [71]. Briefly, 100 µL of test media-diluted antibiotic stock was added to microtiter plate wells in column 1, and 50 µL of test media was added to wells in columns 2 through 11. 50 µL of solution in column 1 were pipetted into column 2 to make a 2-fold dilution in column 2. The same serial dilutions were repeated for wells in columns 3 through 10. 50 µL of solution from wells in column 10 were discarded to ensure the same volume of antibiotic in wells. 100 µL of test media was added to wells in column 12 to serve as a negative control. Overnight cultures were diluted to 10^6 CFU/mL (2× bacterial inoculum) based on the optical density at 600 nm (OD_{600}) (assuming OD_{600} of 1.0 is equal to 8×10^8 CFU/mL) in test media and 50 µL of the inoculum was added in all wells except column 12. The cells were incubated at 37°C for overnight (18-24 h) without shaking. After the incubation period, a visual reading was performed to determine the MIC, which is defined as the lowest antibiotic concentration in which there was no visible bacterial growth.

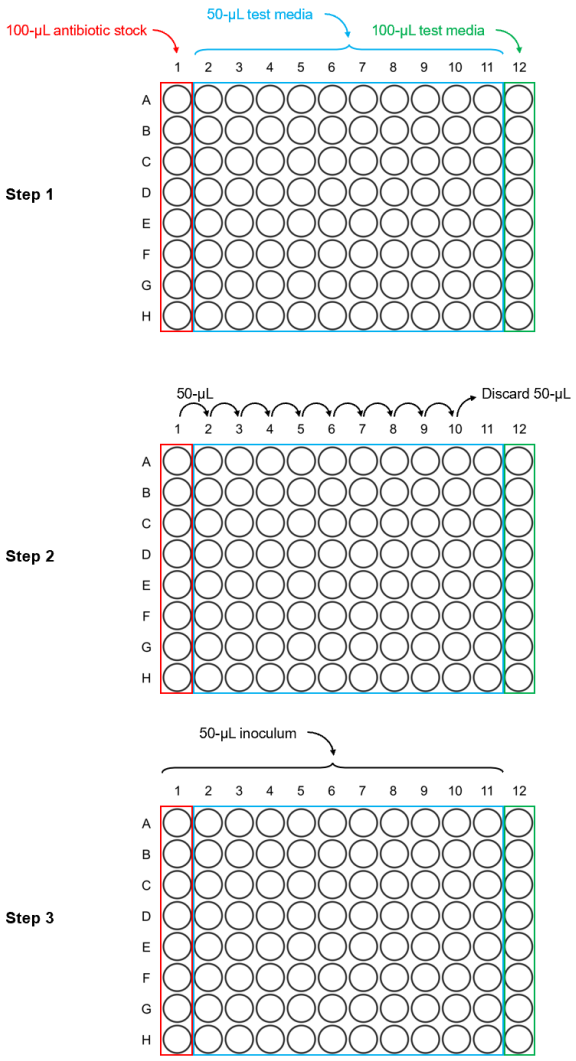

Figure 2.1. Schematic illustration of MIC test.

3.4. Mutation Frequency

Overnight cultures were prepared as described in the protocol for the viability assay. The overnight cultures were back-diluted at a ratio of 1:10,000 in test media and grown at 37°C with shaking at 200 rpm to an optical density at 600 nm (OD_{600}) of 0.2. Cultures were subsequently divided into aliquots, with each aliquot added with a specified concentration of arabinose, which allowed a sufficient number of viable cells for at least one mutant colony to form, or treatment of sub-MIC of CIP (0.5× or 0.75× MIC). Cultures were then grown for 8 h at 37°C with shaking at

200 rpm. Following incubation, cultures were centrifuged, and the pellets were resuspended in volumes empirically determined to ensure the presence of sufficient colonies resistant to RIF or TMP for counting methods, using either sterile 0.9% saline solution or test medium. Appropriate volumes of the cell resuspensions were then plated on solid LB or M9 agar plates supplemented with appropriate antibiotics and 1% glucose to maintain the selection of the *parE*-encoding plasmid as well as antibiotic RIF or TMP at 3× or 5× MIC to determine the number of colonies harboring a mutation allowing growth with RIF or TMP. The total number of viable cells was determined as CFUs by plating the cell resuspensions on solid LB or M9 agar plates supplemented with appropriate antibiotics and lacking RIF or TMP. Mutation frequency was calculated by dividing the number of colonies resistant to RIF or TMP by the total number of viable cells per unit volume.

3.5. Antibiotic Susceptibility Assays

Cultures were prepared as described in the protocol for determining mutation frequency. Following the 8-h incubation, culture density was normalized either by dilution in sterile 0.9% saline solution or by centrifugation and subsequent resuspension in sterile 0.9% saline solution. The normalized cultures were then smeared on LB or M9 agar plates using cotton swabs. These plates were supplemented with appropriate antibiotics to maintain the selection of the *parE*-encoding plasmid. Disks or E-test strips of specified antibiotics were placed on the agar plates, and the plates were incubated at 37°C for overnight (18-24 h). Antibiotic susceptibilities were evaluated by assessing the size of the inhibition zone for disks, or by determining the MIC using the scale printed on the strip.

4. Results

Two *parE* genes were amplified from the *Pseudomonas aeruginosa* PAO1 strain and *Mycobacterium tuberculosis* Rv1960c strain, respectively, according to gene annotations in TADB. These *parE* genes were subsequently cloned into appropriate vectors as detailed in **Table 2.2**. Beyond *P. aeruginosa* PAO1 strain, this study also included *P. aeruginosa* PA14 strain, which possess only the PaParDE1 TA system on the chromosome, and *E. coli* MG1655 strain, which lack any of those four ParDE TA systems on the chromosome, as experimental strains for the expression of ParE toxins. *P. aeruginosa* PAO1 and PA14 strains maintained the intact chromosomally encoded TA systems. To induce the expression of the ParE toxin, a specified concentration range of arabinose was used under standard liquid growth conditions. The impact of ParE toxin expression on cell viability was assessed by measuring viable cell counts, expressed as colony-forming units per milliliter (CFU/ml), on solid media.

Table 2.2

ParDE toxin and antitoxin sources, abbreviations and construct formats used in this study.

Bacterial species of origin	Abbreviation in text	Vector (affinity tag)
Mycobacterium tuberculosis	MtParDE1	pMindBAD (none)
Mycobacterium tuberculosis	MtParDE2	pMindBAD (N-terminal Strep tag)
Pseudomonas aeruginosa	PaParDE1	pHerd20T (N-terminal 6×His tag)
Pseudomonas aeruginosa	PaParDE2	pHerd20T (N-terminal 6×His tag)

4.1. Expression of Different ParE Toxins Revealed Variances in the Toxic Effects on Bacterial Cells

Among the four ParE toxins tested, the PaParE1 toxin was the only one that exhibited essentially no toxicity over 8 h in both *P. aeruginosa* PA14 and PAO1 host cells, regardless of the induction strength (**Fig. 2.2A** and **B**). Furthermore, when expressed in *E. coli* MG1655 cells, the PaParE1

toxin did not lead to a noticeable loss in cell counts (**Fig. 2.2D**). The resulting CFU counts closely aligned with those of the controls, including the empty vector (EV), the PaParD1 antitoxin alone, and the PaParDE1 toxin-antitoxin co-expression (**Fig. S2.1A-C** and **Fig. S2.2A**). Despite this lack of toxicity, sodium dodecyl-sulfate polyacrylamide gel electrophoresis (SDS-PAGE) confirmed the expression of PaParE1 toxin in *E. coli* MG1655, *P. aeruginosa* PA14 and PAO1 cells (**Fig. 2.3**), indicating that the non-toxic nature of PaParE1 toxin was attributed to its intrinsic properties rather than to inadequate expression levels.

In contrast, the expression of PaParE2 toxin led to a dose-dependent decline in the cell viability of *P. aeruginosa* PAO1 cells (**Fig. 2.2C**). Notably, attempts to transform the PaParE2-expressing plasmid into *P. aeruginosa* PA14 cells were unsuccessful. This failure may be attributed to the absence of the *paparDE2* operon on the chromosome of *P. aeruginosa* PA14 cells, resulting in the lack of endogenous PaParD2 antitoxin to partially neutralize the induced PaParE2 toxin expression. When expressing the PaParE2 toxin in *P. aeruginosa* PAO1 cells, a 0.2% induction strength caused a maximum approx. 3.2-log reduction in cell counts within 4 h, while a 2% induction strength led to cell counts below the limit of detection (an approx. 5.0-log reduction) in the same time frame (**Fig. 2.2C**). When no arabinose was added, cell counts increased by approx. 1.0-fold (**Fig. 2.2C**) over the same 4-hour period, consistent with the approx. 0.9-fold increase in cell counts observed with the EV, PaParD2, PaParDE2 controls (**Fig. S2.1D-F**). Furthermore, a similar pattern of dose-dependent decrease in cell counts could be observed when inducing the PaParE2 toxin expression in *E. coli* MG1655 cells with same induction strengths (**Fig. 2.2E**). Collectively, these findings highlighted the contrasting characteristics of two PaParE toxins from the same species, showcasing one as inert and the other as highly active.

The impact of MtParE toxin expression was assessed in *E. coli* MG1655 cells. Both MtParE1 and MtParE2 toxins exhibited a dose-dependent toxicity profile in *E. coli* MG1655 cells (**Fig. 2.4**). Specifically, the MtParE1 toxin expression led to a maximum approx. 2.7-log reduction in cell counts at a 2% induction strength within 2 h of induction (**Fig. 2.4A**), whereas the MtParE2 toxin expression led to cell counts below the limit of detection (an approx. 4.5-log reduction)

after 8 h of induction at both 0.2% and 2% induction strengths (**Fig. 2.4B**). In comparison, the expression of EV, MtParD antitoxin or MtParDE antitoxin-toxin didn't change the cell growth (**Fig. S2.2B-F**). Moreover, the MtParE2 toxin appeared to exhibit stronger toxicity to cells than the MtParE1 toxin, as evidenced by the lower cell counts at the same induction strengths. Furthermore, the MtParE2 toxin expression at a 0.001% induction strength still resulted in a decrease in cell counts (**Fig. S2.3**). Even at the 0% induction strength, unlike the MtParE1 toxin, the potential leaky expression of MtParE2 toxin also caused a reduction in cell counts after 2 h of incubation (**Fig. 2.4D** and **E**).

Overall, despite a conserved 3-dimensional structure, this comparative analysis of four ParE toxins from two species, along with the analysis of ParE toxins from other species (collaborators' data, not shown), revealed a significant variance in their toxic effects on bacterial cells.

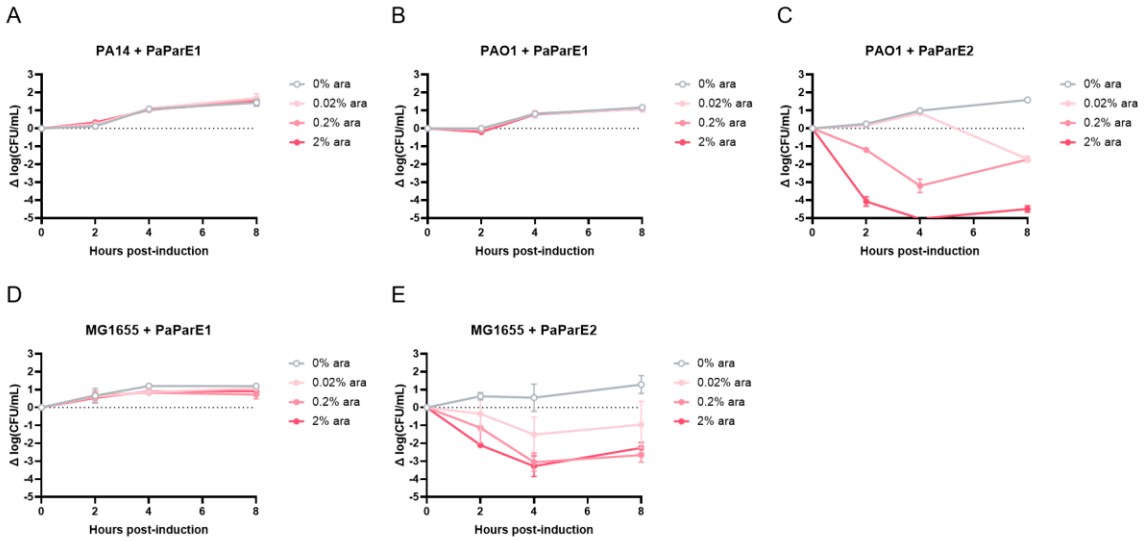

Figure 2.2. Impact of PaParE toxin expression on bacterial cell viability. The expression of the toxin protein PaParE1 (**A, B,** and **D**) or PaParE2 (**C** and **E**) was induced in *P. aeruginosa* PA14 (**A** and **B**), PAO1 (**C**), or *E. coli* MG1655 (**D** and **E**) cells using specified concentrations of arabinose (ara) in M9 minimal medium (**A** to **C**) or LB medium (**D** and **E**). Colony-forming units per milliliter (CFU/mL) were measured as described in methods and normalized to the initial

count at time zero to calculate the change in CFU/mL (ΔCFU/mL), which was plotted on the y-axis. Notably, the PaParE1 toxin exhibited essentially no toxicity, whereas the other ParE toxins exhibited induction-strength-dependent toxicity to the cells. Each data point on the graph includes the standard error of the mean (SEM), derived from at least two independent experiments with replicates.

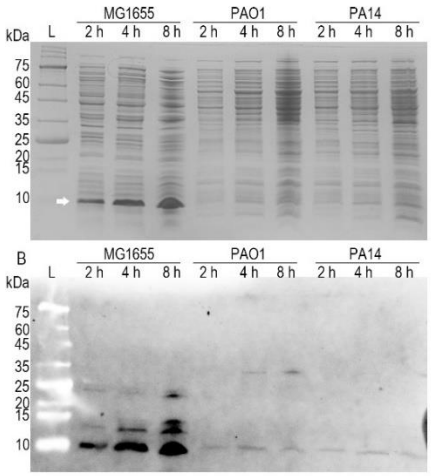

Figure 2.3. Protein expression analysis of PaParE1 toxin in bacterial cells. Following viability assays, cultures of PaParE1-expressing *E. coli* MG1655, *P. aeruginosa* PA14, and PAO1 cells were aliquoted at 2, 4 and 8 h of induction. Cultures were centrifuged and pellets were resuspended in 1× SDS sample dye and heated at 95°C for 5 min. Protein expression levels were analyzed by SDS-PAGE (**A**) and Western blot with anti 6× His tag antibody (**B**). White arrow indicates the expected position of PaParE1 toxin protein. L: protein ladder.

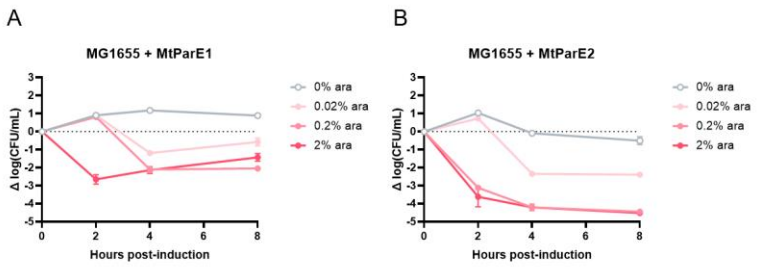

Figure 2.4. Impact of MtParE toxin expression on *E. coli* cell viability. The expression of the toxin protein MtParE1 (**A**) or MtParE2 (**B**) was induced in *E. coli* MG1655 cells using specified concentrations of arabinose (ara) in LB medium. Colony-forming units per milliliter (CFU/mL) were measured as described in methods and normalized to the initial count at time zero to calculate the change in CFU/mL (ΔCFU/mL), which was plotted on the y-axis. Notably, both MtParE toxins exhibited induction-strength-dependent toxicity to *E. coli* MG1655 cells. Each data point on the graph includes SEM, derived from at least two independent experiments with replicates.

4.2. Expression of ParE Toxins Resulted in the Increased Mutation Frequency

The expression of ParE toxins has been shown to induce a filamentation phenotype, which is consistent with the observations from other DNA gyrase inhibitors [23]. Inhibition of DNA gyrase causes DSBs in DNA, which rapidly trigger cellular repair pathways like SOS response to repair this DNA damage [59,61]. However, the low fidelity of these repair processes can lead to an increase in genetic mutations, which may contribute to the emergence of antibiotic resistance. To evaluate the impact of ParE-mediated DNA gyrase on genetic mutations, the mutation frequency because of ParE toxicity was determined.

Mutation frequency, defined as the proportion of mutants within a population, was determined using a selection method that identifies rifampicin (RIF) or trimethoprim (TMP) resistant mutants, adapted from an established protocol [72]. Major modifications to published protocols were required to accommodate the expression of a potential mutagen rather than an external

treatment, such as with a compound. Additional development was needed to establish specific growth conditions that minimized further mutation events after treatment, as well as robust imaging techniques and standardized data processing procedures. RIF-resistant (RIF^R) mutants emerge from single-point mutations in the RNA polymerase beta subunit, whereas TMP-resistant (TMP^R) mutants develop through single-point mutations affecting dihydrofolate reductase activity [73,74]. In addition, ciprofloxacin (CIP), a quinolone antibiotic, was used in this chapter as a positive control. CIP is known for its effect on gyrase inhibition and has been shown to increase mutagenesis at concentrations below its minimum inhibitory concentration (MIC) [75–77], making it an ideal standard for comparison. The MICs for RIF, TMP, and CIP against the experimental strains were determined in the test media, and the results aligned with previously published values (**Table 2.3**). The study then proceeded to use the highest induction strength that allowed the emergence of at least one mutant on the selection plate for mutant screening.

Table 2.3

MICs (μg/mL) of RIF, TMP and CIP for test bacterial cells in test media.

Bacteria strain	RIF	Reference	TMP	Reference	CIP	Reference
P. aeruginosa PA14 [a]	>500	*unreported* [d]	100	*unreported* [d]	0.05	0.064 [b] [78]
P. aeruginosa PAO1 [a]	*n.t.*	*unreported* [d]	100	>32 [c] [79]	0.07	0.063-0.09 [b] [80,81]
E. coli MG1655 [b]	10	12-25 [82,83]	0.25	0.2-1 [84,85]	0.04	0.016-0.035 [86,87]

[a] MIC was tested in M9 minimal medium. [b]: MIC was tested in LB medium. [c] MIC was tested in tryptic soy broth (TSB). [d]: Extensive literature searches did not reveal a published value. *n.t.*: not tested.

Not surprisingly, the PaParE1 toxin, which exhibited minimal impact on cell viability (**Fig. 2.2A** and **B**), did not lead to a marked increase in mutation frequency in either *P. aeruginosa* PA14 or

PAO1 cells, even with the maximum induction strength of 2% (**Fig. 2.5A** and **B**). In comparison, the treatments of sub-MICs of CIP resulted in approx. 2.4- and 1.5-fold increases in mutation frequency in *P. aeruginosa* PA14 and PAO1 cells, respectively. In contrast, when expressing the PaParE2 toxin in *P. aeruginosa* PAO1 cells, the induction strengths of 0.2% and 2% led to approx. 5.54- and 14.24-fold increases in mutation frequency, respectively (**Fig. 2.5C**), while the treatments of sub-MICs of CIP led to approx. 2.2- and 3.3-fold increase in mutation frequency for 0.5× MIC and 0.75× MIC, respectively (**Fig. 2.5C**). Though PaParE2 toxin expression led to an approx. 1.7-log reduction in cell counts at a 0.02% induction strength within 8 h, it did not impact cell growth until 4 h of induction (**Fig. 2.2C**). This delay of the toxin's effect appeared to render the later 4 h of expression insufficient for a significant number of mutants to accumulate so as there was not a significant increase in mutation frequency (**Fig. 2.5C**).

As the focus shifted to the highly toxic MtParE toxins, both MtParE1 and MtParE2 toxins exhibited significant, dose-dependent increases in mutation frequency even at low induction strengths (**Fig. 2.5D** and **E**). Specifically, the MtParE1 toxin expression resulted in approx. 12.3-fold and 16.6-fold increases in mutation frequency at 0.01% and 0.02% induction strengths, respectively, in comparison to that observed from the 0% induction baseline (**Fig. 2.5D**). Interestingly, these increases in mutation frequency induced by the MtParE1 toxin expression surpassed those observed with treatments of sub-MICs of CIP, which showed approx. 2.4-fold and 4.0-fold increases for 0.5× MIC and 0.75× MIC, respectively (**Fig. 2.5D**). In contrast, the MtParE2 toxin expression resulted in more pronounced increases in mutation frequency, approx. 27.2-fold and 50.6-fold at 0.0005% and 0.001% induction strengths, respectively, while treatments of sub-MICs of CIP led to approx. 1.8-fold and 2.3-fold increases for 0.5× MIC and 0.75× MIC, respectively (**Fig. 2.5E**).

Collectively, the attenuated PaParE1 toxin expression didn't affect mutation frequency while the expression of other three potent ParE toxins led to a dose-dependent increase in mutation frequency. Given the distinct toxicity profiles and the dose-dependent killing patterns of PaParE2, MtParE1 and MtParE2 toxins, these findings also suggest a direct correlation between

the toxicity of ParE toxins and the resulting increased mutation frequency.

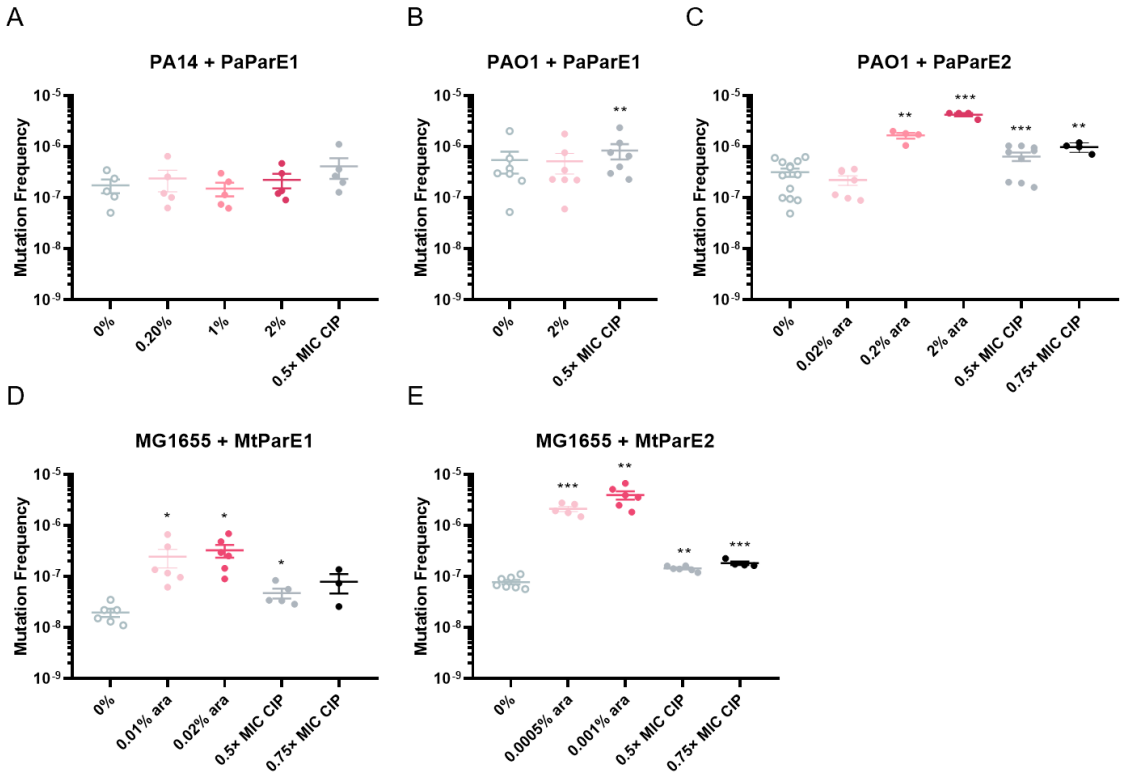

Figure 2.5. Mutation frequency induced by ParE toxin expression or treatment with sub-MICs of CIP. MIC of CIP against each strain was shown in **Table 2.3**. The expression of toxin protein PaParE1 (**A** and **B**), PaParE2 (**C**), MtParE1 (**D**), or MtParE2 (**E**) was induced in *P. aeruginosa* PA14 (**A**), PAO1 (**B** and **C**), or *E. coli* MG1655 (**D** and **E**) cells using specified concentrations of arabinose (ara) or treatment of sub-MICs of CIP (0.5× and 0.75× MIC) for 8 h in test medium. Mutation frequency was defined as the proportion of cells resistant to TMP (**A** to **C**) or RIF (**D** and **E**) in population, which was calculated by dividing the number of RIF^R or TMP^R cells by the number of viable cells per unit volume. Each measurement with SEM represents at least three independent experiments. Mutation frequency of arabinose-added or sub-MIC-CIP-treated groups (solid circle) were compared to that of the 0%-arabinose-added group (hollow circle) and one-tailed paired Student's *t*-test was performed: *, $P < 0.05$; **, $P < 0.01$; ***, $P < 0.001$.

4.3. Expression of ParE Toxins did not Reduce Cell Antibiotic Susceptibility

Given the increased mutation frequency resulting from the ParE toxin toxicity (**Fig. 2.5**), it was questioned whether this could contribute to the emergence of antibiotic resistance, enhancing the bacterial cells' ability to withstand current antibiotic treatments.

To investigate that, cells were treated with commonly used clinical antibiotics following 8 h of ParE expression at the highest induction strengths that triggered an increase in mutation frequency and permitted subsequent adequate cell growth (as a lawn) on agar plates. At the time of adding cultures to plated media, a disk containing a defined amount of antibiotic or a commercial "E-test" strip containing a gradient of impregnated antibiotics was carefully placed on the plate. After incubation, a zone of clearing (inhibition zone) around the disk or strip is indicative of susceptibility to the antibiotic.

Inducing the PaParE1 toxin expression by 2% arabinose did not significantly alter the MIC values of any tested antibiotics against *P. aeruginosa* PA14 and PAO1 cells (**Fig. 2.6, Table 2.4**, **Fig. S2.4**). This observation aligned with the expected attenuated toxicity of the PaParE1 toxin. In contrast, the expression of the potent PaParE2 toxin did not alter the MIC values of most tested antibiotics against *P. aeruginosa* PAO1 cells, but it moderately lowered the MIC values of two antibiotics that target cell wall synthesis (**Fig. 2.6, Table 2.4**, **Fig. S2.4**). Specifically, the MIC value of piperacillin against *P. aeruginosa* PAO1 cells was reduced moderately from 4 μg/mL (0% induction) to 3 μg/mL (0.2% and 2% inductions) and the diameter of the inhibition zone of meropenem was increased from 30.8 ± 1.3 mm (0% induction) to 35.1 ± 0.8 mm (0.2% induction) and 34.4 ± 1.5 mm (2% induction). This data indicated that the expression of PaParE2 toxin increased the cell's susceptibility to certain antibiotics.

Similarly, the expression of MtParE1 and MtParE2 toxins led to a noticeable decrease in the MIC value of meropenem against *E. coli* MG1655 cells (**Fig. 2.6, Table 2.5**, **Fig. S2.5**). Additionally, the expression of MtParE1 and MtParE2 toxins also increased the cell susceptibility to other antibiotics. For example, a minimal 0.02% induction of MtParE1 toxin expression decreased

MIC value of ciprofloxacin from 0.008 μg/mL to 0.004 μg/mL and increased the diameter of the inhibition zone of trimethoprim from 26.3 ± 0.5 mm to 33.0 ± 1.2 mm (**Table 2.5**, **Fig. S2.5**). Moreover, the expression of the more potent MtParE2 toxin exhibited a similar effect in enhancing cell susceptibility but required even lower levels of induction (**Table 2.5**, **Fig. S2.5**). These results also aligned with the expected toxicity of the MtParE toxins.

Collectively, these results demonstrated that exposure to ParE toxin expression enhanced cell susceptibility to certain antibiotics, especially those targeting cell wall synthesis (**Fig. 2.6**, **Table 2.4** and **2.5**, **Fig. S2.4** and **S2.5**). While the ParE toxin activity has the potential to contribute to antibiotic resistance through increased mutation frequency, it did not lead to antibiotic resistance for most tested antibiotics within the observation period. Instead, the ParE toxin activity can weaken the bacterial cell's ability to survive, and this effect was additive or synergistic with existing antibiotic treatments.

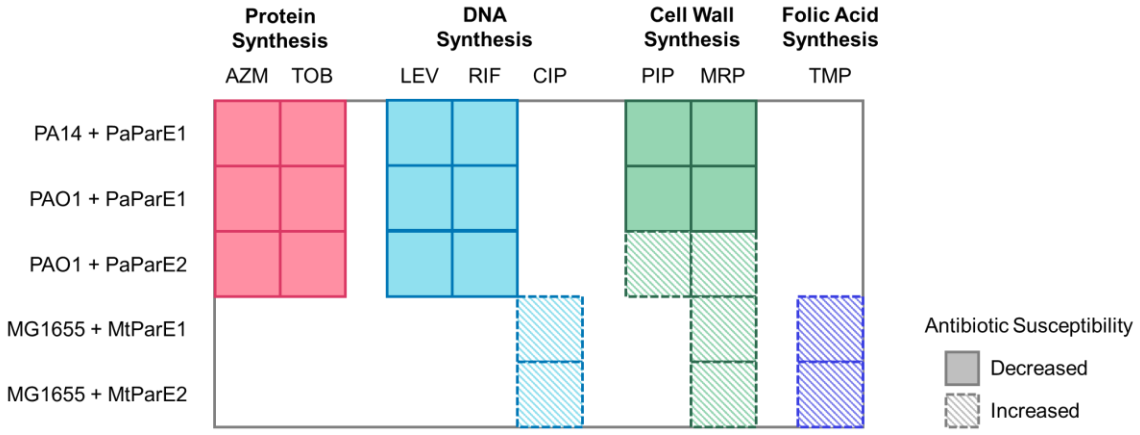

Figure. 2.6. Impact of ParE toxin expression on cell antibiotic susceptibility. Summary for data of tested samples; note that "increased" indicates the susceptibility is better, such that the MIC value (for AZM, LEV, RIF, and CIP) will have decreased, or the diameter of the inhibition zone (for TOB, MRP, and TMP) will have increased. AZM: azithromycin; TOB: tobramycin; LEV: levofloxacin; PIP: piperacillin; MRP: meropenem; TMP: trimethoprim.

Table 2.4

MIC values (μg/mL) or diameters of inhibition zones (mm) of antibiotics against *P. aeruginosa* PA14 and PAO1 strains with and without the induction of PaParE toxin expression.

Cells and ParE toxin	Ara	AZM	LEV	PIP	RIF	MRP [a]	TOB [a]
PA14 + PaParE1	0%	>64 ± 0	0.23 ± 0.02	6 ± 2	>128	30.8 ± 0.1	21.9 ± 1.3
	2%	>64 ± 0	0.23 ± 0.02	6 ± 2	>128	30.8 ± 0.1	22.3 ± 0.9
PAO1 + PaParE1	0%	>256 ± 0	0.32 ± 0.07	8 ± 0	6	27.9 ± 0.1	21.9 ± 0.1
	2%	>256 ± 0	0.32 ± 0.07	6 ± 2	6	27.8 ± 0.2	22.2 ± 0.2
PAO1 + PaParE2	0%	>256 ± 0	0.125 ± 0	4 ± 0	6 ± 2	30.8 ± 1.3	26.2 ± 0.1
	0.2%	>256 ± 0	0.125 ± 0	3 ± 0	7 ± 1	35.1 ± 0.8	25.6 ± 0.1
	2%	>256 ± 0	0.125 ± 0	3 ± 0	6 ± 2	34.4 ± 1.5	25.9 ± 0.1

[a] Discs of antibiotics were used, and the diameters of the inhibition zones are presented. *n.t.*: not tested. Data represented in the format of "mean±SEM" was derived from at least 2 independent experiments. Ara: arabinose. AZM: azithromycin; LEV: levofloxacin; PIP: piperacillin; RIF: rifampicin; MRP: meropenem of 10 μg; TOB: tobramycin of 10 μg.

Table 2.5

MIC values (μg/mL) or diameters of inhibition zones (mm) of antibiotics against *E. coli* MG1655 strains with and without the induction of MtParE toxin expression.

Cells and ParE toxin	Ara	CIP	MRP [a]	TMP [a]
MG1655 + MtParE1	0%	0.008 ± 0	34.2 ± 0.4	26.3 ± 0.5
	0.02%	0.004 ± 0	39.3 ± 0.6	33.0 ± 1.2
	0.2%	0.004 ± 0	41.5 ± 0.4	34.0 ± 0.8
	2%	0.005 ± 0.001	41.5 ± 0.2	35.6 ± 0.1
MG1655 + MtParE2	0%	0.006 ± 0	29.0 ± 0.5	25.3 ± 0.3
	0.00001%	0.006 ± 0	30.3 ± 2.8	26.6 ± 2.0
	0.0001%	0.004 ± 0	33.8 ± 0.3	32.1 ± 0.9
	0.001%	0.004	36	30.9

[a] Discs of antibiotics were used, and the diameters of the inhibition zones are presented. *n.t.*: not tested. Data represented in the format of "mean±SEM" was derived from at least 2 independent experiments. Ara: arabinose. CIP: ciprofloxacin; MRP: meropenem of 10 μg; TMP: trimethoprim

of 5 μg.

5. Discussion

The findings presented in this chapter provide important insights into the potential outcomes of co-opting ParE toxins as a strategic tool to fight bacterial infections. This study not only emphasizes the different impacts of expression of different ParE toxins on bacterial viability and mutation frequency, but also highlights the understanding of the role of toxins in the combat against bacterial infections.

The differential toxicities were observed among different ParE toxin members despite their conserved structure [23,26], where the PaParE1 toxin showed a minimal toxicity and the PaParE2, MtParE1, and MtParE2 toxin showed pronounced effects (**Fig. 2.2** and **2.4**). While the source of this variability remains unknown, increasing evidence suggests that ParE toxins have limited solubility such that sequence-specific variations may impact both interactions with the gyrase target as well as cellular location [23,88]. This difference in toxicity highlights the potential of specific toxins as components of new antibacterial strategies.

Furthermore, the dose-dependent increase in mutation frequency was observed upon ParE toxin expression, as shown in **Table 2.4** and **2.5**. This observation of increased mutation frequency underlines the capacity of ParE toxins to induce mutagenesis within bacterial populations, a phenomenon that could theoretically accelerate the emergence of antibiotic resistance. However, within the timeframe of observation, this study observed no direct promotion of new antibiotic resistance. On the contrary, an increase in cell susceptibility to a broad spectrum of antibiotics in the presence of ParE toxin expression was observed (**Table 2.4** and **2.5**, **Fig. S2.4** and **S2.5**). This finding suggests that while the ParE toxins increase the frequency of single point mutations, these do not translate into functional resistance mechanisms for common antibiotics. This implied that the single point mutations are unlikely to accumulate into usable resistance mechanisms before the cell dies.

Although these data highlighted the potential of TA-system-based antibacterial strategies, it is still too early to successfully translate these concepts into real-world therapeutic approaches. It is essential to carefully choose the correct TA systems to target. This selection should consider not only the potency of the toxins but also their prevalence in pathogens, as well as additional effects such as the formation of persister cells and biofilms [44]. The ParDE TA system, prevalent in pathogenic bacteria like *P. aeruginosa* and *M. tuberculosis*, has shown significant potential for a correct target, as demonstrated in this chapter. Future investigations targeting different TA systems and bacterial species will need tailored approaches.

In conclusion, this study reveals the dual functions of ParE toxins as agents causing mutagenesis and as modulators of antibiotic susceptibility. By clarifying effects of ParE toxins, this study opens the door to manipulate these bacterial "time bombs" in developing innovative treatments, which may change the struggle against antibiotic-resistant infections. The role of ParE toxins in enhancing antibiotic efficacy sets a promising paradigm for their strategic application in antibacterial therapy and makes an important contribution to the ongoing global efforts to combat antibiotic resistance.

Author Contributions

S.R. collected all data reported in this chapter; S.R. and C.R.B. participated in the project design, data analysis, manuscript drafting, and editing.

Data Availability

All data are included in this manuscript and Appendix A; DNA clones for constructs made in this work are available upon request. Information for the proteins used in this work is available online (PaParE1, UniProtKB Q9I708; PaParE2, UniProtKB Q9I5J9; MtParE1, UniProtKB P9WHG7; MtParE2, UniProtKB P9WHG5).

Acknowledgements

Research reported in this publication was supported by the Department of Defense under Grant

No. W81XWH-20-1-0121. The content is solely the responsibility of the authors and does not necessarily represent the official views of the Department of Defense. We appreciate use of equipment in the Protein Production and Characterization Core at OU.

Chapter III: *Escherichia coli* Cells Evade Inducible ParE Toxin Expression by Reducing Plasmid Copy Number

Shengfeng Ruan and Christina R. Bourne

Department of Chemistry and Biochemistry, University of Oklahoma, Norman OK USA

This chapter represents unpublished research conducted in the Bourne lab, located within the Department of Chemistry and Biochemistry at the University of Oklahoma. The manuscript has been accepted by *the Journal of ASM Microbiology Spectrum* on April 15th, 2024.

I collected and processed all the data for the manuscript. All figures were produced by me. Writing of the manuscript was performed by me with assistance from Dr. Christina Bourne. Editing and feedback on all writing was provided by Dr. Christina Bourne.

1. Abstract

Plasmids play important roles in microbial ecosystems, serving as carriers of antibiotic resistance and virulence. In the laboratory, they are essential tools for genetic manipulation and recombinant protein expression. We uncovered an intriguing survival phenotype in a fraction of the bacterial population while using plasmid-mediated arabinose inducible gene expression to monitor production of toxic ParE proteins. This phenotype was not correlated with changes to the plasmid sequence and could not be rescued by increasing arabinose uptake. Instead, survival correlates with a marked reduction in plasmid copy number (PCN). Reduced PCN was reproducible, not a function of pre-existing population, and can be sequentially enriched by continual passage with induction. The reduction in PCN appears to allow mitigation of toxicity from expression of ParE proteins while balancing the need to maintain a threshold PCN to withstand selection conditions. This indicates an adaptive cellular response to stressful

conditions likely by altering regulation of plasmid replication. Furthermore, this survival mechanism appears to not be limited to a specific bacterial strain of *Escherichia coli* or ParE toxin family member, suggesting a generalized response. Lastly, bacterial whole genome sequencing indicated a N845S residue substitution in DNA polymerase I, which correlates with the observed reduction in PCN and has been previously reported to impact plasmid replication. Further understanding this molecular mechanism has broader implications for this adaptive response of the dynamics of plasmid-mediated gene expression, microbial adaptation, and genetic engineering methodologies.

2. Introduction

Plasmids are circular, double-stranded DNA molecules that are naturally present in the microbial world, including bacteria and archaea [62]. They exist as a physically distinct entity from cell's chromosomal DNA that can replicate independently and have evolved over time as part of these organisms' genetic makeup. These natural plasmids often bring their hosts beneficial traits, such as antibiotic resistance and virulence, thereby offering survival advantages in competitive environments. [89–92]. They are also important drivers of bacterial evolution due to their intercellular transfer by conjugation or mobilization [93–95].

In the laboratory, plasmids are important tools in genetic engineering procedures such as gene cloning and recombinant protein expression. Laboratory-based plasmids canonically possess a minimal set of essential components, including an origin of replication (*ori*), a selection marker, and a cloning site for the insertion of genes of interest. In order to control the expression of an inserted recombinant gene, these recombinant plasmids frequently incorporate catabolic repression systems as inducible promoters [96]. The arabinose-inducible (*ara*BAD) promoter is commonly used and is tightly controlled by the presence or absence of arabinose in the environment [97]. Notably, due to catabolite repression, the induction of *ara*BAD is easily repressed by the presence of excess glucose or lactose [98]. This specificity ensures that the

induction of the *ara*BAD promoter is tightly controlled and limited to the presence of arabinose, enabling modest induction levels for toxic protein expression [99], making it more suitable for certain applications.

The ease of modifying recombinant plasmids [100,101] as well as their capacity for self-replication and tunable recombinant protein expression [102,103] within host cells render them useful for ectopically expressing recombinant proteins in bacteria. Although, under particular conditions, the host cells benefit from the survival advantages conferred by the plasmid, the presence of plasmids can impose a metabolic burden on the host cells, potentially leading to adverse effects on plasmid stability and quality [104,105]. Given the important role of plasmid stability in ensuring research reliability and validity, the problem of plasmid instability is a concern. This is especially the case for studies expressing toxic proteins, such as those from toxin-antitoxin (TA) systems, where standard characterization sometimes relies on demonstration of toxicity upon induction of toxin and rescue upon induction of antitoxin [23,106–108]. We have previously noted toxins that are active in their native hosts but were not toxic in the commonly used *Escherichia coli* surrogate host [108], and in the current work have uncovered additional confounding issues with these strategies.

Our research focuses on the ParE toxin proteins, components of the type-II ParDE TA system. It is one of few known toxin proteins that target DNA gyrase [26], an essential enzyme involved in DNA replication and maintenance [32,109,110]. The first ParDE system to be characterized is carried on the broad host range low copy number RK2 plasmid [111]. In this capacity, the TA system serves an addiction function to enforce maintenance of the plasmid through the gyrase-inhibiting function of the ParE toxin. However, it was reported that under some growth conditions the plasmid could be lost, and, paradoxically, viability was restored over time. Later other ParE family members have been studied, including one encoded within a pathogenicity island on the chromosome of *Mycobacteria tuberculosis* (Mt) [112]. It was found that the overexpression in an *E. coli* host caused potent toxicity but was followed by a full recovery of growth.

Our studies have also observed a robust reduction in cell viability upon ParE protein expression but, in some instances, this is followed by a recovery of viable cell counts, indicating some survival mechanism may be induced. To investigate the underlying mechanism of this recovery phenotype, the ParE proteins were cloned from the Mt chromosome (MtParE1 and MtParE2) and were ectopically expressed in *E. coli*. These exerted a maximum toxicity on cells within 4 hr of induction, after which cultures either maintain a steady population or recover growth, which is consistent with previous observations [112]. Unexpectedly, we observed an insensitivity to subsequent re-induction of ParE protein expression after initial exposure and recovery. Through culture-based assays, we find that the loss of toxicity upon re-induction of ParE protein expression does not result from mutations of the plasmids or by alteration of arabinose uptake. Instead, we captured cells within the population with a consistent and stably reduced plasmid copy number (PCN); further, this phenotype could be enriched from the culture population with subsequent ParE exposure via continual induction. Our investigation suggests that the observed reduction in PCN may be attributed to a mutation at the N845S residue in DNA polymerase I, and potentially the ratio of replication regulators RNA I and RNA II. These factors are intricately connected to the replication process of the plasmid under investigation.

In summary, our studies highlight a pervasive reduction in PCN, which could be a confounding variable for standard studies of recombinant toxic proteins in engineered plasmids. We have thus characterized a phenotypic balance between two toxic contrasting outcomes: maintaining PCN to support survival by ensuring sufficient expression of the antibiotic-resistant selection maker versus reducing the PCN to limit expression of the ParE toxin protein.

3. Experimental Details

3.1. Bacterial Strains and Plasmids

The bacterial strains, plasmids and primers used in this study are listed in **Table S1** and **Table S2**. Standard protocols were followed for DNA manipulation, PCR cloning and DNA

purification. DNA fragments were PCR amplified from *Mycobacterium tuberculosis* strain H37Rv genomic DNA and plasmid DNA using Q5® High-Fidelity DNA Polymerase (NEB) and assembled by Gibson Assembly using Gibson Assembly® Master Mix (NEB) according to the manufacturer's instructions. The chemically competent cells of *Escherichia coli* MG1655 or TOP10 strains were prepared according to standard protocols and aliquoted as "starting" cells for transformation. Plasmid was transformed into competent cells by heat shock method according to standard protocols. Plasmid was extracted and purified using Zyppy™ Plasmid Miniprep Kit (Zymo Research) and sequenced by GENEWIZ (USA) or Plasmidsaurus (USA). Genomic DNA was extracted and purified using Wizard® Genomic DNA Purification Kit (Promega) and sequenced by Plasmidsaurus (USA). Genome annotations are sourced from GenBank: U00096.3.

Construction of Plasmids

(i) *pMindBAD::mtparE1*

The fragments of the *mtparE1* gene and the pMind vector were separately PCR amplified and subsequently assembled to generate the pMind::*mtparE1* plasmid. This construction process involved utilizing the mtparE1 primer set for the gene fragments and the pMind primer set for the vector. The *tetRO* promoter of pMind::*mtparE1* was substituted with the *araC*-pBAD promoter to generate the pMindBAD::*mtparE1* plasmid. This replacement involved assembling the fragment of *araC*-pBAD promoter, which was amplified from pHerd20T using the araC-pBAD primer set, with the fragment amplified from pMind::*mtparE1* using the pMind+araC-pBAD primer set.

(ii) *pMindBAD::Strep-mtparE2*

The fragments of the *mtparD2E2* gene and the pMind vector were separately PCR amplified. These fragments were then assembled to generate the pMind::*mtparD2E2* plasmid, using mtparD2E2 and pMind primer sets. The *mtparD2* gene of pMind::*mtparD2E2* was subsequently removed, and a *Strep* tag was fused upstream of the *mtparE2* gene to generate the pMind::*Strep-mtparE2* plasmid. This modification was achieved by performing a PCR amplification of

pMind::*mtparD2E2* using the mtparE2+Strep primer set. The resulting amplicon was subjected to KLD treatment using the KLD Enzyme Mix (NEB, Cat# M0554S), according to the manufacturer's instructions. Finally, the *tetRO* promoter was replaced with the *araC*-pBAD promoter to generate the pMindBAD::*Strep-mtparE2* plasmid, following the same method as described above.

3.2. Growth of Cultures and Measurements of Cell Viability

Overnight cultures were inoculated from -80°C frozen 20%-glycerol stocks or single colonies on LB agar plates into LB media supplemented with appropriate antibiotic and 1% glucose, and grown overnight (18–20 hr) at 37°C with shaking at 200 rpm. The overnight cultures were then back-diluted 1:20 in fresh LB media and added with arabinose to final concentrations of 0% to 2%, and grown at 37°C with shaking at 200 rpm. Aliquots of cultures were collected at the defined time intervals and 10-fold serial dilutions in sterile 0.9% saline solution were performed and spotted onto LB agar plates supplemented with 50 μg/mL Kanamycin and 1% glucose for determination of the colony-forming units (CFUs). The CFUs were subsequently converted to CFU/mL based on the initial spotting volumes. Kanamycin was added at 50 μg/mL. Carbenicillin was added at 100 μg/mL. Gentamycin was added at 10 μg/mL. The limit of detection for CFU/mL measurements was 200 CFU/mL. Figures were generated using GraphPad Prism 8.01.

3.3. Determination of the Ratio of Plasmid to Chromosome per Cell

3.3.1. DNA sample preparation for qPCR

The method described previously by Anindyajati and Skulj et al. [113,114] was modified in this study. Briefly, overnight cultures were inoculated from frozen glycerol stocks into 8 mL of LB media supplemented with 50 μg/mL Kanamycin and grown overnight (18-20 hr) at 37°C with shaking at 200 rpm. The cells were then harvested through centrifugation and resuspended in 80

μL of distilled water. The cell suspension was heated at 99°C for 20 minutes, frozen at -80°C and heated again at 99°C for 20 minutes. Supernatants were collected by centrifugation at 16,000 ×g for 10 minutes, followed by a series of 10-fold dilution as a template source.

3.3.2. Design of primer sets for qPCR and RT-qPCR

The constitutively expressed *gapA* gene, encoding d-glyceraldehyde-3-phosphate dehydrogenase, was chosen as the reference gene to normalize the expression levels of target genes. The primer sequences for *gapA* were sourced from the study by Robbins-Manke et al [115]. Primers for the target genes were designed with a similar melting temperature to the gapA primer set using IDT PrimerQuest™ Tool. Primers were synthesized by IDT (USA). Primer specificity was tested by the PCR product electrophoretogram and the product melting curve analysis following qPCR amplification.

3.3.3. Real-time qPCR using SYBR Green dye

4 μL of at least 3 template dilutions (*e.g.,* 10^{-1}, 10^{-2} and 10^{-3} dilutions) was then amplified using Fast SYBR™ Green Master Mix (Applied Biosystems) and the appropriate primer set in separated reaction on Roche LightCycler® 480 II Real-Time PCR system using the following cycling conditions for all amplicons: 5 min at 95°C (pre-incubation), followed by 45 cycles of 5 sec at 95°C, 30 sec at 58°C and 20 sec at 58°C. At the end, a dissociation stage was added: 5 sec at 95°C, 1 min from 60°C to 97°C. Cycle threshold (Ct) values were determined automatically using the built-in analysis function of "Abs Quant/Fit Points" in LightCycler® 480 software version 1.5.1.62.

The determination of the ratio of the plasmid to chromosome (P/C) was reported by Anindyajat and Skulj et al. [113,114]. Briefly, in each run, the curve for each primer set was constructed by placing the log value of the dilution fold (*e.g.,* -1, -2 and -3) on the x axis and Ct value on the y axis. The calculation of amplification efficiency (E) involved utilizing the average slope value from the curves obtained with the same primer set in the same run, as per the formula outlined in equation (1).

$$E = 10^{-\frac{1}{slope}} \quad (1)$$

The determination of the ratio of target A to target B (A/B) was accomplished by applying equation (2), which considered distinct amplification efficiencies (E) and Ct values corresponding to the targets.

$$A/B = \frac{{E_A}^{-Ct_A}}{{E_B}^{-Ct_B}} \quad (2)$$

The ratio of P/C was defined as the ratio of plasmid (*parE* gene, target A) to chromosome (*gapA* gene, target B) and determined across all dilutions within each sample, followed by the calculation of the mean and standard deviation (SD) for these values. Figures were generated using GraphPad Prism 8.01.

3.4. Determination of the Ratio of RNA II to RNA I

3.4.1. cDNA sample preparation for RT-qPCR

Overnight cultures were inoculated from frozen glycerol stocks into LB media supplemented with appropriate antibiotic and 1% glucose, and grown overnight (18-20 hr) at 37°C with shaking at 200 rpm. The overnight cultures were then back-diluted 1:20 in 50 mL of fresh LB media supplemented with appropriate antibiotic and grown at 37°C with shaking at 200 rpm. The cells were then harvested through centrifugation when an optical density (OD_{600}) of 0.6-0.8 was reached. Total RNA was extracted using the Direct-zol™ RNA Miniprep Plus Kit (Zymo Research) according to the manufacturer's instructions. Contaminating genomic and plasmid DNA was removed and total RNA was cleaned using RNA Clean & Concentrator Kit (Zymo Research) according to the manufacturer's instructions. DNA contamination was tested by qPCR using appropriate primer sets. RNA samples with a Ct value of not less than 35 were considered to contain limited or no DNA contamination. Once the RNA sample was free of DNA contamination, it was reverse-transcribed into cDNA using the High Capacity cDNA Reverse

Transcription Kits (Applied Biosystems), followed by a series of 10-fold dilution as a template source. When the elimination of DNA contamination cannot be accomplished, a control group was introduced, *i.e.*, the reverse transcriptase was replaced with an equal volume of water in the reverse transcription reaction.

3.4.2. Real-time qPCR using SYBR Green dye

4 μL of cDNA template or control template was then amplified by qPCR as described above. The ratio of *RNA II* (target A) to *RNA I* (target B) was determined across all dilutions within each sample as described above by applying equation (2) or equation (3), followed by the calculation of the mean and standard deviation (SD) for these values. Figures were generated using GraphPad Prism 8.01.

$$A/B = \frac{(E_A{}^{-Ct_A})_{exp} - (E_A{}^{-Ct_A})_{Ctrl}}{(E_B{}^{-Ct_B})_{exp} - (E_B{}^{-Ct_B})_{Ctrl}} \quad (3)$$

3.5. Determination of the *araE* mRNA

Overnight cultures were inoculated from frozen glycerol stocks into LB media supplemented with appropriate antibiotic(s) and grown overnight (15 hr) at 37°C with shaking at 200 rpm. The overnight cultures were divided into two portions. Arabinose was added to one portion to achieve a final concentration of 2% and the same amount of water was added to the other portion as a control (0%). Subsequently, both portions were grown at 37°C with shaking at 200 rpm for 5 hr. cDNA samples were prepared and data analysis was performed as described above.

3.6. Imaging of Fluorescent Cells

Overnight cultures were inoculated from frozen glycerol stocks into LB media supplemented appropriate antibiotic(s) and 1% glucose and grown overnight (15 hr) at 37°C with shaking at

200 rpm. Arabinose was then added to a final concentration of 0.2% or 2% to induce mCherry protein expression and grown at 37°C with shaking at 200 rpm for 4-5 hr. 5 μL of the cultures were applied to a microscope slide (Fisher Scientific, USA) and a cover glass (Fisher Scientific, USA) was then sealed into place. The cells were imaged using a Leica Microsystems Model DMi8 with appropriate settings.

4. Results

4.1. A Subset of Cells within a Population Exhibited Survival during Ectopic ParE1 Protein Expression

The expression of the ParE1 toxin protein, derived from *Mycobacteria tuberculosis* (Mt), was induced in *Escherichia coli* MG1655 cells at multiple induction strengths (**Fig. 1A**). Induction by arabinose relied on an inserted arabinose-inducible (*ara*BAD) promoter, cloned from a pBAD vector to replace the existing *tetRO* promoter on the pMind vector, generating the "pMindBAD" plasmid. The resulting colony-forming units per milliliter (CFU/mL) sampled over time revealed a dose-dependent decline in cell viability, confirming the toxicity of ParE1 protein expression to cells (**Fig. 1B**). Under a standard liquid growth condition in Luria-Bertani broth, a 0.02% induction level led to a 1.3-log reduction in cell counts within 4 hr, while a 2% induction resulted in a more pronounced 3.1-log reduction in the same time frame (**Fig. 1B**). In contrast, when no arabinose was added during the same time frame, cell counts increased by 1.4-fold, which aligns with the 1.6-fold increase in cell counts for *E. coli* cells harboring the pMind "empty" vector lacking the inserted ParE1-encoding gene over the same 4-hr period (**Fig. S1**). However, the induction of ParE1 protein expression did not result in a complete cell loss; instead, cells demonstrated the ability to either recover growth or maintain a steady population beyond 4 hr post-induction (**Fig. 1B**).

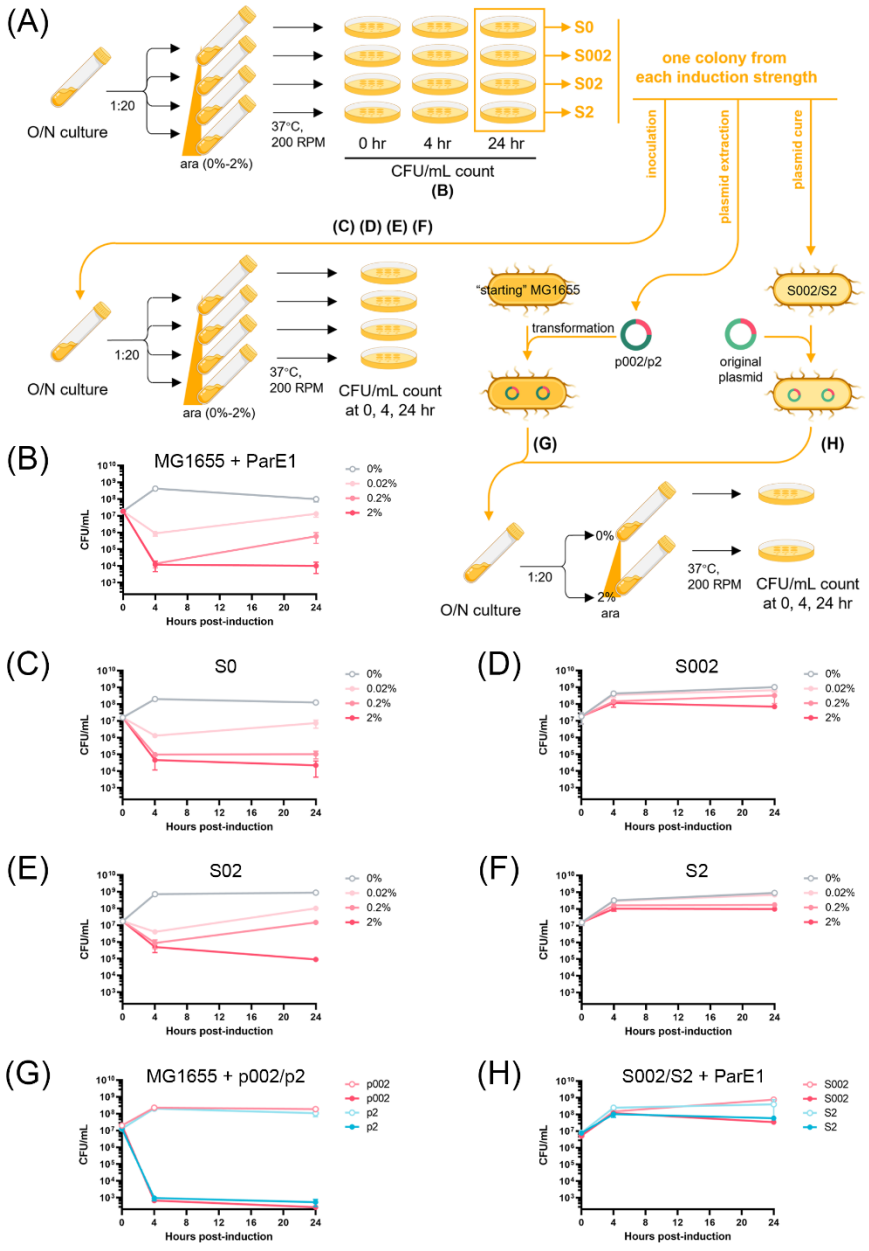

Figure 3.1. Impact of the induction of ParE1 protein expression on *E. coli* cell viability. (**A**) Schematic representation of the experimental workflow. ara: arabinose. (**B**) The induction of ParE1 protein expression in *E. coli* MG1655 cells exhibited an induction-strength-dependent pattern. (**C** to **F**) Following a 24-hr induction of ParE1 protein expression, the reinduction of ParE1 protein expression in the isolated cells exerted two different toxicity profiles: cells S0 (**C**) and S02 (**E**) remained sensitive to the reinduction of ParE1 protein expression, while cells S002

(**D**) and S2 (**F**) lost the sensitivity. (**G**) The induction of ParE1 protein expression from the extracted plasmids exhibited a strong toxicity profile to the "starting" *E. coli* MG1655 cells. (**H**) Plasmid-cured S002 and S2 cells lost the sensitivity to the induction of ParE1 protein expression from the transformed original plasmid construct. Each data point is presented with the standard error of the mean (SEM), representing at least two independent experiments.

To further investigate the underlying mechanism of this phenotype, following the 24-hr induction period, one colony from each induction strength (designated as surviving cell "S" and corresponding arabinose concentration: S0, S002, S02 and S2, **Fig. 1A, 1C-F**) was isolated and re-grown to stationary phase in the absence of the arabinose inducer. Subsequently, the stationary culture was diluted 1:20 and ParE1 protein expression was re-induced with the same inducer concentrations (**Fig. 1A**). Unexpectedly, the re-induction of ParE1 protein expression exerted markedly two different toxicity profiles: cells originating from 0% induction remained sensitive to the induction of ParE1 protein expression (S0, **Fig. 1C**) as did the culture originating from the 0.2% induced surviving colony (S02, **Fig. 1E**). However, there was no sensitivity remaining for cells originating from 0.02% induction (S002, **Fig. 1D**) and 2% induction (S2, **Fig. 1F**) conditions. This unexpected differential response to ParE protein re-induction implies that the recovery in cell growth was not solely a consequence of the depletion of arabinose inducer at longer growth time points. It emphasizes the complexity of the cellular response to ParE1 toxin expression and prompted further exploration into the underlying mechanisms.

4.2. Loss of Re-induction Sensitivity does not Result from Plasmid Mutations

As a gyrase inhibitor, the action of ParE toxins raises the possibility of mutation-prone repair as a means of cell rescue and subsequent survival [116]. Further, previous studies have indicated mutations in promoter regions as a common means for cellular escape of toxin effects [117]. To investigate if mutations on the plasmid contributed to the observed diminished toxicity profile,

plasmids from the surviving cells S002 and S2 (designated as plasmids p002 and p2) were extracted and purified. These purified plasmids were subsequently transformed into the "starting" *E. coli* MG1655 cells and viability was assessed over time with 0% or 2% arabinose (**Fig. 1A**). Surprisingly, the growth profiles of both S002 and S2 cells exhibited similar sensitivity to the re-induction of ParE protein expression (**Fig. 1G**) as the original ParE1-expressing cells (**Fig. 1B**), suggesting the plasmid was unlikely to contain mutations that would prevent ParE1 protein expression.

In parallel, S002 and S2 cells were cured of the plasmids via sequential plating without selection pressure. After confirming the plasmid removal through the absence of qPCR amplification and restored sensitivity to the selective antibiotic, these surviving cells were re-transformed with the original ParE1-expressing plasmid construct and viability was assessed over time with 0% or 2% arabinose (**Fig. 1A**). As shown in **Fig. 1H**, these cells did not regain the sensitivity to the induction of ParE1 protein expression, indicating the phenotype is associated with the *E. coli* culture rather than with the plasmid.

Attempts to directly sequence the plasmids p002 and p2 were not successful, likely due to a noted reduction in yields. Therefore, polymerase chain reaction (PCR) was used to amplify the full plasmid using the extracted samples as templates, and two different priming regions were used to ensure overlapping full coverage (**Table S2** and **Fig. S2**. pMind+araC_FWD with araC-pBAD_REV and araC-pBAD_FWD with pMind+araC_REV). Nanopore sequencing revealed no alterations in the base sequences as compared to the starting sample, further confirming that the lack of sensitivity to re-induction was not associated with plasmid defects.

These findings collectively indicated the observed difference in toxicity profiles between the surviving cells and their original counterparts is not attributed to mutations within the plasmids. Instead, other factors, possibly related to cellular adaptations or responses, including plasmid maintenance mechanisms, could be influencing the reduced impact of ParE1 protein expression on viability. This speculation shifts the focus from genetic changes in the plasmid to possibly

epigenetic or physiological changes within the cells that confer a survival advantage induced by the presence of the ParE1 toxin protein.

4.3. The Phenotypic Loss of Re-induction Sensitivity cannot be Complemented by Increasing Inducer Uptake

In the recombinant pMindBAD plasmid system, expression of the ParE1 protein is contingent on the presence of arabinose inducer. This system is sensitive to the intracellular levels of arabinose, which are regulated by specific transport proteins, primarily the AraE permease [118]. To evaluate the arabinose uptake and its subsequent effect on protein expression, a reporter pHerd20T plasmid encoding the fluorescent protein mCherry downstream of the same *ara*BAD promoter was introduced by transformation into the plasmid-cured surviving cells S002 and S2, as well as into the "starting" MG1655 *E. coli* cells. Induction of mCherry protein expression was achieved through the addition of 2% arabinose, followed by visualization using fluorescence via microscopy. As expected, the MG1655 cells that had not previously been subjected to ParE1 protein expression exhibited clear fluorescence within cells across the observed field and this was dependent on the inducer (**Fig. 2A**), indicating efficient mCherry expression. In contrast, the fluorescence was notably absent in the ParE1-expressing plasmid-cured S002 and S2 cells, even with the highest level (2%) of arabinose inducer (**Fig. 2A**), suggesting a marked reduction in mCherry expression within these cells.

To quantify this observation at the mRNA level, subsequent reverse transcription-quantitative polymerase chain reaction (RT-qPCR) assays were conducted to measure *araE* mRNA levels in cells. This unveiled a consistent pattern of upregulated *araE* transcription level following the addition of arabinose in both "starting" and surviving cells, with an approx. 80-fold increase in MG1655 cells, an approx. 28-fold increase in S002 cells and an approx. 11-fold increase in S2 cells (**Fig. 3.2B**). However, despite this consistent pattern of transcriptional upregulation, the *araE* mRNA levels were significantly lower in the surviving cells than in the "starting" cells both

before and after upregulation. To further investigate if these decreased transcription levels affect mCherry expression, a secondary pRK2 plasmid constitutively expressing AraE protein was co-transformed into these surviving cells. However, although the presence of the AraE-expressing plasmid significantly increased the transcription level of *araE*, the fluorescence was still absent in these surviving cells (**Fig. S3.4**). Despite this transcription increase, the absence of fluorescence in the surviving cells implies a discrepancy between *araE* mRNA levels and functional mCherry protein expression. When integrated with the observation of inefficient mCherry expression in these surviving cells, this insight underscores that arabinose transport remains partially functional despite the alterations introduced by ParE1 toxin expression.

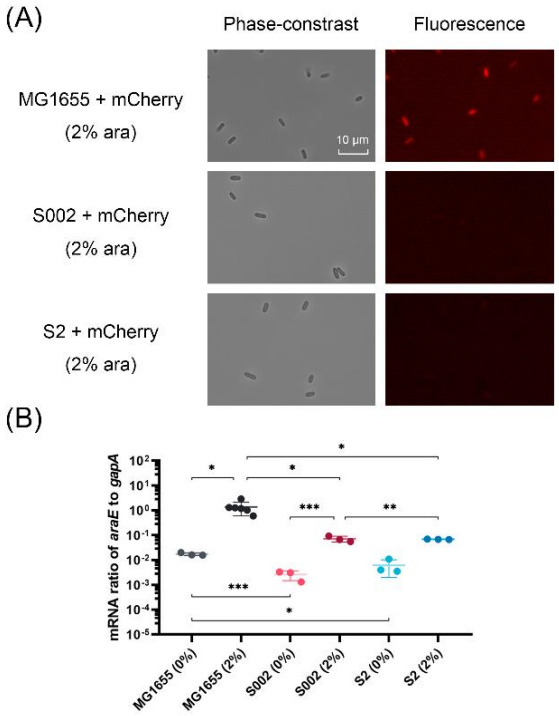

Figure 3.2. *araE* mRNA levels are sensitive to arabinose induction in ParE1-surviving cultures, despite the lack of fluorescent protein mCherry signal. (**A**) Fluorescence microscopy of the "starting" MG1655 as well as the S002 and S2 cells with ParE-expressing plasmid removed ("cured") induced for the expression of fluorescent protein mCherry from a

plasmid, pHerd20T, also under control of the arabinose inducible promoter. However, fluorescence of mCherry protein is only visualized in the "starting" MG1655 cells. ara: arabinose. (**B**) The mRNA ratio of the arabinose transporter *araE* to chromosomal *gapA* in these cells after incubation with 0% and 2% arabinose. Each measurement with standard deviation (SD) contains at least 3 technical replicates. Unpaired two-tailed Student's *t*-test was performed: *, $P < 0.05$; **, $P < 0.01$; ***, $P < 0.001$.

4.4. Cells Modulate Plasmid Copy Number to Survive ParE1 Protein Expression

Persistently low yields when extracting plasmids from these surviving cells suggested that the plasmid copy number (PCN) may have undergone alterations. To investigate this, the change of PCN in cells before and after ParE1 protein exposure was determined using quantitative polymerase chain reaction (qPCR) analysis. The ratio of plasmid to chromosome (P/C) was calculated using efficiencies of the individual primers and the threshold cycle (Ct) values arising from the *parE1* gene on plasmids and the chromosomal *gapA* gene. Two different primer sets, targeting the plasmid *ori* region or toxin gene (**Table S3.2**, **Fig. S3.2**. ori-qPCR and parE1-qPCR primer sets), were used. The data indicated a consistent result irrespective of which plasmid region was detected (**Fig. S3.5**). Strikingly, when compared to the pre-induction MG1655 cells, the surviving cells S002 and S2 exhibited an approx. 40-fold reduction in PCN, resulting in an average change from 697.4 ± 163.4 plasmid copies per chromosome pre-induction to 17.3 ± 9.4 plasmid copies per chromosome with re-induction insensitivity (**Fig. 3.3**). It suggests that the reduction in PCN can be a survival mechanism, potentially diminishing the ParE1 toxin's impact by reducing the number of toxin protein molecules produced per cell.

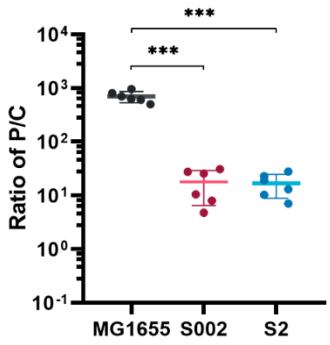

Figure 3.3. Cells modulate plasmid copy number (PCN) to survive ParE1 protein expression. The ratio of P/C was defined as the amplification signal ratio of plasmid to chromosome, as described in the methods. The surviving S002 and S2 cells exhibited a significantly reduced PCN, compared to the pre-induction MG1655 cells. Each measurement with SD represents 2 independent experiments, with each containing three technical replicates. Unpaired two-tailed Student's *t*-test was performed: ***, $P < 0.001$.

4.5. There is a Direct Correlation Between Reduced Plasmid Copy Number and Survival Phenotype

The survival phenotype was limited within the population of the "starting" cells, with only two out of the four tested colonies (*i.e.*, S002 and S2 cells) persisting during re-induction (**Fig. 3.1C-F**). To assess if this persisting fraction could be further enriched, following the initial 24-hr induction cultures of MG1655 *E. coli* cells expressing ParE1 toxin were subjected to successive passages in fresh medium while maintaining the arabinose inducer at the same concentration (**Fig. 3.4A**). Notably, in the three groups subjected to induction with arabinose, the cultures displayed progressively higher cell viability with each successive passage at all induction strengths (0.02% to 2%) (**Fig. 3.4B**). This suggests that the population of induction-surviving cells becomes more predominant over successive passages.

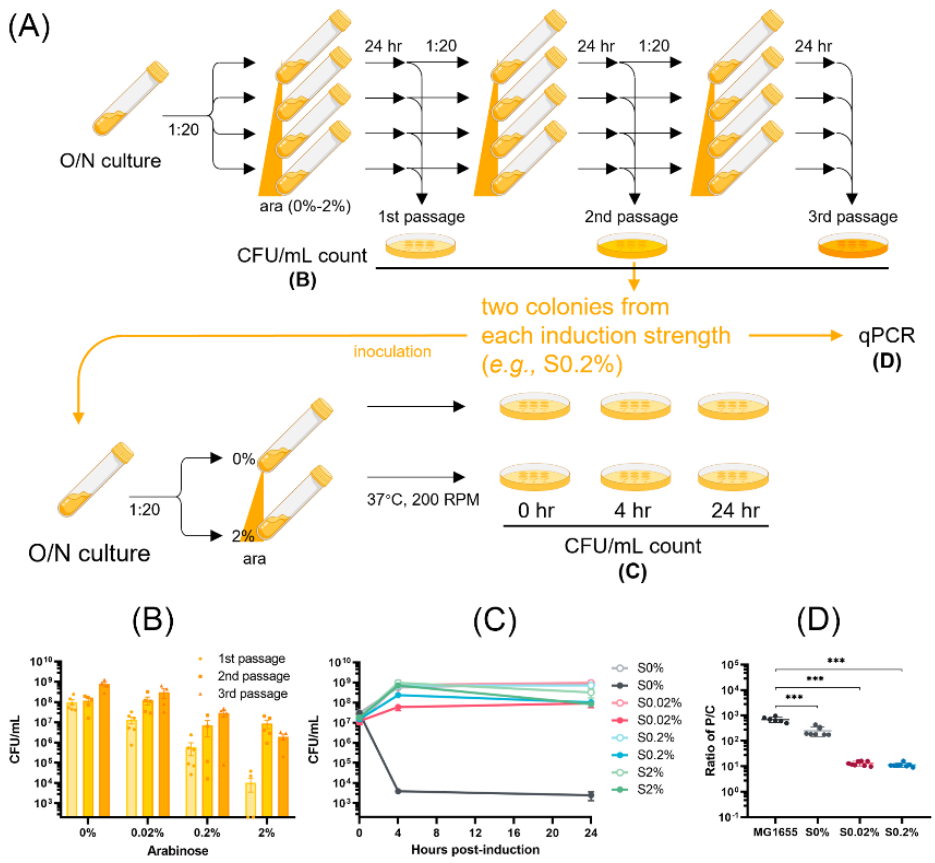

Figure 3.4. Assessment of *E. coli* MG1655 cell viability and plasmid copy numbers upon induction of ParE1 Toxin Expression. (**A**) Schematic presentation of the passage workflow. ara: arabinose. (**B**) Cultures of MG1655 cells harboring ParE1-expressing plasmids were passaged every 24 hr at the indicated induction levels, and all successive cultures had increased numbers of viable cells. (**C**) Cell viability was subsequently determined for two colonies isolated after 2 passages and re-induced with the addition of 0% (hollow circle) or 2% (solid circle) arabinose. All re-grown colonies apparently exhibited the same growth pattern at 0% reinduction, indicating there were no growth defects for those nonsensitive cells. Each data point represents the mean value of the two colonies, shown with SEM. (**D**) The PCNs of these surviving cells were determined by qPCR analysis. All cells that lost partial or complete sensitivity to reinduction exhibited a decreased PCN. Graph shows SD from 2 independent experiments performed in triplicates. Unpaired two-tailed Student's *t*-test was performed: ***, $P < 0.001$.

Following the second passage, two colonies from each induction strength were isolated and re-grown in the absence of the arabinose inducer. Cultures were diluted at 1:20 ratio and ParE1 toxin expression was subsequently re-induced with 2% arabinose. Strikingly, upon re-induction, the toxicity profiles of all re-grown colonies with previous ParE1 toxin exposure remained viable at all induction concentrations (0.02% to 2%) (**Fig. 3.4C**). In contrast, the colonies derived from cells with no prior ParE1 exposure remained as sensitive as the initial observation, with only a minor fraction surviving (**Fig. 3.4C**, colonies S0%).

Quantification of PCN for the cultures of these surviving colonies shows a consistent reduction for all surviving cells **(Fig. 3.4D)**, with a more pronounced reduction correlated with higher inducer concentration. For cells maintained at a 0.02% inducer concentration there was an approx. 53-fold reduction, resulting in an average from 697.4 ± 163.4 plasmid copies per chromosome for sensitive cells to 13.1 ± 2.7 plasmid copies per chromosome in insensitive cells. For cells maintained at 0.2% inducer concentration there was an approx. 50-fold reduction, resulting in an average 11.3 ± 2.1 plasmid copies per chromosome. However, for cells maintained at 2% inducer concentration the PCN was below the limit of quantification (a P/C ratio of 0.25, corresponding to one plasmid to four chromosomes) even under constant antibiotic selection pressure. These data collectively provide evidence that the strategy of survival through the reduction of PCN to mitigate toxin expression is a reproducible phenomenon directly correlated with the amount of ParE1 protein induction.

We questioned if toxicity was the driver for reduced PCN. Experiments were carried out using a control pMind plasmid without the insertion of the ParE1-encoding gene. When this “empty” plasmid was introduced into the “starting” MG1655 *E. coli* cells, no reduction in PCN was found upon arabinose induction (**Fig. S3.6A**). Considering the inconsistency between the promoters on this control plasmid and the pMindBAD plasmid, another control pHerd20T plasmid was introduced, which contains the same *ori* and *ara*BAD promoter, but with a non-toxic fluorescent protein mCherry gene. Consistently, no reduction in PCN was found **(Fig. S3.6B)**. This demonstrated that the decrease in PCN, and hence cell survival, was specifically driven by the

toxic expression of ParE1 protein and not merely by the presence of the plasmid or the induction process. Collectively, these results indicate that survival of ParE1 protein expressing cells is driven by reducing PCN, thereby limiting the available DNA template for transcription.

4.6. Reduced Plasmid Copy Number is a Generalized Phenotype for MG1655 *E. coli* Survival of ParE Protein Expression

To further explore whether this phenomenon is limited to only the specific ParE1 toxin protein, the ParE2 toxin protein from Mt was cloned into the same pMindBAD plasmid (**Fig. S3.3**). While these two toxin proteins belong to the same family, and both exert their impacts by inhibition of DNA gyrase, their protein sequence similarity is limited to 37% (**Fig. S3.7**). The viability of MG1655 cells expressing ParE2 protein was monitored following induction with arabinose, again documenting a toxicity profile that correlated to induction strength, and notably, displayed even greater potency than ParE1 protein. At 2% induction, the ParE2 protein expression induced a complete cell loss at 24-hr post-induction, while at 0% induction, presumably leaky expression of ParE2 protein resulted in a lower CFU when compared to ParE1 protein (**Fig. 3.5A**). As observed with ParE1 protein, cultures slowly recovered growth between the 4 hr and 24 hr timepoints.

Given the stronger toxicity of ParE2 protein, a lower concentration range of arabinose was employed for subsequent culture passages. As shown in **Fig. 3.5B**, the culture CFU counts have a pattern similar to that observed with ParE1 protein, albeit at lower induction strengths. However, the population of cells exposed to the highest induction (0.02%) did not exhibit a progressive enrichment, and instead essentially the same number of the CFU counts was obtained for each passage. This could potentially be attributed to the heightened toxicity of ParE2 relative to ParE1 at the 0.02% induction strength. As before, following the second passage two colonies from each induction strength were selected and re-grown, and ParE2 protein expression was reinduced with 0% or 2% arabinose (**Fig. 3.5A**). Strikingly, upon re-induction there were varied toxicity

profiles: one cell from the 0.02% induction group (S0.02% (#1)) had the survivor phenotype, colonies derived from the 0% induction group retained sensitivity to ParE2 expression induction, and all other cultures had an intermediate phenotype with partial survival (**Fig. 3.5C**).

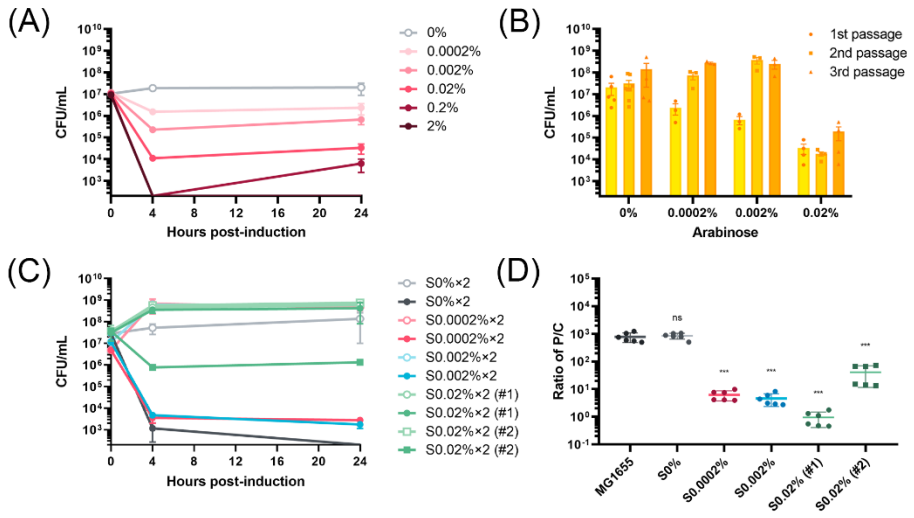

Figure 3.5. Assessment of *E. coli* MG1655 cell viability and plasmid copy numbers upon induction of ParE2 Protein Expression. (**A**) The induction of ParE2 protein expression in *E. coli* MG1655 cells exhibited an induction-strength-dependent pattern, with 2% induction leading to a cell count below the detection limit (200 CFU/mL). (**B**) Cultures of MG1655 cells harboring ParE2-expressing plasmids were passaged every 24 hr at the indicated induction levels, and all successive cultures had increased numbers of viable cells. (**C**) Cell viability was subsequently determined for two colonies isolated after 2 passages and re-induced with the addition of 0% (hollow circle) or 2% (solid circle) arabinose. All re-grown colonies apparently exhibited the same growth pattern at 0% reinduction, indicating there were no growth defects for those nonsensitive cells. Each data point represents the mean value of the two colonies, shown with SEM. (**D**) The PCNs of these surviving cells were determined by qPCR analysis. All cells that lost partial or complete sensitivity to reinduction exhibited a decreased PCN. Graph shows SD from 2 independent experiments performed in triplicates. The ratios of P/C of surviving cells were compared to that of the pre-induction MG1655 cells and unpaired two-tailed Student's *t*-

test was performed: ns, non-significant, ***, $P < 0.001$.

Subsequent quantification of PCN showed a substantial reduction for all cultures exhibiting decreased sensitivity to ParE2 protein re-induction (**Fig. 3.5D**). Specifically, in the 0.0002% and 0.002% induction groups, the average reduction in PCN exceeded 125-fold, resulting in an average from 779.0 ± 300.0 for sensitive cells to 5.4 ± 2.3 plasmid copies per chromosome for insensitive cells. In the 0.02% induction group, one culture (S0.02% (#1)) with the survivor phenotype upon ParE2 protein re-induction exhibited an average 824-fold reduction in PCN (to 0.9 ± 0.5 plasmid copies per chromosome), while the other culture (S0.02% (#2)) that retained some sensitivity to ParE2 protein re-induction had an intermediate but significant 19-fold reduction in PCN (to 41.0 ± 29.5 plasmid copies per chromosome). Consistently, colonies derived from the 0% induction group, which retained sensitivity to ParE2 protein re-induction, exhibited no essential change in PCN.

4.7. Reduced Plasmid Copy Number is a Generalized Phenotype for *E. coli* Survival of ParE Toxin Expression

We questioned if the reduction in PCN in response to ParE toxin expression was somehow limited to the MG1655 strain. To evaluate this, *E. coli* TOP10 cells were transformed with the pMindBAD plasmid encoding the ParE1 protein, allowing assessment of the viability and induction response in a different strain. We specifically selected the TOP10 strain, which lacks a functional *ara*BAD operon, including the *araB*, *araA*, and *araD* genes responsible for converting arabinose into metabolites that can be used by the cell [119]. The selection of this strain allows a stable induction strength over the time course of the experiment. Induction of ParE1 protein in TOP10 *E. coli* cells demonstrated a direct correlation between the induction strength and the toxicity of ParE1 toxin **(Fig. 6A)**. The trend is similar to that seen with the MG1655 strain (**Fig. 1B**), although this strain was much more sensitive to inducer and necessitated lowering the

arabinose concentrations in subsequent experiments.

When the TOP10 strain cultures were subjected to the serial passage assay, they exhibited a pattern similar to that observed with ParE2 protein but not ParE1 protein in MG1655 cells: cultures exhibited a greater increase in CFU counts at low (0.00002%) and medium (0.0002%) induction strengths compared to high (0.002%) induction strengths **(Fig. 3.6B)**. When colonies from each induction strength were isolated and re-grown, followed by re-induction of the ParE1 protein expression, all cells showed a decrease in CFU counts at the 4 hr timepoint, followed by a robust recovery in growth, while cells from 0.02%-induction group exhibited a complete cell loss within 24 hr **(Fig. 3.6C)**. Consistent with the MG1655 strain, only cultures with the ability to recover CFUs exhibited a reduction in PCN, with an average reduction exceeding 56-fold, resulting in an average plasmid copies per chromone change from 416.1 ± 53.2 to 7.4 ± 2.3 **(Fig. 3.6D)**. This indicates that the reduction in PCN is independent of strain and instead arises from toxicity, or potentially from the specific mechanism of the toxins, rather than the specific cellular context.

Collectively, when considering both ParE toxin types and the two *E. coli* strains, a noteworthy trend emerges: out of the total 24 tested colonies, 20 colonies exhibited either partial or complete reduction in both toxicity profile and PCN, while in comparison 4 colonies had no significant change in either toxicity profile or PCN. Continual exposure to the expressed toxin could enrich the population, with increased numbers of surviving cells in subsequent passages. ParE2 toxin protein exhibits a stronger toxicity profile than ParE1 toxin protein, hence cells need to maintain a lower expression level of ParE2 to avoid being killed. These findings underscore the consistency of the observed phenomenon across different conditions and reinforce the notion that survival by reducing PCN as a response to toxic protein expression is a reproducible and potentially adaptive cellular strategy.

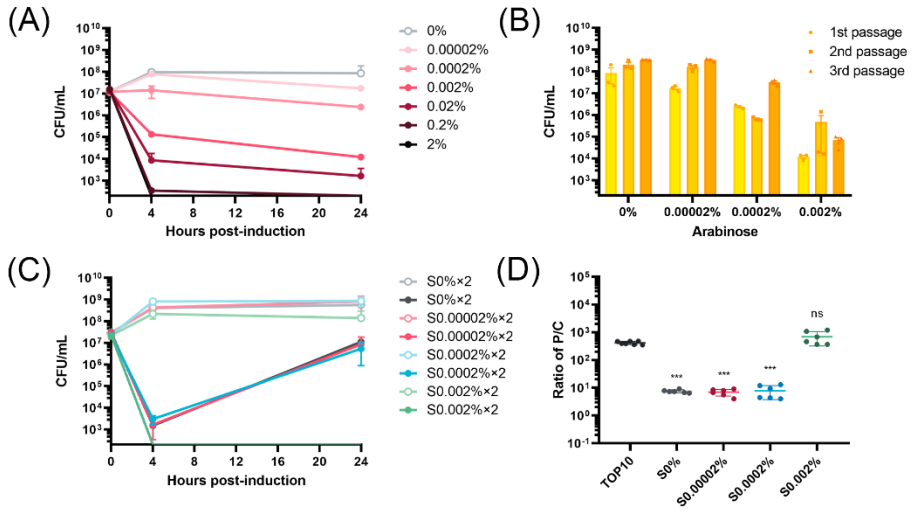

Figure 3.6. Assessment of *E. coli* TOP10 cell viability and plasmid copy numbers upon induction of ParE1 Protein Expression. (**A**) The induction of ParE1 protein expression in *E. coli* TOP10 cells exhibited an induction-strength-dependent pattern. (**B**) Cultures of TOP10 cells harboring ParE1-expressing plasmids were passaged every 24 hr at the indicated induction levels, and all successive cultures had increased numbers of viable cells. (**C**) Cell viability was subsequently determined for two colonies isolated after 2 passages and re-induced with the addition of 0% (hollow circle) or 2% (solid circle) arabinose. All re-grown colonies apparently exhibited the same growth pattern at 0% reinduction, indicating there were no growth defects for those nonsensitive cells. Each data point represents the mean value of the two colonies, shown with SEM. (**D**) The PCNs of these surviving cells were determined by qPCR analysis. All cells that lost partial or complete sensitivity to reinduction exhibited a decreased PCN. Graph shows SD from 2 independent experiments performed in triplicates. The ratios of P/C of surviving cells were compared to that of the pre-induction MG1655 cells and unpaired two-tailed Student's *t*-test was performed: ns, non-significant, ***, $P < 0.001$.

5. Discussion

In this study, we observed a distinct phenotype characterized by a reduction in plasmid copy number (PCN) following arabinose-induced-expression of ParE proteins imparting levels of toxicity to *Escherichia coli* cells starting from lag phase. This led to a robust (typically 4 logs) but not complete decrease in cell viability, followed by a consistent recovery of culture growth (**Fig. 1B**, **5A** and **6A**). Furthermore, within the population of surviving cells, a subset exhibited a loss of apparent toxicity upon re-induction (**Fig. 4C**, **5C** and **6C**). These findings collectively suggest that, while the initial induction of the ParE toxin expression leads to a reduction in cell viability, a portion of the bacterial population adapts to the toxic conditions and ultimately regains growth. Importantly, our examination of the plasmids carried by these insensitive cells revealed a consistent and stably reduced PCN (**Fig. 4D**, **5D** and **6D**). This indicates that the reduction in PCN might serve as a reproducible mechanism enabling cells to mitigate the toxic effects of ParE toxin expression (**Fig. 7**).

Plasmid stability, which refers to the ability of a plasmid to persist within a population of host cells, has crucial impacts on the expression of genes encoded in the plasmid. PCN is influenced by various factors, such as origin of replication proteins, plasmid topology, segregation machinery and selection pressure [120]. Dumon-Seignovert et al. observed that the overexpression of several heterologous proteins in *E. coli* cells becomes toxic and diminishes plasmid stability, as assessed by the percentage of colonies that could survive on both non-selection and selection agar plates in their study [121]. In our investigation, we provide evidence that the toxic expression of ParE toxins leads to a reduction in PCN, directly impacting the accessible gene dosage for toxin expression. These findings raise important questions about potential confounding variables in studies that rely on the ectopic expression of genes to explore their physiological effects. Based on the current study, this phenotypic adaptation arises within 4-8 hr of induction. In the current study this effect correlates directly with the extent of toxicity, such that more toxic expression results in quicker adaptation. The observed reduction in PCN suggests that gene expression studies conducted in plasmid-based systems may not accurately reflect the

physiological responses of cells, particularly when dealing with toxic proteins.

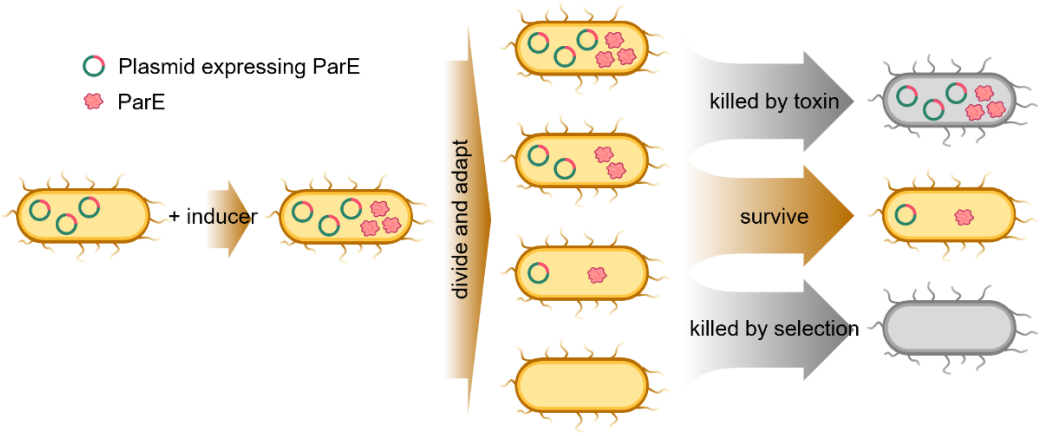

Figure 3.7. Plasmid copy number (PCN) reduction as a survival mechanism against ParE toxin proteins expressed in *E. coli*. In our study, the stationary cultures of *E. coli* cells harboring ParE-expressing plasmids were diluted in fresh media and added with arabinose for induction of ParE toxin expression. Antibiotics were always added in the media to select plasmid-harboring cells. When the plasmids were present in cells at high copy numbers, the cells were susceptible to the lethal dose of ParE toxin. When the plasmid copy number was reduced, the cells had a chance to survive exposure to a sub-lethal dose of ParE toxin. However, if the PCN was reduced beyond some threshold level, antibiotic selection would reduce cell survival due to the reduced expression of the encoded antibiotic resistant gene.

Plasmids used in this study are ColE1-like plasmids featuring a pUC origin, the replication and maintenance of which rely on the dynamic balance between two small RNAs, RNA I and RNA II. Our findings indicated a notable decrease in the transcription level of RNA II within these insensitive cells with reduced PCN (**Fig. S8**). Notably, the transcription level of RNA I was undetectable under these conditions. This observation suggests that the decrease in PCN might be accompanied by a proportional reduction in RNA I's absolute transcript level, potentially

leading to its undetectability. Further investigations into the expression of RNA I in these insensitive cells to reveal the balance change between these two RNAs would provide insight into the molecular regulation of the plasmid.

On the other hand, our analysis, comparing the complete genomes of *E. coli* cell samples S002 and S2 (**Fig. 1**) with the *E. coli* K-12 MG1655 reference sequences (sourced from GenBank accessions U00096.1, U00096.2, U00096.3, and ATCC references 70926 and 47076), revealed seven variants in the reference genomes and our samples as detailed in **Table S3**. Among these variants, only the N845S substitution in the DNA polymerase I (Pol I) appeared exclusively in our samples. This mutation may be causally linked to the observed phenotype of reduced PCN. Research has highlighted the crucial role that DNA polymerase I plays in the replication of ColE1-like plasmids within *E. coli*. It has been observed that mutants deficient in DNA polymerase I activity are incapable of sustaining the ColE1 plasmid [122,123]. Further, the N845 residue has been reported to be involved in the recognition of correct terminal base pairs in the DNA substrate [124] and in the incorporation of ribonucleotides [125], and contribute to the polymerase fidelity [126] and catalytic activity [127]. The surviving S002 and S2 cells both demonstrated the same mutation in DNA polymerase I, a change we hypothesize arose as an adaptive response to evade the effects of ParE toxin expression. This mutation likely resulted from the toxin's gyrase inhibition, representing a random yet prevalent adaptation selected in our study to mitigate toxicity while promoting survival. To explore this hypothesis further, investigation into the N845S mutation's impact on DNA replication and expression of other gyrase-inhibiting agents would offer deeper insights into the mechanisms driving the observed reduction in PCN.

In conclusion, our studies highlight a potential technical limitation to studies of toxic proteins in engineered inducible systems, as well as the phenotypic balance between two opposing effects of the ParE toxin. The ability of some cells to recover or become insensitive to toxin expression when exposed to arabinose again raises intriguing questions about the underlying mechanisms of this phenomenon. It also underscores the complexity of bacterial responses to toxic proteins and

the role of plasmid copy number in mediating these responses. Further investigation is needed to elucidate the precise mechanisms involved in PCN determination and to apply these findings in various biotechnological and medical contexts.

Author Contributions

S.R. collected all data reported in this chapter; S.R. and C.R.B. participated in the project design, data analysis, manuscript drafting, and editing.

Data Availability

All data are included in this manuscript and Appendix B; DNA clones for constructs made in this work are available upon request. Information for the proteins used in this work is available online (MtParE1, UniProtKB P9WHG7; MtParE2, UniProtKB P9WHG5).

Acknowledgements

The author would like to thank Bourne lab members for their suggestions and assistance with various experiments. Research reported in this chapter was supported by the Department of Defense under Grant No. W81XWH-20-1-0121. The content is solely the responsibility of the authors and does not necessarily represent the official views of the Department of Defense. Financial support for publication was provided by the University of Oklahoma Libraries' Open Access Fund.

Chapter IV: Quantification of PaParE1 Protein Molecules in Bacterial Cell Lysate using Bio-Layer Interferometry

Shengfeng Ruan, Christina R. Bourne

Department of Chemistry and Biochemistry, University of Oklahoma, Norman OK USA

This chapter reports currently unpublished research conducted in the Bourne lab, located within the Department of Chemistry and Biochemistry at the University of Oklahoma.

I collected and processed all the data for the manuscript. All figures were produced by me. Writing of the manuscript was performed by me with assistance from Dr. Christina Bourne. Editing and feedback on all writing was provided by Dr. Christina Bourne.

1. Abstract

Members of the ParE toxin protein subfamily, despite their conserved three-dimensional structures, demonstrate differential toxic effects on cells. These differences in toxicity may be attributed to variations in their sequences and expression levels. When quantifying toxin proteins, traditional methods such as Western blot and mass spectrometry are effective for less potent toxins but do not reliably detect highly potent, and therefore low abundance toxins. To address this issue, this chapter proposed and validated the feasibility of using bio-layer interferometry (BLI)-based methods to quantify toxin proteins in cell lysate, specifically using an attenuated PaParE1 toxin for this proof-of-concept study. The work also included determining the optimal cell lysate as a percentage of the test solution, and optimizing the loading step to enhance signal clarity relative to high background signals. Furthermore, the performance and efficacy of two different biosensors were compared. The antibody-based biosensor exhibited more precise quantification across a range of toxin concentrations, whereas the nickel-ion-based

biosensor was more susceptible to non-specific binding but capable of larger signals. This validation of the BLI-based method highlights its potential to quantify bacterial proteins in cell lysate, providing the possibility for the quantification of potent toxins that is important for enhancing our understanding of the dynamics of bacterial TA systems.

2. Introduction

The bacterial ParDE toxin-antitoxin (TA) system harbors non-secreted ParE toxin proteins that interfere with DNA gyrase activity, which is crucial for DNA replication and transcription [26,32] Despite their conserved three-dimensional structure, the ParE toxin subfamily members exhibited differential toxicity levels (as shown in chapter II and previous work [23]). This differential toxicity may stem from the variation in the protein sequence and expression levels. A comparison of nine different ParE toxins from various species revealed a low sequence identity (approximately 12%), with similarity ranging from 30% to 80% [23], suggesting conserved residues may contribute to the toxicity. However, the detailed molecular mechanism of ParE toxin binding to gyrase remains unclear due to the unresolved structure of the ParE-gyrase complex, making it hard to identify the region involved in the binding with DNA gyrase. On the other hand, protein expression levels are influenced by factors such as plasmid copy number, promoter strength, host strain selection, and induction conditions [128,129]. These variations present a challenge in directly comparing the toxicity of each ParE toxin using conventional methods like cell count reduction.

Traditional protein quantification methods, such as Western blot and mass spectrometry, have provided valuable tools for researchers when working with less potent toxins. However, the high toxicity of some ParE variants severely limits their abundance in the population by reducing the number of cells, resulting in unsuccessful quantification attempts through Western blotting [23]. Similarly, mass spectrometry has challenges to quantify individual proteins within a complex due to insufficient detection sensitivity for these low-abundance proteins. This challenge highlights

the need to develop a reliable quantitative method that can accurately measure the concentration of toxic, low-abundant ParE toxins in cell lysates, overcoming its deleterious effects on cell viability and limitations imposed by traditional detection techniques.

Bio-layer interferometry (BLI) is a promising technology in this context, offering a label-free, real-time method for protein quantification. BLI overcomes many of the limitations associated with traditional quantification methods by directly measuring the interaction between the immobilized molecules and the molecules of interest without the need for secondary detection strategies. By measuring the binding mass of molecules to a biosensor surface, BLI provides a sensitive and direct measurement. This technique is particularly well-suited to quantifying proteins with variable expression levels or those that are difficult to detect due to their toxic nature, such as the ParE toxin subfamily, providing insights into their molecular concentrations that were previously unattainable with conventional methods.

This study validates the application of BLI-based method to quantify toxin molecules within cell lysates using an attenuated PaParE1 toxin variant, illustrating the potential of this method to address the challenges associated with toxic protein quantification. Through the comparison of different biosensor types pre-immobilized with specific bio-recognition elements, such as antibodies or nickel-charged groups, this research also highlights the importance of selecting the appropriate biosensor based on sample complexity to circumvent the limitation of non-specific binding (NSB). The application of the BLI-based method in this study offers a precise and sensitive approach for quantifying toxin protein concentrations within cell lysates. By overcoming the challenges presented by traditional techniques, the BLI-based method can facilitate a deeper understanding of the biological roles and dynamics of toxin proteins from TA systems. The adaptability and accuracy of this methodology sets the stage for further research into microbial physiology and pathogenic mechanisms, offering potential insights that could inform the development of new therapeutic strategies and biotechnological applications.

3. Experimental Details

3.1. Expression and Purification of the *P. aeruginosa* ParE1 toxin protein

To construct a standard response line for BLI binding signal per known amount of protein, the attenuated ParE1 toxin from *Pseudomonas aeruginosa* was purified. *Escherichia coli* BL21(DE3) cells harboring either the *paparE1*-encoding pET-15b plasmid were obtained from the laboratory inventory, and have been previously described [17]. In brief, the *paparE1* gene was cloned into the pET-15b plasmid in frame with an N-terminal hexa histidine-tag (6× his-tag) and thrombin cleavage site. A 1-L culture was inoculated at a 1:20 ratio with an overnight Luria-Bertani (LB) broth culture started from -80°C frozen glycerol stocks and incubated at 37°C, 200 RPM, until it reached an optical density (OD) unit of 0.6-0.8. Then the expression of PaParE1 protein was induced at 18°C, 125 RPM, with the addition of 1 mM isopropyl β-d-1-thiogalactopyranoside (IPTG), and was harvested after an overnight (~16 hours) incubation.

The purification of the 6× His-tagged PaParE1 protein was conducted as previously described [45]. In summary, cell pellets were harvested through centrifugation and then resuspended in 5-mL lysis buffer per gram of cell pellet. This lysis buffer solution was composed of 20 mM Hepes-HCl (pH 7.5 at room temperature), 150 mM NaCl, 5% glycerol and 40 mM imidazole. The cells were then lysed using a high-pressure homogenizer (Emulsiflex), and the lysate was clarified by further centrifugation. The clear supernatant was collected and passed through a 1-mL HisTrap FF Ni-NTA column (GE Healthcare) and eluted using a buffer consisting of 20 mM Hepes-HCl (pH 7.5 at room temperature), 150 mM NaCl, 5% glycerol and 500 mM imidazole, in an order of 10% (10 column volume (CV)), 15% (10 CV), and 15% to 100% (10 CV). Finally, the eluted protein was subjected to desalting in a buffer consisting of 20 mM Hepes-HCl (pH 7.5 at room temperature), 150 mM NaCl and 5% glycerol, using a HiPrep 26/10 desalting column (GE Healthcare).

3.2. Bio-Layer Interferometry Assay

E. coli BL21(DE3) cells carrying the pET-15b empty vector (EV) were induced with IPTG following the same protocol above. The harvested cell pellets were resuspended in a lysis buffer without imidazole, consisting of 20 mM Hepes-HCl (pH 7.5 at room temperature), 150 mM NaCl and 5% glycerol, at a ratio of 5 mL buffer per gram of cell pellet. The cells were lysed using a high-pressure homogenizer (Emulsiflex) and the lysate was then clarified through centrifugation. The clear supernatant was collected as an EV lysate to spike in the BLI running buffer of purified protein for subsequent bio-layer interferometry (BLI) assays.

Prior to BLI assays, samples were diluted to specified concentration in the BLI running buffer containing 20 mM Hepes-HCl (pH 7.5 at room temperature), 150 mM NaCl, 5% glycerol, 0.5% BSA and 0.05% Tween-20. All solutions were matched to this buffer condition. BLI assays were performed at 25°C, 1000 RPM, using a 96-well plate with each well containing a 200-µL volume. An Octet RED96 interferometer (Pall ForteBio) was employed for these assays, using either Anti-Penta-His (HIS1K) or Ni-NTA biosensor tips for detection. The purified 6× His-tagged PaParE1 protein was serially diluted in the running buffer with or without EV lysate spiked in, with concentrations ranging from 600 to 0.78125 µg/mL.

The detection protocol for the PaParE1 protein was as follows: an initial baseline measurement in pure running buffer for 120 seconds, followed by three consecutive loading steps of 500-second in specified samples, and a final 500-second washing step in pure running buffer. After the baseline measurement, binding signals were normalized to zero, ensuring all further collected response data were calibrated accordingly. The regeneration of the biosensor tips was conducted in accordance with the manufacturer's instructions. A 10 mM glycine solution at pH 1.7 was used for the regeneration process of HIS1K and Ni-NTA biosensor tips, while a 10 mM $NiCl_2$ solution was used for recharging the nickel ions on the Ni-NTA biosensor tips.

4. Results

4.1. Assay Development

The polyhistidine-tag (His-tag) is a widely used peptide tag for recombinant proteins and many tools have been developed to facilitate their detection and purification, such as the Octet® HIS1K and Ni-NTA biosensor tips. These biosensor tips' surfaces are pre-immobilized with either the monoclonal Penta-His antibody or nickel-charged tris-nitrilotriacetic (Tris-NTA) groups, providing a rapid and label-free approach for the analysis of His-tagged proteins. The working process of the BLI assay is presented in **Fig. 4.1**. When the biosensor tip was dipped into a sample, the binding signal represented the sum of His-tagged protein molecules and any non-specific binding (NSB) molecules. To isolate the specific binding signal for the 6× His-tagged PaParE1 protein from the total binding signal, the signal from the negative control (buffer matched but lacking PaParE1 protein) was aligned with and deducted from the PaParE1 sample signal following the baseline step. The minimum binding signals, measured at the end of the washing step, represented the total amount of PaParE1 molecules that had bound to the biosensor tips at different steps, respectively. For typical BLI experiments, significant disassociation after loading is not expected; however, we routinely found this to be the case with tips manufactured in the previous few years for unknown reasons. To provide another reference, the minimum binding signals, measured at the end of the washing phase, were also collected.

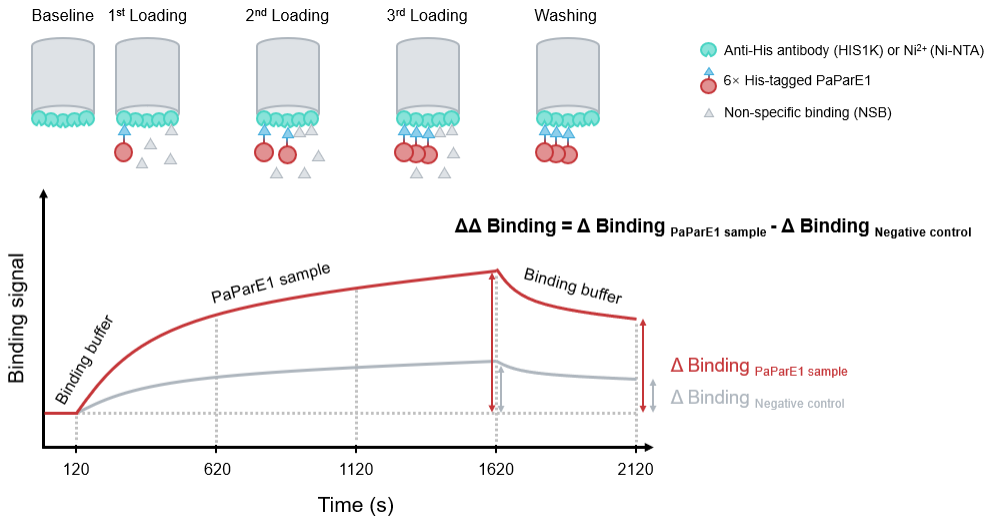

Figure 4.1. Schematic illustration of the BLI-based detection process for 6× His-tagged PaParE1 protein in running buffer with or without cell lysate. The specific binding signal (ΔΔ binding) for PaParE1 protein was isolated by deducting the binding signal of negative control (*i.e.*, NSB) from the binding signal of PaParE1 sample. PaParE1 sample: purified PaParE1 protein was spiked in the running buffer in specified concentrations with or without EV lysate spiked in. Negative control: pure running buffer with or without EV lysate spiked in.

4.2. Assay Optimization

The application of BLI-based method for the quantification of biomarkers, virus vaccines, and antibodies, has been recently reported in samples with uncomplicated compositions, such as vaccines and tears [130–134]. This study, however, aims to extend the BLI-based method to the quantification of PaParE1 toxin proteins within bacterial cell crude lysate. Compared to vaccines and tears, *E. coli* cell lysate contains over thousands of heterogeneous proteins, which compete with PaParE1 proteins and non-specifically bind to the biosensor. These NSB events result in more complex matrices that could potentially affect assay performance. Following the manufacturer's recommendation, dilution of lysate sample by more than tenfold may be an effective strategy for mitigating matrix effects. To assess whether dilution of lysate was needed, a

5% EV lysate was first spiked in the running buffer containing 100 µg/mL of purified PaParE1 protein and compared to an identical solution without EV lysate. As shown in **Fig. 4.3A**, the 5% cell lysate in the running buffer had a noticeable impact on the specific binding signals when compared to assays performed without lysate. There was a significant reduction—more than 50%—in the specific binding signals using HIS1K biosensor. This pronounced decline in signal strength underscores the influence of NSB from the cell lysate, which competes with the specific binding of PaParE1 protein to the binding sites on the biosensor surface.

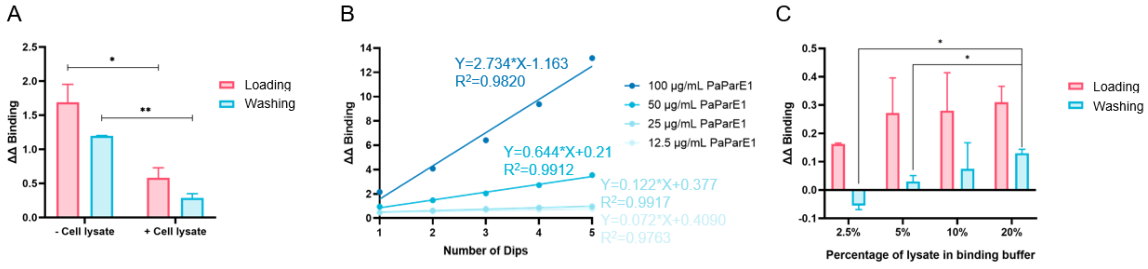

Figure 4.2. Impacts of the number of dips and lysate percentage in the running buffer on signal clarity. (**A**) The purified PaParE1 protein was diluted to 100 µg/mL in the running buffer with or without 5% EV lysate spiked in. The graph shows the specific binding signals of PaParE1 protein from the loading and washing steps in the absence or presence of cell lysate in the running buffer, using HIS1K biosensor tip. Each data point with the standard deviation (SD) represented two independent experiments. (**B**) A series of dilutions of purified PaParE1 protein, ranging from 100 to 12.5 µg/mL, was prepared in the running buffer containing a constant 5% EV lysate. Identical solutions without the purified PaParE1 protein served as negative controls. The graph shows the specific binding signal of PaParE1 protein from the washing step against the dip replicates, using Ni-NTA biosensor tips. Each data point represented one experiment. (**C**) The purified PaParE1 protein was initially diluted to 50 µg/mL in the running buffer containing 20% EV lysate. Further dilutions were made in the running buffer devoid of EV lysate to adjust the PaParE1 concentration from 50 µg/mL to 6.125 µg/mL, simultaneously reducing the lysate percentage from 20% to 2.5%. Identical solutions without the purified PaParE1 protein served as

negative controls. The graph shows the specific binding signals of PaParE1 protein from the loading and washing steps against the percentage of lysate in the running buffer, using HIS1K biosensor tips. Each data point with SD represented two independent experiments. Two-tailed unpaired Student's *t*-test was performed: *, $P < 0.05$; **, $P < 0.01$.

Considering the toxic nature of ParE toxins to cells that limits their growth, which may limit the abundance of ParE toxin molecules in the cell lysate, it is hypothesized that the amount of ParE molecules bound to the biosensor surface could be enriched by dipping the tips into multiple sample solutions successively. This approach assumes that each dip allows more ParE molecules to bind to the biosensor surface, thereby incrementally increasing the binding signal in proportion to the number of dips.

To test this hypothesis, the purified 6× His-tagged PaParE1 protein was diluted in the running buffer containing a constant 5% EV lysate, ranging from 100 to 12.5 μg/mL. As shown in **Fig. 4.2B**, the binding signals for PaParE1 protein showed robust linear relationships with the number of dips at all tested concentrations. For the 100 μg/mL PaParE1 concentration, the binding signal increased sharply with the number of dips, as indicated by the steep slope (the slope is 2.734), while the 12.5 μg/mL concentration showed the least increase in binding signal per dip (the slope is 0.072). These data suggested that increasing the numbers of dips enhances the binding signal for all concentrations. Combined with the consistently high R square values across all concentrations, these results supported the hypothesis that dipping the biosensor tips multiple times can enrich the PaParE1 molecules on the biosensor surface, with the effect being concentration dependent. It is noteworthy that dipping four times at a 50 μg/mL concentration failed to produce the binding signal observed with two dips at a concentration of 100 μg/mL, which may be ascribed to the presence of NSB. At higher concentrations, the binding signal likely predominantly arise from specific interactions, as there's a higher chance of the PaParE1 molecules encountering the biosensor surface. However, at lower concentrations, NSB could

constitute a more significant portion of the overall signal when multiple dips were performed, given the reduced availability of target molecules for binding.

Apart from the approach of multiple dips, increasing the percentage of the cell lysate in the running buffer could potentially enrich the amount of ParE molecules bound to the biosensor surface. Nevertheless, a higher lysate percentage may introduce more opportunities for NSB by other molecules in the mixture, which could cloud the specific PaParE1 interaction signal. While such an increase can potentially enrich the detection of PaParE1 molecules, identifying the optimal lysate percentage in the running buffer was essential to balance the trade-off between maximizing specific binding signals and minimizing NSB. To find this balance, the purified PaParE1 protein was spiked in a running buffer at 50 μg/mL and containing 20% EV lysate. This solution was further diluted in the lysate-free running buffer to concurrently reduce PaParE1 and NSB molecules. As shown in **Fig. 4.2C**, as the percentage of lysate in the running buffer was increased from 2.5% to 20%, there is an overall upward trend in the binding signals of PaParE1 protein for both loading and washing steps. Notably, for the loading step, the binding signal of PaParE1 protein started to plateau beyond a 5% lysate percentage. This plateau suggested that when the lysate percentage exceeds 5%, NSB may become more pronounced. However, following the application of a washing step to remove NSB, the binding signals of PaParE1 protein were more distinct, peaking at a lysate percentage of 20%. This indicates that while NSB can mask the true binding signal at higher lysate percentages, proper washing protocols can help in retrieving a clearer and more accurate signal attributable to specific binding events. For the following BLI assays, a 20% lysate percentage was used in the running buffer to ensure the maximum binding signal for PaParE1 protein.

4.3. Standard Curve Generation

The measurable PaParE1 protein concentration range with the optimized settings was first determined. Seven concentrations (600, 400, 200, 50, 12.5, 3.125 and 0.78125 μg/mL) of the

purified PaParE1 protein were spiked in the running buffer, respectively, which is within the dynamic range of binding according to the manufacturer. A running buffer without the spiked lysate was used as a negative control to measure NSB from buffer background. The blank running buffer exhibited a minimal background signal with both HIS1K and Ni-NTA biosensor tips (**Fig. S4.2**), indicating a minimal NSB background from the running buffer matrix.

When PaParE1 protein was spiked in the running buffer, the specific binding signals showed linear correlations with the concentrations of PaParE1 protein in two defined ranges (for concentrations lower than 12.5 μg/mL and for those higher than 12.5 μg/mL) for both the loading and washing steps when using HIS1K (**Fig. 4.3A**) and Ni-NTA (**Fig. 4.3B**) biosensor tips. These linear relationships within the designated ranges confirm the effectiveness of the biosensor tips for detecting and quantitating specific interactions with the PaParE1 protein in a minimal NSB background.

To assess the specificity and quantitation capability of the biosensor tips in the presence of background noise from NSB due to cell lysate, the assay was conducted with the purified PaParE1 protein spiked into a running buffer that contained 20% EV lysate. A running buffer containing 20% EV lysate, but without the PaParE1 protein spike, served as a negative control to measure NSB. Under these conditions, HIS1K biosensor tips produced specific binding signals that displayed a similar pattern to that observed in **Fig. 4.3A**, where linear relationships with the protein concentrations were observed in two ranges (**Fig. 4.4A**). In contrast, Ni-NTA biosensor tips exhibited a different response in the presence of cell lysate. It was observed that the specific binding signal for PaParE1 protein concentrations below 12.5 μg/mL was indistinguishable from the background signal (data not shown). Despite this, a linear relationship between the PaParE1 concentration and the binding signals was still evident at concentrations higher than 12.5 μg/mL for loading step or 50 μg/mL for washing step (**Fig. 4.4B**).

Overall, these comparisons demonstrated the differing sensitivities of HIS1K and Ni-NTA biosensor tips to NSB when quantifying low concentrations of PaParE1 protein in a complex

lysate environment. While HIS1K tips appear to have a robust quantification ability regardless of the NSB, Ni-NTA tips may require higher protein concentrations to overcome NSB and accurately quantify the PaParE1 protein.

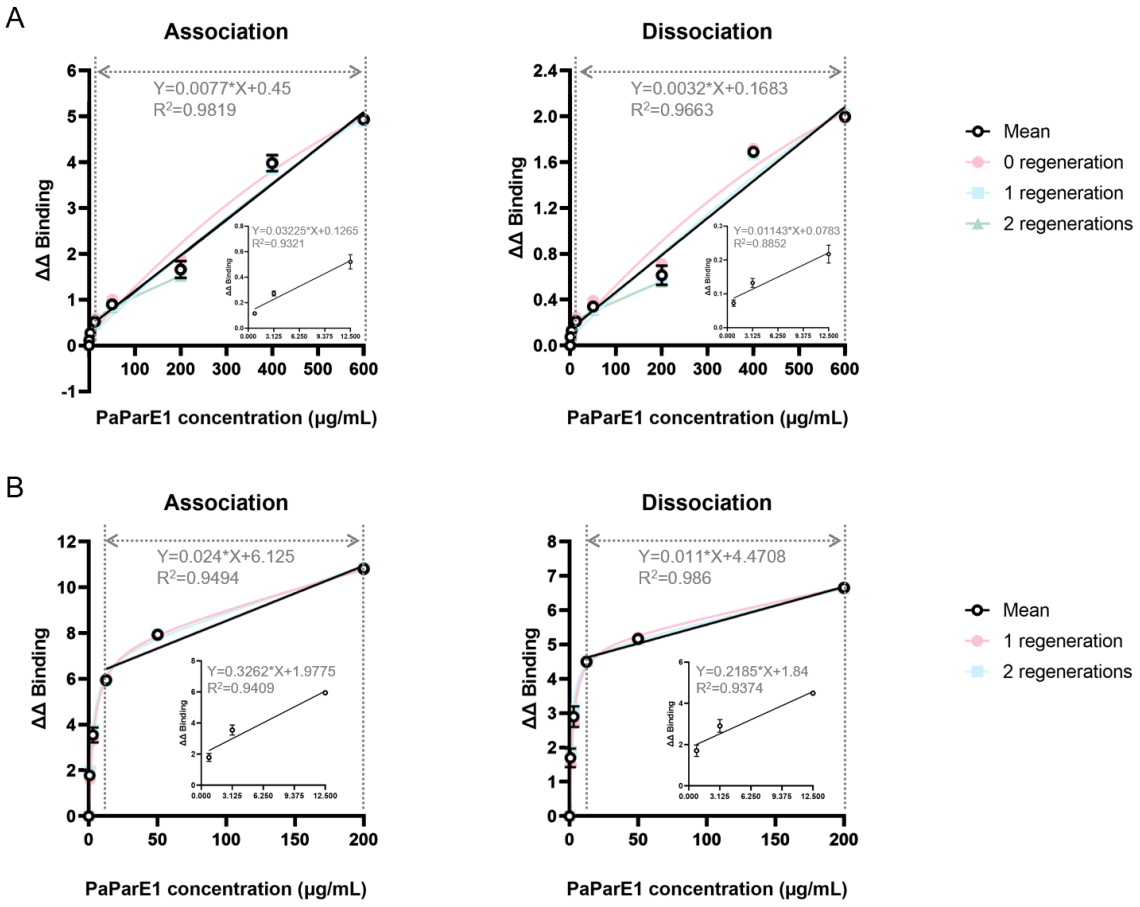

Figure 4.3. The calibration curve for PaParE1 protein in the running buffer. This figure presents graphs showing the specific binding signals of PaParE1 protein from 3-dip loading and washing steps against the concentration of PaParE1 protein in the running buffer, ranging from 0 to 600 µg/mL when using HIS1K biosensor tips (**A**), and 0 to 200 µg/mL when using Ni-NTA biosensor tips (**B**). Each graph represented independent data from multiple regenerations of the biosensor tips. The mean value of the data points, shown along with their SD, represented the results of all independent experiments. For each set of data corresponding to different

regeneration cycles, nonlinear regression analysis was performed using GraphPad Prism. Additionally, linear regression analysis of the mean values across the indicated concentration range is shown through dashed lines or an inset.

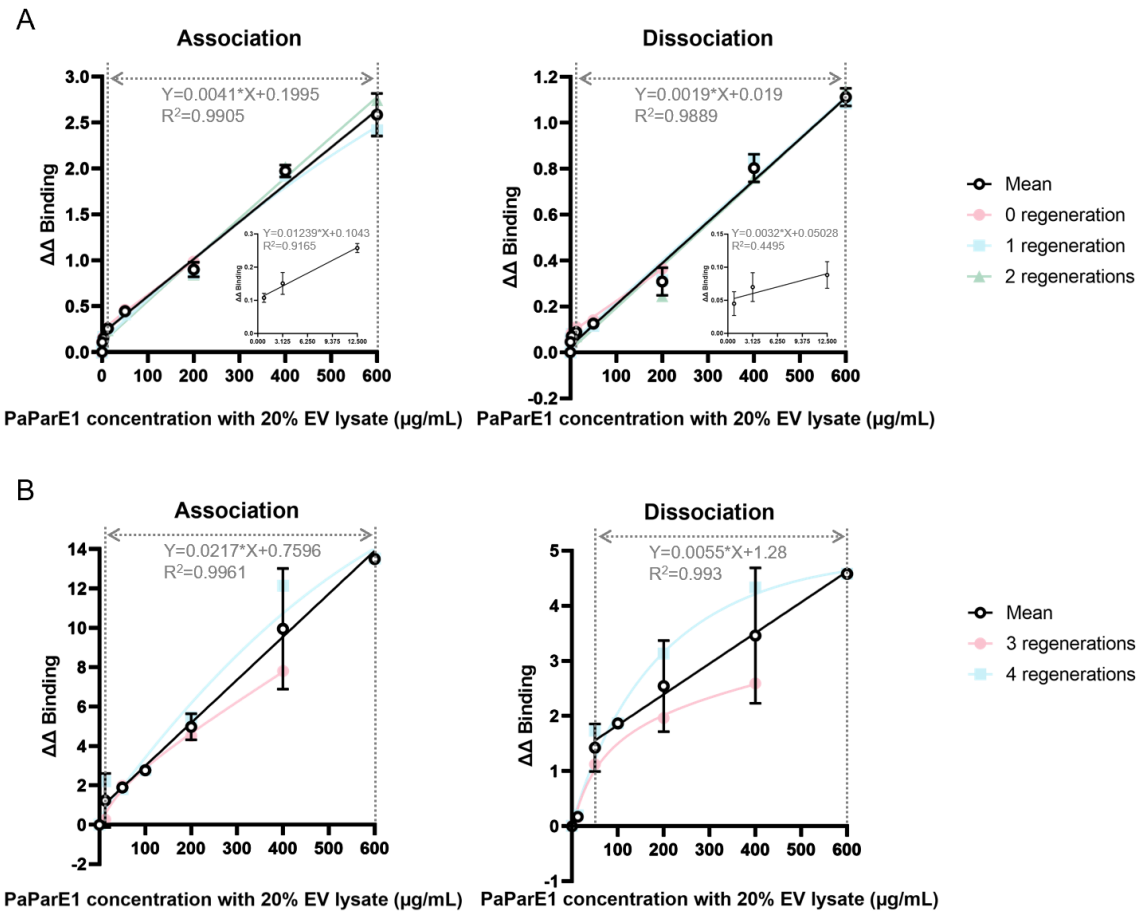

Figure 4.4. The calibration curve for PaParE1 in the running buffer with 20% EV lysate. This figure presents graphs showing the specific binding signals of PaParE1 protein from 3-dip loading and washing steps against the concentration of PaParE1 protein in the running buffer with 20% EV lysate, ranging from 0 to 600 μg/mL when using HIS1K biosensor tips (**A**) and Ni-NTA biosensor tips (**B**). Each graph represented independent data from multiple regenerations of the biosensor tips. The mean value of the data points, shown along with their SD, represented the results of all independent experiments. For each set of data corresponding to different

regeneration cycles, nonlinear regression analysis was performed using GraphPad Prism. Additionally, linear regression analysis of the mean values across the indicated concentration range is shown with dashed lines (**A** and **B**) or an inset (**A**).

4.4. Accuracy Evaluation

To evaluate accuracy of the BLI-based quantification method, a lysate sample of *E. coli* MG1655 cells expressing PaParE1 protein was obtained under the same expression conditions to those used for the purification process, assuming an equivalent level of PaParE1 protein expression. It was diluted in the running buffer in a percentage of 20% and analyzed using both HIS1K and Ni-NTA biosensor tips. Another running buffer containing 20% EV lysate was prepared as a negative control. As shown in **Table 4.1**, with the HIS1K biosensor, the observed binding signals aligned with the second linear regression ranges for both loading and washing steps. These signals correspond to derived concentrations of 208.05 μg/mL and 268.95 μg/mL, respectively. In contrast, when using the Ni-NTA biosensor, the binding signals fell near to the edges of the linear regression ranges for both loading and washing steps. Due to variations between regeneration cycles with the Ni-NTA biosensor, the analysis was adjusted for each specific cycle, resulting in calculated concentrations of 137.12 μg/mL for the loading step and 144.36 μg/mL for the washing step.

Table 4.1.

Readings and calculated concentrations of PaParE1 protein in cell lysate using HIS1K and Ni-NTA biosensors

	HIS1K		Ni-NTA	
	Loading	Washing	Loading	Washing
ΔΔ Binding	1.05 ± 0.01	0.53 ± 0.01	3.34 ± 0.23	1.67 ± 0.13
Calculated Concentration (μg/mL)	208.05 ± 2.59	268.95 ± 3.68	118.91 ± 10.60 [a]	70.31 ± 22.73 [b]

[a, b]: When only applying the measurement of PaParE1 sample into the standard curve of the corresponding regeneration cycle, the calculated concentration was 137.12 μg/mL for loading step and 144.36 μg/mL for wash step.

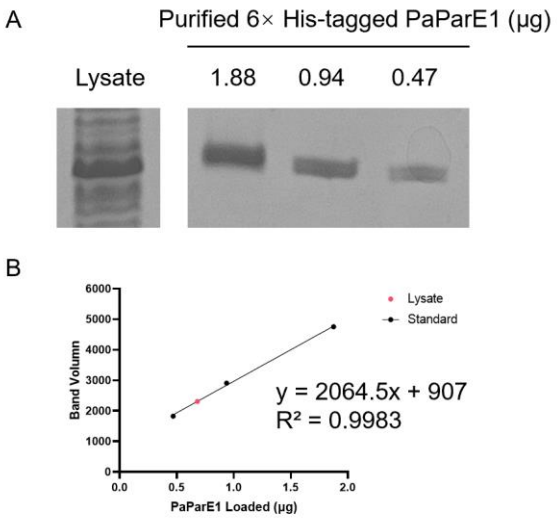

Figure 4.5. Quantification of the concentration of PaParE1 protein in cell lysate by SDS-PAGE. (**A**) Lysate of MG1655 cells expressing 6× His-tagged PaParE1 protein and purified 6× His-tagged PaParE1 protein were diluted in 4× SDS loading dye and analyzed by SDS-PAGE. The concentration of purified PaParE1 protein was measured using a microplate spectrophotometer. (**B**) Band volumes on gel were analyzed using GelAnalyzer 23.1.1. Linear

regression analysis of band volume against the loaded mass of PaParE1 protein was performed. The band volume of PaParE1 in the lysate was 2312, corresponding to a mass of 0.68 μg loaded and a concentration of 181.48 μg/mL in the lysate.

The concentration of PaParE1 protein in the lysate was also estimated by sodium dodecyl-sulfate polyacrylamide gel electrophoresis (SDS-PAGE) (**Fig. 4.5**), indicating a concentration of 181.48 μg/mL for PaParE1 in the lysate sample. The calculated concentrations from the HIS1K biosensor displayed a +16% to +50% variance from the SDS-PAGE-estimated concentration, whereas those from the Ni-NTA biosensor exhibited a -19% to -23% difference. These discrepancies highlight the distinct sensitivities and response behaviors of the two biosensor types within the assay environment. Such differences are critical to consider for accurate data interpretation, indicating the necessity for biosensor-specific calibration and validation to ensure reliable protein quantification. Despite these variances, these outcomes validated the capability of BLI-based method to quantify PaParE1 toxin molecules in cell lysate, demonstrating its practicality though with some deviations that warrant careful consideration in analysis.

5. Discussion

The differential effects on bacterial cell viability exhibited by the ParE toxin subfamily members necessitate an innovative approach for their quantification. When attempting to detect potent ParE proteins in cell lysate, such as *Mycobacterium tuberculosis* ParE toxins, traditional methods like Western blot, fall short due to the toxins' toxic nature to limit cell growth and their resultant low abundance in cells [23]. This study proposed the use of a BLI-based quantification approach and validated its feasibility for quantifying ParE toxin molecules within cell lysate using a non-toxic PaParE1 variant, providing a promising strategy to addressing these challenges.

Key to this study’s success was the demonstration that the BLI-based method could effectively

quantify PaParE1 toxin molecules across a range of concentrations, even in the presence of a complex cell lysate background. While both biosensors demonstrated linear responses to specific concentration intervals of PaParE1 toxin (**Fig. 4.3** and **Fig. 4.4**), a side-by-side comparison highlighted the importance of biosensor selection based on the precise needs of the assay. Ni-NTA biosensor, pre-immobilized with nickel ions, exhibited a stronger response to binding events (**Fig. 4.3B** and **Fig. 4.4B**) and high consistency in performance between regeneration cycles in the absence of cell lysate (**Fig. 4.3B**). However, NSB to Ni-NTA can arise from the attraction between electronegative atoms, typically aromatic nitrogen, and the nickel ions. This interaction may result in the inadvertent binding of proteins with histidine residues, other than the intended target protein. When proteins that bind non-specifically predominate in the solution, these NSB events can restrict the Ni-NTA's ability to detect PaParE1 protein at concentrations lower than 12.5 µg/mL (**Fig. S4.1**). In the presence of cell lysate, this sensitivity to NSB, coupled with inconsistent signal performance across regeneration cycles, complicates the calibration process. On the other hand, due to the high level of binding specificity of the pre-immobilized Penta-His antibody, HIS1K biosensor exhibited more refined response to binding events (**Fig. 4.3A** and **Fig. 4.4A**). However, the limited number of regenerations makes it less cost-effective than Ni-NTA biosensor.

Furthermore, the study's findings highlight the critical role of assay optimization, particularly in minimizing the effects of NSB, a common challenge when working with cell lysates. The observed reduction in binding signals by approximately 50% in the presence of cell lysate (**Fig. 4.3** and **Fig. 4.4**) underscored the competitive nature of specific versus non-specific interactions on the biosensor surface, emphasizing the need for careful assay design and execution. Dubrow et al. have proposed that incorporating 20 mM imidazole and 0.6 M sucrose into the assay could significantly reduce NSB in scenarios involving weak ligand-analyte interactions with the Ni-NTA biosensor, without markedly affecting the affinity of His-tagged proteins [135]. While these adjustments had minimal impact on reducing NSB with the HIS1K biosensor (**Fig. S4.2**), further investigation into these and other modifications is essential to enhance the performance of the

Ni-NTA biosensor, aiming to improve its specificity and resolution in detecting targeted proteins. In addition to reducing NSB, the biosensor's capacity to resolve proteins at lower concentrations can be enhanced by amplifying the specific binding signals of target proteins. Many approaches have been proposed to achieve this, including the introduction of aptamers, secondary antibodies, or the conjugation of enzymes like horseradish peroxidase (HRP) to improve specificity and signal strength [130,134,136]. Overall, these optimization efforts will be necessary for future tasks using this BLI-based method to detect toxic and low abundant ParE toxins.

In conclusion, this study's validation of a BLI-based approach for quantifying ParE toxins paves the way for more accurate and detailed studies into TA systems and their implications for bacterial physiology and pathogenicity. By addressing the technical challenges, the BLI-based quantification method not only enhances our ability to study the ParE toxin subfamily but also broadens the scope of toxic protein research. This methodology could be adapted for other proteins where traditional quantification methods are ineffective, potentially unlocking new insights into protein toxicity, cellular interactions, and the molecular underpinnings of bacterial virulence. Future research should aim to further refine this method, exploring its application to a wider array of proteins and investigating the biological insights that precise quantification can reveal.

Author Contributions

S.R. collected all data reported in this chapter; S.R. and C.R.B. participated in the project design, data analysis, manuscript drafting, and editing.

Data Availability

All data are included in this manuscript and supplement document; DNA clones for constructs made in this work are available upon request. Information for the protein used in this work is available online (PaParE1, UniProtKB Q9I708).

Acknowledgements

We thank the Price Family Foundation for providing funds for the purchase of the Octet RED96 interferometer (Pall ForteBio) and the OU Protein Production and Characterization Core facility for access and expertise. This facility is supported by Institutional Development Awards (IDeA) from the National Institute of General Medical Sciences of the National Institutes of Health (Grants P20GM103640 and P30GM145423), the OU Vice President for Research and Partnerships, and the OU College of Arts and Sciences. National Institute of General Medical Sciences of the National Institutes of Health Grant P30GM145423 also provided financial support for this work through a voucher program. Additional funding support was from the Department of Defense, grant number W81XWH-20-1-0121.

Chapter V: Research Impact and Future Directions

The research introduced in Chapters II to IV discuss the impacts of bacterial toxin-antitoxin (TA) systems, particularly the ParE toxin subfamily, which helps us to understand the role of TA systems in bacterial physiology and their potential use as a novel antibacterial strategy. Through a series of detailed studies, including phenotypic analysis, molecular characterization, and innovative method applications, this dissertation work provides new insights into the variable toxicity of ParE toxins, the survival mechanisms employed by bacteria in response to plasmid born ParE toxin expression, and the quantification of toxic ParE proteins within bacterial cells. The findings from this dissertation have contributed to several key areas of bacterial physiology, molecular biology, and antibacterial research.

1.1. Enhanced Understanding of the Potential of Co-Opting TA Systems as an Antibacterial Strategy

Chapter II discusses research on the differential effects of ParE toxins from *Pseudomonas aeruginosa* and *Mycobacterium tuberculosis* on the *P. aeruginosa* hosts as well as the *E. coli* surrogate host. Consistent with previous studies [23], PaParE1 toxin showed a minimal effect while other ParE toxins significantly reduced bacterial viability. This difference in toxicity highlights the potential of certain ParE toxins as components of new antibacterial strategies [137]. Importantly, a dose-dependent increase in mutagenic potential following ParE toxin expression was observed. Interestingly, it did not immediately lead to the emergence of antibiotic resistance within the observed timeframe. Instead, increased cell susceptibility to a variety of existing antibiotics was noted, indicating that the expression of ParE toxins can be used to enhance the effectiveness of existing antibiotic treatments.

The results of this chapter have significantly promoted our understanding of TA systems in bacteria and emphasized the complex dynamics between toxin activity and bacterial survival. By

demonstrating the differential effects of ParE toxins on bacterial physiology and antibiotic susceptibility, this work opens a new way for developing innovative antibacterial therapies. These strategies may change the current situation of bacterial infections, especially in the context of rising antibiotic resistance. Furthermore, the study observed that increased mutation frequence did not translate into antibiotic resistance and in some instances improved antibiotic susceptibility, increasing the potential of the use of ParE toxins in combination with existing antibiotics to combat drug-resistant bacterial strains. This approach could provide a valuable supplement for the current efforts to combat bacterial infections and provide a potential new method to curb the spread of antibiotic resistance.

Based on the results of this chapter, future research will primarily target how to artificially disrupt the toxin-antitoxin interaction to liberate the toxin to kill cells. One strategy that has been explored is the use of antisense peptide nucleic acids to inhibit antitoxin translation, which led to an effective inhibition of *E. coli* growth [138]. However, the practicality of this strategy is questionable due to the high binding affinity that PNA oligomers exhibit for natural nucleic acids, resulting in their toxicity to eukaryotic cells [139,140]. Another strategy involves screening small molecules, such as peptides, that bind to the antitoxin at the toxin-antitoxin interaction site, preventing the toxin from associating with the antitoxin, thereby liberating the toxin [141]. Our previous research has identified the minimal antitoxin unit required for binding to the PaParE1 toxin (data not shown). Utilizing structure-based rational design, we aim to further develop a protein-protein interaction inhibitor that binds more effectively to this site. This would competitively inhibit ParD1 binding to ParE1, enhancing the strategy's efficacy.

1.2. Novel Insights into Bacterial Survival Strategies

Chapter III demonstrated a phenotype that a fraction of *Escherichia coli* populations survived the expression of toxic ParE proteins by significantly reducing the plasmid copy number (PCN). This adaptation was observed across different *E. coli* strains and with the expression of different

members of the ParE toxin subfamily. The reduction in PCN was found to be a reproducible response not attributable to mutations within the plasmid sequence or to alterations in arabinose uptake, which induces the expression of the ParE proteins. Instead, this survival strategy balances the need to maintain essential plasmid functions, such as antibiotic resistance, with the necessity to mitigate the toxicity of overexpressed ParE proteins.

This phenomenon was further investigated through various experiments, including growth and viability assays and qPCR analyses to determine PCN. The results showed that the observed reduction in PCN was an adaptive cellular response likely mediated by altering the regulation of plasmid replication. Additionally, whole genome sequencing of surviving *E. coli* cells identified a specific mutation (N845S) in DNA polymerase I, which correlates with reduced PCN and has been previously suggested to be related to the maintenance of the plasmid in this study [123,142].

To clarify the molecular mechanism of PCN reduction observed, the future direction may focus on studying the role of N845S mutation in DNA polymerase I and its influence on plasmid replication and stability. In addition, further investigations into the expression of RNA I in these insensitive cells to reveal the balance change between these two RNAs would provide insight into the molecular regulation of the plasmid. Lastly, exploring whether bacteria adopt similar survival strategies under the stress conditions of toxins from other TA systems will enhance our understanding of bacterial adaptability.

Overall, the impact of this chapter goes beyond the specific study of ParE toxin expression. It emphasizes the potential confounding factors in genetic studies with plasmid-based expression systems, especially when expressing toxic proteins. Understanding the dynamics of PCN under stress conditions such as toxin expression could inform the design of more stable genetic constructs for research and biotechnological applications. Furthermore, this study contributes to our broader understanding of bacterial survival mechanisms under adverse conditions, providing insights that could be leveraged in developing novel antibacterial strategies or improving the efficacy of existing ones.

1.3. Progress in Quantitative Method of Toxic Proteins

In Chapter IV, a new approach for directly measuring the concentration of toxic ParE proteins directly within bacterial cell lysates is introduced. The research focuses on the quantification of the PaParE1 toxin (an attenuated variant from *Pseudomonas aeruginosa*) and validates the feasibility and effectiveness of detecting and quantifying ParE toxin proteins in complex biological samples using BLI-based method. The research compared the efficacy of two types of biosensors (HIS1K and Ni-NTA) in the specific binding and quantification of PaParE1 toxin variant, highlighting the importance of selecting appropriate biosensors according to the complexity of samples to minimize non-specific binding (NSB). Through careful experimental design, PaParE1 toxin in cell lysates was successfully quantified in this chapter. By providing a method to quantitatively compare the toxic effects of different ParE toxins, which was unsuccessful by traditional methods like Western blot [23] and mass spectrometry, this work fills a major gap in microbial physiology research.

The observed reduction in binding signals by approximately 50% in the presence of cell lysate underscored the competitive nature of specific versus non-specific interactions on the biosensor surface, emphasizing the need for careful assay design and execution. Given the toxic nature of toxins, which will limit the number of toxin molecules in cell populations, it may be necessary to enhance the signal clarity from NSB. Therefore, future directions should include the optimization work in reducing these NSB. Reports suggested that incorporating 20 mM imidazole and 0.6 M sucrose can decrease NSB [135], yet initial tests with these NSB blockers have yielded limited results. Consequently, further research into these and other NSB blockers is crucial for improving biosensor efficiency. Beyond reducing NSB, enhancing signal detection through methods such as incorporating aptamers, secondary antibodies, or enzyme conjugations like horseradish peroxidase is also vital. These enhancements are essential for the advancement of BLI-based methods in quantifying those toxic and low-abundance toxin proteins.

Overall, the impact of this research is extensive and important. By providing a reliable method for quantifying toxic proteins that limit bacterial growth, this study enhances our ability to study TA systems and their roles in bacterial physiology. Moreover, the method established in this chapter can be adapted for a wide range of applications beyond the scope of TA systems, including but not limited to, the study of other low-abundance proteins, the development of new antibacterial strategies, and the improvement of biotechnological processes.

References

(1) Hutchings, M. I.; Truman, A. W.; Wilkinson, B. Antibiotics: Past, Present and Future. *Current Opinion in Microbiology* **2019**, *51*, 72–80. https://doi.org/10.1016/j.mib.2019.10.008.

(2) Peterson, E.; Kaur, P. Antibiotic Resistance Mechanisms in Bacteria: Relationships Between Resistance Determinants of Antibiotic Producers, Environmental Bacteria, and Clinical Pathogens. *Front. Microbiol.* **2018**, *9*. https://doi.org/10.3389/fmicb.2018.02928.

(3) Munita, J. M.; Arias, C. A. Mechanisms of Antibiotic Resistance. *Microbiol Spectr* **2016**, *4* (2), 10.1128/microbiolspec.VMBF-0016–2015. https://doi.org/10.1128/microbiolspec.VMBF-0016-2015.

(4) Salam, Md. A.; Al-Amin, Md. Y.; Salam, M. T.; Pawar, J. S.; Akhter, N.; Rabaan, A. A.; Alqumber, M. A. A. Antimicrobial Resistance: A Growing Serious Threat for Global Public Health. *Healthcare (Basel)* **2023**, *11* (13), 1946. https://doi.org/10.3390/healthcare11131946.

(5) Murray, C. J. L.; Ikuta, K. S.; Sharara, F.; Swetschinski, L.; Robles Aguilar, G.; Gray, A.; Han, C.; Bisignano, C.; Rao, P.; Wool, E.; Johnson, S. C.; Browne, A. J.; Chipeta, M. G.; Fell, F.; Hackett, S.; Haines-Woodhouse, G.; Kashef Hamadani, B. H.; Kumaran, E. A. P.; McManigal, B.; Achalapong, S.; Agarwal, R.; Akech, S.; Albertson, S.; Amuasi, J.; Andrews, J.; Aravkin, A.; Ashley, E.; Babin, F.-X.; Bailey, F.; Baker, S.; Basnyat, B.; Bekker, A.; Bender, R.; Berkley, J. A.; Bethou, A.; Bielicki, J.; Boonkasidecha, S.; Bukosia, J.; Carvalheiro, C.; Castañeda-Orjuela, C.; Chansamouth, V.; Chaurasia, S.; Chiurchiù, S.; Chowdhury, F.; Clotaire Donatien, R.; Cook, A. J.; Cooper, B.; Cressey, T. R.; Criollo-Mora, E.; Cunningham, M.; Darboe, S.; Day, N. P. J.; De Luca, M.; Dokova, K.; Dramowski, A.; Dunachie, S. J.; Duong Bich, T.; Eckmanns, T.; Eibach, D.; Emami, A.; Feasey, N.; Fisher-Pearson, N.; Forrest, K.; Garcia, C.; Garrett, D.; Gastmeier, P.; Giref, A. Z.; Greer, R. C.; Gupta, V.; Haller, S.; Haselbeck, A.; Hay, S. I.; Holm, M.; Hopkins, S.; Hsia, Y.; Iregbu, K. C.; Jacobs, J.; Jarovsky, D.; Javanmardi, F.; Jenney, A. W. J.; Khorana, M.; Khusuwan, S.; Kissoon, N.; Kobeissi, E.; Kostyanev, T.; Krapp, F.; Krumkamp, R.; Kumar, A.; Kyu, H. H.; Lim, C.; Lim, K.; Limmathurotsakul, D.; Loftus, M. J.; Lunn, M.; Ma, J.; Manoharan, A.; Marks, F.; May, J.; Mayxay, M.; Mturi, N.; Munera-Huertas, T.; Musicha, P.; Musila, L. A.; Mussi-Pinhata, M. M.; Naidu, R. N.; Nakamura, T.; Nanavati, R.; Nangia, S.; Newton, P.; Ngoun, C.; Novotney, A.; Nwakanma, D.; Obiero, C. W.; Ochoa, T. J.; Olivas-Martinez, A.; Olliaro, P.; Ooko, E.; Ortiz-Brizuela, E.; Ounchanum, P.; Pak, G. D.; Paredes, J. L.; Peleg, A. Y.; Perrone, C.; Phe, T.; Phommasone, K.; Plakkal, N.; Ponce-de-Leon, A.; Raad, M.; Ramdin, T.; Rattanavong, S.; Riddell, A.; Roberts, T.; Robotham, J. V.; Roca, A.; Rosenthal, V. D.; Rudd, K. E.; Russell, N.; Sader, H. S.; Saengchan, W.; Schnall, J.; Scott, J. A. G.; Seekaew, S.; Sharland, M.; Shivamallappa, M.; Sifuentes-Osornio, J.; Simpson, A. J.; Steenkeste, N.; Stewardson, A. J.; Stoeva, T.; Tasak, N.; Thaiprakong, A.; Thwaites, G.; Tigoi, C.; Turner, C.; Turner, P.; van Doorn, H. R.; Velaphi, S.; Vongpradith, A.; Vongsouvath, M.; Vu, H.; Walsh, T.; Walson, J. L.; Waner, S.; Wangrangsimakul, T.; Wannapinij, P.; Wozniak, T.; Young Sharma, T. E. M. W.; Yu, K. C.; Zheng, P.; Sartorius, B.; Lopez, A. D.; Stergachis, A.; Moore, C.; Dolecek, C.; Naghavi, M. Global Burden of Bacterial Antimicrobial Resistance in 2019: A

Systematic Analysis. *The Lancet* **2022**, *399* (10325), 629–655. https://doi.org/10.1016/S0140-6736(21)02724-0.

(6) Centers for Disease Control and Prevention (U.S.). *Antibiotic Resistance Threats in the United States, 2019*; Centers for Disease Control and Prevention (U.S.), 2019. https://doi.org/10.15620/cdc:82532.

(7) Neil, J. O. Report on Antimicrobial Resistance. *Report on Antimicrobial Resistance* **2016**.

(8) Hegemann, J. D.; Birkelbach, J.; Walesch, S.; Müller, R. Current Developments in Antibiotic Discovery. *EMBO Rep* **2022**, *24* (1), e56184. https://doi.org/10.15252/embr.202256184.

(9) Bubnoff, A. von. Seeking New Antibiotics in Nature's Backyard. *Cell* **2006**, *127* (5), 867–869. https://doi.org/10.1016/j.cell.2006.11.021.

(10) Równicki, M.; Lasek, R.; Trylska, J.; Bartosik, D. Targeting Type II Toxin-Antitoxin Systems as Antibacterial Strategies. *Toxins (Basel)* **2020**, *12* (9), E568. https://doi.org/10.3390/toxins12090568.

(11) Yamaguchi, Y.; Park, J.-H.; Inouye, M. Toxin-Antitoxin Systems in Bacteria and Archaea. *Annual Review of Genetics* **2011**, *45* (1), 61–79. https://doi.org/10.1146/annurev-genet-110410-132412.

(12) Guan, J.; Chen, Y.; Goh, Y.-X.; Wang, M.; Tai, C.; Deng, Z.; Song, J.; Ou, H.-Y. TADB 3.0: An Updated Database of Bacterial Toxin–Antitoxin Loci and Associated Mobile Genetic Elements. *Nucleic Acids Research* **2023**, gkad962. https://doi.org/10.1093/nar/gkad962.

(13) Qiu, J.; Zhai, Y.; Wei, M.; Zheng, C.; Jiao, X. Toxin–Antitoxin Systems: Classification, Biological Roles, and Applications. *Microbiological Research* **2022**, *264*, 127159. https://doi.org/10.1016/j.micres.2022.127159.

(14) Jurėnas, D.; Fraikin, N.; Goormaghtigh, F.; Van Melderen, L. Biology and Evolution of Bacterial Toxin–Antitoxin Systems. *Nat Rev Microbiol* **2022**, *20* (6), 335–350. https://doi.org/10.1038/s41579-021-00661-1.

(15) Kamruzzaman, M.; Wu, A. Y.; Iredell, J. R. Biological Functions of Type II Toxin-Antitoxin Systems in Bacteria. *Microorganisms* **2021**, *9* (6), 1276. https://doi.org/10.3390/microorganisms9061276.

(16) Leplae, R.; Geeraerts, D.; Hallez, R.; Guglielmini, J.; Drèze, P.; Van Melderen, L. Diversity of Bacterial Type II Toxin–Antitoxin Systems: A Comprehensive Search and Functional Analysis of Novel Families. *Nucleic Acids Res* **2011**, *39* (13), 5513–5525. https://doi.org/10.1093/nar/gkr131.

(17) Snead, K. J.; Moore, L. L.; Bourne, C. R. ParD Antitoxin Hotspot Alters a Disorder-to-Order Transition upon Binding to Its Cognate ParE Toxin, Lessening Its Interaction Affinity and Increasing Its Protease Degradation Kinetics. *Biochemistry* **2022**, *61* (1), 34–45. https://doi.org/10.1021/acs.biochem.1c00584.

(18) Chan, W. T.; Garcillán-Barcia, M. P.; Yeo, C. C.; Espinosa, M. Type II Bacterial Toxin–Antitoxins: Hypotheses, Facts, and the Newfound Plethora of the PezAT System. *FEMS Microbiology Reviews* **2023**, *47* (5), fuad052. https://doi.org/10.1093/femsre/fuad052.

(19) Griffin, M. A.; Davis, J. H.; Strobel, S. A. Bacterial Toxin RelE: A Highly Efficient Nuclease with Exquisite Substrate Specificity Using Atypical Catalytic Residues. *Biochemistry* **2013**, *52* (48), 8633–8642. https://doi.org/10.1021/bi401325c.

(20) Pedersen, K.; Zavialov, A. V.; Pavlov, M. Y.; Elf, J.; Gerdes, K.; Ehrenberg, M. The Bacterial Toxin RelE Displays Codon-Specific Cleavage of mRNAs in the Ribosomal A Site. *Cell* **2003**, *112* (1), 131–140. https://doi.org/10.1016/S0092-8674(02)01248-5.

(21) Han, J.-S.; Lee, J. J.; Anandan, T.; Zeng, M.; Sripathi, S.; Jahng, W. J.; Lee, S. H.; Suh, J.-W.; Kang, C.-M. Characterization of a Chromosomal Toxin–Antitoxin, Rv1102c–Rv1103c System in Mycobacterium Tuberculosis. *Biochemical and Biophysical Research Communications* **2010**, *400* (3), 293–298. https://doi.org/10.1016/j.bbrc.2010.08.023.

(22) Vang Nielsen, S.; Turnbull, K. J.; Roghanian, M.; Bærentsen, R.; Semanjski, M.; Brodersen, D. E.; Macek, B.; Gerdes, K. Serine-Threonine Kinases Encoded by Split hipA Homologs Inhibit Tryptophanyl-tRNA Synthetase. *mBio* **2019**, *10* (3), e01138-19. https://doi.org/10.1128/mBio.01138-19.

(23) Ames, J. R.; Muthuramalingam, M.; Murphy, T.; Najar, F. Z.; Bourne, C. R. Expression of Different ParE Toxins Results in Conserved Phenotypes with Distinguishable Classes of Toxicity. *Microbiologyopen* **2019**, *8* (10), e902. https://doi.org/10.1002/mbo3.902.

(24) Bahassi, E. M.; O'Dea, M. H.; Allali, N.; Messens, J.; Gellert, M.; Couturier, M. Interactions of CcdB with DNA Gyrase: INACTIVATION OF GyrA, POISONING OF THE GYRASE-DNA COMPLEX, AND THE ANTIDOTE ACTION OF CcdA*. *Journal of Biological Chemistry* **1999**, *274* (16), 10936–10944. https://doi.org/10.1074/jbc.274.16.10936.

(25) Dao-Thi, M.-H.; Van Melderen, L.; De Genst, E.; Afif, H.; Buts, L.; Wyns, L.; Loris, R. Molecular Basis of Gyrase Poisoning by the Addiction Toxin CcdB. *Journal of Molecular Biology* **2005**, *348* (5), 1091–1102. https://doi.org/10.1016/j.jmb.2005.03.049.

(26) Ruan, S.; Tu, C.-H.; Bourne, C. R. Friend or Foe: Protein Inhibitors of DNA Gyrase. *Biology* **2024**, *13* (2), 84. https://doi.org/10.3390/biology13020084.

(27) Ogura, T.; Hiraga, S. Mini-F Plasmid Genes That Couple Host Cell Division to Plasmid Proliferation. *Proceedings of the National Academy of Sciences* **1983**, *80* (15), 4784–4788. https://doi.org/10.1073/pnas.80.15.4784.

(28) Tsang, J. Bacterial Plasmid Addiction Systems and Their Implications for Antibiotic Drug Development. *Postdoc J* **2017**, *5* (5), 3–9.

(29) Fraikin, N.; Goormaghtigh, F.; Van Melderen, L. Type II Toxin-Antitoxin Systems: Evolution and Revolutions. *Journal of Bacteriology* **2020**, *202* (7), e00763-19. https://doi.org/10.1128/JB.00763-19.

(30) Fraikin, N.; Melderen, L. V. Single-Cell Evidence for Plasmid Addiction Mediated by Toxin-Antitoxin Systems. bioRxiv August 29, 2023, p 2023.08.29.555305. https://doi.org/10.1101/2023.08.29.555305.

(31) Gerdes, K.; Rasmussen, P. B.; Molin, S. Unique Type of Plasmid Maintenance Function: Postsegregational Killing of Plasmid-Free Cells. *Proceedings of the National Academy of Sciences* **1986**, *83* (10), 3116–3120. https://doi.org/10.1073/pnas.83.10.3116.

(32) Tu, C.-H.; Holt, M.; Ruan, S.; Bourne, C. Evaluating the Potential for Cross-Interactions of Antitoxins in Type II TA Systems. *Toxins (Basel)* **2020**, *12* (6), 422. https://doi.org/10.3390/toxins12060422.

(33) Van Melderen, L.; Bernard, P.; Couturier, M. Lon-Dependent Proteolysis of CcdA Is the Key Control for Activation of CcdB in Plasmid-Free Segregant Bacteria. *Molecular Microbiology* **1994**, *11* (6), 1151–1157. https://doi.org/10.1111/j.1365-2958.1994.tb00391.x.

(34) Van Melderen, L.; Thi, M. H. D.; Lecchi, P.; Gottesman, S.; Couturier, M.; Maurizi, M. R. ATP-Dependent Degradation of CcdA by Lon Protease: EFFECTS OF SECONDARY STRUCTURE AND HETEROLOGOUS SUBUNIT INTERACTIONS*. *Journal of Biological Chemistry* **1996**, *271* (44), 27730–27738. https://doi.org/10.1074/jbc.271.44.27730.

(35) Yuan, J.; Yamaichi, Y.; Waldor, M. K. The Three Vibrio Cholerae Chromosome II-Encoded ParE Toxins Degrade Chromosome I Following Loss of Chromosome II. *Journal of Bacteriology* **2011**, *193* (3), 611–619. https://doi.org/10.1128/jb.01185-10.

(36) Saavedra De Bast, M.; Mine, N.; Van Melderen, L. Chromosomal Toxin-Antitoxin Systems May Act as Antiaddiction Modules. *Journal of Bacteriology* **2008**, *190* (13), 4603–4609. https://doi.org/10.1128/jb.00357-08.

(37) Schuster, C. F.; Bertram, R. Toxin–Antitoxin Systems Are Ubiquitous and Versatile Modulators of Prokaryotic Cell Fate. *FEMS Microbiology Letters* **2013**, *340* (2), 73–85. https://doi.org/10.1111/1574-6968.12074.

(38) Gerdes, K.; Maisonneuve, E. Bacterial Persistence and Toxin-Antitoxin Loci. *Annual Review of Microbiology* **2012**, *66* (Volume 66, 2012), 103–123. https://doi.org/10.1146/annurev-micro-092611-150159.

(39) Fineran, P. C.; Blower, T. R.; Foulds, I. J.; Humphreys, D. P.; Lilley, K. S.; Salmond, G. P. C. The Phage Abortive Infection System, ToxIN, Functions as a Protein–RNA Toxin–Antitoxin Pair. *Proceedings of the National Academy of Sciences* **2009**, *106* (3), 894–899. https://doi.org/10.1073/pnas.0808832106.

(40) Lobato-Márquez, D.; Díaz-Orejas, R.; García-del Portillo, F. Toxin-Antitoxins and Bacterial Virulence. *FEMS Microbiology Reviews* **2016**, *40* (5), 592–609. https://doi.org/10.1093/femsre/fuw022.

(41) Bardaji, L.; Añorga, M.; Echeverría, M.; Ramos, C.; Murillo, J. The Toxic Guardians — Multiple Toxin-Antitoxin Systems Provide Stability, Avoid Deletions and Maintain Virulence Genes of Pseudomonas Syringae Virulence Plasmids. *Mobile DNA* **2019**, *10* (1), 7. https://doi.org/10.1186/s13100-019-0149-4.

(42) Yang, Q. E.; Walsh, T. R. Toxin–Antitoxin Systems and Their Role in Disseminating and Maintaining Antimicrobial Resistance. *FEMS Microbiol Rev* **2017**, *41* (3), 343–353. https://doi.org/10.1093/femsre/fux006.

(43) Bleriot, I.; Blasco, L.; Pacios, O.; Fernández-García, L.; Ambroa, A.; López, M.; Ortiz-Cartagena, C.; Cuenca, F. F.; Oteo-Iglesias, J.; Pascual, Á.; Martínez-Martínez, L.; Domingo-Calap, P.; Wood, T. K.; Tomás, M. The Role of PemIK (PemK/PemI) Type II TA System from Klebsiella Pneumoniae Clinical Strains in Lytic Phage Infection. *Sci Rep* **2022**, *12* (1), 4488. https://doi.org/10.1038/s41598-022-08111-5.

(44) Wang, X.; Wood, T. K. Toxin-Antitoxin Systems Influence Biofilm and Persister Cell Formation and the General Stress Response ▿. *Appl Environ Microbiol* **2011**, *77* (16), 5577–5583. https://doi.org/10.1128/AEM.05068-11.

(45) Muthuramalingam, M.; White, J. C.; Murphy, T.; Ames, J. R.; Bourne, C. R. The Toxin from a ParDE Toxin-antitoxin System Found in Pseudomonas Aeruginosa Offers Protection to Cells Challenged with Anti-gyrase Antibiotics. *Mol Microbiol* **2019**, *111* (2), 441–454. https://doi.org/10.1111/mmi.14165.

(46) Singh, G.; Yadav, M.; Ghosh, C.; Rathore, J. S. Bacterial Toxin-Antitoxin Modules: Classification, Functions, and Association with Persistence. *Curr Res Microb Sci* **2021**, *2*, 100047. https://doi.org/10.1016/j.crmicr.2021.100047.

(47) Boss, L.; Kędzierska, B. Bacterial Toxin-Antitoxin Systems' Cross-Interactions—Implications for Practical Use in Medicine and Biotechnology. *Toxins* **2023**, *15* (6), 380. https://doi.org/10.3390/toxins15060380.

(48) Fernández-García, L.; Blasco, L.; Lopez, M.; Bou, G.; García-Contreras, R.; Wood, T.; Tomas, M. Toxin-Antitoxin Systems in Clinical Pathogens. *Toxins (Basel)* **2016**, *8* (7), 227. https://doi.org/10.3390/toxins8070227.

(49) Roberts, R. C.; Burioni, R.; Helinski, D. R. Genetic Characterization of the Stabilizing Functions of a Region of Broad-Host-Range Plasmid RK2. *J Bacteriol* **1990**, *172* (11), 6204–6216.

(50) Weinstein, M.; Roberts, R. C.; Helinski, D. R. A Region of the Broad-Host-Range Plasmid RK2 Causes Stable in Planta Inheritance of Plasmids in Rhizobium Meliloti Cells Isolated from Alfalfa

Root Nodules. *Journal of Bacteriology* **1992**, *174* (22), 7486–7489. https://doi.org/10.1128/jb.174.22.7486-7489.1992.

(51) Spencer, A. C.; Panda, S. S. DNA Gyrase as a Target for Quinolones. *Biomedicines* **2023**, *11* (2), 371. https://doi.org/10.3390/biomedicines11020371.

(52) Villain, P.; Catchpole, R.; Forterre, P.; Oberto, J.; da Cunha, V.; Basta, T. Expanded Dataset Reveals the Emergence and Evolution of DNA Gyrase in Archaea. *Molecular Biology and Evolution* **2022**, *39* (8), msac155. https://doi.org/10.1093/molbev/msac155.

(53) Bax, B. D.; Murshudov, G.; Maxwell, A.; Germe, T. DNA Topoisomerase Inhibitors: Trapping a DNA-Cleaving Machine in Motion. *Journal of Molecular Biology* **2019**, *431* (18), 3427–3449. https://doi.org/10.1016/j.jmb.2019.07.008.

(54) Gubaev, A.; Klostermeier, D. The Mechanism of Negative DNA Supercoiling: A Cascade of DNA-Induced Conformational Changes Prepares Gyrase for Strand Passage. *DNA Repair* **2014**, *16*, 23–34. https://doi.org/10.1016/j.dnarep.2014.01.011.

(55) Williams, J. S.; Tumbale, P. P.; Arana, M. E.; Rana, J. A.; Williams, R. S.; Kunkel, T. A. High-Fidelity DNA Ligation Enforces Accurate Okazaki Fragment Maturation during DNA Replication. *Nat Commun* **2021**, *12* (1), 482. https://doi.org/10.1038/s41467-020-20800-1.

(56) Anderson, V. E.; Zaniewski, R. P.; Kaczmarek, F. S.; Gootz, T. D.; Osheroff, N. Quinolones Inhibit DNA Religation Mediated by Staphylococcus Aureus Topoisomerase IV: CHANGES IN DRUG MECHANISM ACROSS EVOLUTIONARY BOUNDARIES *. *Journal of Biological Chemistry* **1999**, *274* (50), 35927–35932. https://doi.org/10.1074/jbc.274.50.35927.

(57) Barnard, F. M.; Maxwell, A. Interaction between DNA Gyrase and Quinolones: Effects of Alanine Mutations at GyrA Subunit Residues Ser83 and Asp87. *Antimicrob Agents Chemother* **2001**, *45* (7), 1994–2000. https://doi.org/10.1128/AAC.45.7.1994-2000.2001.

(58) Alam, M. K.; Alhhazmi, A.; DeCoteau, J. F.; Luo, Y.; Geyer, C. R. RecA Inhibitors Potentiate Antibiotic Activity and Block Evolution of Antibiotic Resistance. *Cell Chemical Biology* **2016**, *23* (3), 381–391. https://doi.org/10.1016/j.chembiol.2016.02.010.

(59) Revitt-Mills, S. A.; Wright, E. K.; Vereker, M.; O'Flaherty, C.; McPherson, F.; Dawson, C.; Oijen, A. M. van; Robinson, A. Defects in DNA Double-Strand Break Repair Re-Sensitise Antibiotic-Resistant Escherichia Coli to Multiple Bactericidal Antibiotics. bioRxiv January 25, 2022, p 2022.01.24.477632. https://doi.org/10.1101/2022.01.24.477632.

(60) Baharoglu, Z.; Mazel, D. SOS, the Formidable Strategy of Bacteria against Aggressions. *FEMS Microbiology Reviews* **2014**, *38* (6), 1126–1145. https://doi.org/10.1111/1574-6976.12077.

(61) Mo, C. Y.; Manning, S. A.; Roggiani, M.; Culyba, M. J.; Samuels, A. N.; Sniegowski, P. D.; Goulian, M.; Kohli, R. M. Systematically Altering Bacterial SOS Activity under Stress Reveals Therapeutic Strategies for Potentiating Antibiotics. *mSphere* **2016**, *1* (4), 10.1128/msphere.00163-16. https://doi.org/10.1128/msphere.00163-16.

(62) Shintani, M.; Sanchez, Z. K.; Kimbara, K. Genomics of Microbial Plasmids: Classification and Identification Based on Replication and Transfer Systems and Host Taxonomy. *Front Microbiol* **2015**, *6*, 242. https://doi.org/10.3389/fmicb.2015.00242.

(63) Hernández-Arriaga, A. M.; Chan, W. T.; Espinosa, M.; Díaz-Orejas, R. Conditional Activation of Toxin-Antitoxin Systems: Postsegregational Killing and Beyond. *Microbiology Spectrum* **2014**, *2* (5), 10.1128/microbiolspec.plas-0009–2013. https://doi.org/10.1128/microbiolspec.plas-0009-2013.

(64) Yee, W.-X.; Yasir, M.; Turner, A. K.; Baker, D. J.; Cehovin, A.; Tang, C. M. Evolution, Persistence, and Host Adaption of a Gonococcal AMR Plasmid That Emerged in the Pre-Antibiotic Era. *PLOS Genetics* **2023**, *19* (5), e1010743. https://doi.org/10.1371/journal.pgen.1010743.

(65) Bottery, M.; Brockhurst, M. A. Rapid Evolution Helps Bacteria to Pick up a Plasmid. *Proceedings of the National Academy of Sciences* **2023**, *120* (19), e2304474120. https://doi.org/10.1073/pnas.2304474120.

(66) Buckner, M. M. C.; Ciusa, M. L.; Piddock, L. J. V. Strategies to Combat Antimicrobial Resistance: Anti-Plasmid and Plasmid Curing. *FEMS Microbiol Rev* **2018**, *42* (6), 781–804. https://doi.org/10.1093/femsre/fuy031.

(67) Yao, J.; Zou, P.; Cui, Y.; Quan, L.; Gao, C.; Li, Z.; Gong, W.; Yang, M. Recent Advances in Strategies to Combat Bacterial Drug Resistance: Antimicrobial Materials and Drug Delivery Systems. *Pharmaceutics* **2023**, *15* (4), 1188. https://doi.org/10.3390/pharmaceutics15041188.

(68) Zhang, S.-P.; Wang, Q.; Quan, S.-W.; Yu, X.-Q.; Wang, Y.; Guo, D.-D.; Peng, L.; Feng, H.-Y.; He, Y.-X. Type II Toxin–Antitoxin System in Bacteria: Activation, Function, and Mode of Action. *Biophys Rep* **2020**, *6* (2), 68–79. https://doi.org/10.1007/s41048-020-00109-8.

(69) McKenzie, G. J.; Harris, R. S.; Lee, P. L.; Rosenberg, S. M. The SOS Response Regulates Adaptive Mutation. *Proceedings of the National Academy of Sciences* **2000**, *97* (12), 6646–6651. https://doi.org/10.1073/pnas.120161797.

(70) McKenzie, G. J.; Lee, P. L.; Lombardo, M.-J.; Hastings, P. J.; Rosenberg, S. M. SOS Mutator DNA Polymerase IV Functions in Adaptive Mutation and Not Adaptive Amplification. *Molecular Cell* **2001**, *7* (3), 571–579. https://doi.org/10.1016/S1097-2765(01)00204-0.

(71) Barnes V, L.; Heithoff, D. M.; Mahan, S. P.; House, J. K.; Mahan, M. J. Antimicrobial Susceptibility Testing to Evaluate Minimum Inhibitory Concentration Values of Clinically Relevant Antibiotics. *STAR Protoc* **2023**, *4* (3), 102512. https://doi.org/10.1016/j.xpro.2023.102512.

(72) Blázquez, J.; Gómez-Gómez, J.-M.; Oliver, A.; Juan, C.; Kapur, V.; Martín, S. PBP3 Inhibition Elicits Adaptive Responses in Pseudomonas Aeruginosa. *Molecular Microbiology* **2006**, *62* (1), 84–99. https://doi.org/10.1111/j.1365-2958.2006.05366.x.

(73) Pandey, B.; Grover, S.; Kaur, J.; Grover, A. Analysis of Mutations Leading to Para-Aminosalicylic Acid Resistance in Mycobacterium Tuberculosis. *Sci Rep* **2019**, *9* (1), 13617. https://doi.org/10.1038/s41598-019-48940-5.

(74) Waller, N. J. E.; Cheung, C.-Y.; Cook, G. M.; McNeil, M. B. The Evolution of Antibiotic Resistance Is Associated with Collateral Drug Phenotypes in Mycobacterium Tuberculosis. *Nat Commun* **2023**, *14*, 1517. https://doi.org/10.1038/s41467-023-37184-7.

(75) Valencia, E. Y.; Esposito, F.; Spira, B.; Blázquez, J.; Galhardo, R. S. Ciprofloxacin-Mediated Mutagenesis Is Suppressed by Subinhibitory Concentrations of Amikacin in Pseudomonas Aeruginosa. *Antimicrobial Agents and Chemotherapy* **2017**, *61* (3), 10.1128/aac.02107-16. https://doi.org/10.1128/aac.02107-16.

(76) Wassermann, T.; Meinike Jørgensen, K.; Ivanyshyn, K.; Bjarnsholt, T.; Khademi, S. M. H.; Jelsbak, L.; Høiby, N.; Ciofu, O. The Phenotypic Evolution of Pseudomonas Aeruginosa Populations Changes in the Presence of Subinhibitory Concentrations of Ciprofloxacin. *Microbiology* **2016**, *162* (5), 865–875. https://doi.org/10.1099/mic.0.000273.

(77) Torres-Barceló, C.; Kojadinovic, M.; Moxon, R.; MacLean, R. C. The SOS Response Increases Bacterial Fitness, but Not Evolvability, under a Sublethal Dose of Antibiotic. *Proceedings of the Royal Society B: Biological Sciences* **2015**, *282* (1816), 20150885. https://doi.org/10.1098/rspb.2015.0885.

(78) Sanz-García, F.; Hernando-Amado, S.; López-Causapé, C.; Oliver, A.; Martínez, J. L. Low Ciprofloxacin Concentrations Select Multidrug-Resistant Mutants Overproducing Efflux Pumps in Clinical Isolates of Pseudomonas Aeruginosa. *Microbiology Spectrum* **2022**, *10* (5), e00723-22. https://doi.org/10.1128/spectrum.00723-22.

(79) Jorba, M.; Pedrola, M.; Ghashghaei, O.; Herráez, R.; Campos-Vicens, L.; Luque, F. J.; Lavilla, R.; Viñas, M. New Trimethoprim-Like Molecules: Bacteriological Evaluation and Insights into Their Action. *Antibiotics* **2021**, *10* (6), 709. https://doi.org/10.3390/antibiotics10060709.

(80) Rehman, A.; Jeukens, J.; Levesque, R. C.; Lamont, I. L. Gene-Gene Interactions Dictate Ciprofloxacin Resistance in Pseudomonas Aeruginosa and Facilitate Prediction of Resistance Phenotype from Genome Sequence Data. *Antimicrob Agents Chemother 65* (7), e02696-20. https://doi.org/10.1128/AAC.02696-20.

(81) Morero, N. R.; Argaraña, C. E. Pseudomonas Aeruginosa Deficient in 8-Oxodeoxyguanine Repair System Shows a High Frequency of Resistance to Ciprofloxacin. *FEMS Microbiology Letters* **2009**, *290* (2), 217–226. https://doi.org/10.1111/j.1574-6968.2008.01411.x.

(82) Elitas, M.; Kalayci Demir, G.; Vural Kaymaz, S. Mathematical Model for Growth and Rifampicin-Dependent Killing Kinetics of Escherichia Coli Cells. *ACS Omega* **2023**, *8* (41), 38452–38458. https://doi.org/10.1021/acsomega.3c05233.

(83) Weinstein, Z. B.; Zaman, M. H. Evolution of Rifampin Resistance in Escherichia Coli and Mycobacterium Smegmatis Due to Substandard Drugs. *Antimicrobial Agents and Chemotherapy* **2018**, *63* (1), 10.1128/aac.01243-18. https://doi.org/10.1128/aac.01243-18.

(84) AlRabiah, H.; Allwood, J. W.; Correa, E.; Xu, Y.; Goodacre, R. pH Plays a Role in the Mode of Action of Trimethoprim on Escherichia Coli. *PLoS One* **2018**, *13* (7), e0200272. https://doi.org/10.1371/journal.pone.0200272.

(85) Vinchhi, R.; Jena, C.; Matange, N. Adaptive Laboratory Evolution of Antimicrobial Resistance in Bacteria for Genetic and Phenotypic Analyses. *STAR Protocols* **2023**, *4* (1), 102005. https://doi.org/10.1016/j.xpro.2022.102005.

(86) Pietsch, F.; Bergman, J. M.; Brandis, G.; Marcusson, L. L.; Zorzet, A.; Huseby, D. L.; Hughes, D. Ciprofloxacin Selects for RNA Polymerase Mutations with Pleiotropic Antibiotic Resistance Effects. *Journal of Antimicrobial Chemotherapy* **2017**, *72* (1), 75–84. https://doi.org/10.1093/jac/dkw364.

(87) Pourahmad Jaktaji, R.; Mohiti, E. Study of Mutations in the DNA Gyrase gyrA Gene of Escherichia Coli. *Iran J Pharm Res* **2010**, *9* (1), 43–48.

(88) Fiebig, A.; Rojas, C. M. C.; Siegal-Gaskins, D.; Crosson, S. Interaction Specificity, Toxicity, and Regulation of a Paralogous Set of ParE/RelE-Family Toxin-Antitoxin Systems. *Mol Microbiol* **2010**, *77* (1), 236–251. https://doi.org/10.1111/j.1365-2958.2010.07207.x.

(89) Beceiro, A.; Tomás, M.; Bou, G. Antimicrobial Resistance and Virulence: A Successful or Deleterious Association in the Bacterial World? *Clinical Microbiology Reviews* **2013**, *26* (2), 185–230. https://doi.org/10.1128/cmr.00059-12.

(90) Eberhard, W. G. Why Do Bacterial Plasmids Carry Some Genes and Not Others? *Plasmid* **1989**, *21* (3), 167–174. https://doi.org/10.1016/0147-619X(89)90040-1.

(91) Pal, C.; Bengtsson-Palme, J.; Kristiansson, E.; Larsson, D. G. J. Co-Occurrence of Resistance Genes to Antibiotics, Biocides and Metals Reveals Novel Insights into Their Co-Selection Potential. *BMC Genomics* **2015**, *16* (1), 964. https://doi.org/10.1186/s12864-015-2153-5.

(92) Ramirez, M. S.; Traglia, G. M.; Lin, D. L.; Tran, T.; Tolmasky, M. E. Plasmid-Mediated Antibiotic Resistance and Virulence in Gram-Negatives: The Klebsiella Pneumoniae Paradigm. *Microbiology Spectrum* **2014**, *2* (5), 10.1128/microbiolspec.plas-0016–2013. https://doi.org/10.1128/microbiolspec.plas-0016-2013.

(93) Brockhurst, M. A.; Harrison, E. Ecological and Evolutionary Solutions to the Plasmid Paradox. *Trends in Microbiology* **2022**, *30* (6), 534–543. https://doi.org/10.1016/j.tim.2021.11.001.

(94) Smillie, C.; Garcillán-Barcia, M. P.; Francia, M. V.; Rocha, E. P. C.; de la Cruz, F. Mobility of Plasmids. *Microbiol Mol Biol Rev* **2010**, *74* (3), 434–452. https://doi.org/10.1128/MMBR.00020-10.

(95) Stalder, T.; Rogers, L. M.; Renfrow, C.; Yano, H.; Smith, Z.; Top, E. M. Emerging Patterns of Plasmid-Host Coevolution That Stabilize Antibiotic Resistance. *Sci Rep* **2017**, *7* (1), 4853. https://doi.org/10.1038/s41598-017-04662-0.

(96) Brautaset, T.; Lale, R.; Valla, S. Positively Regulated Bacterial Expression Systems. *Microb Biotechnol* **2009**, *2* (1), 15–30. https://doi.org/10.1111/j.1751-7915.2008.00048.x.

(97) Schleif, R. AraC Protein, Regulation of the l-Arabinose Operon in Escherichia Coli, and the Light Switch Mechanism of AraC Action. *FEMS Microbiol Rev* **2010**, *34* (5), 779–796. https://doi.org/10.1111/j.1574-6976.2010.00226.x.

(98) Ammar, E. M.; Wang, X.; Rao, C. V. Regulation of Metabolism in Escherichia Coli during Growth on Mixtures of the Non-Glucose Sugars: Arabinose, Lactose, and Xylose. *Sci Rep* **2018**, *8* (1), 609. https://doi.org/10.1038/s41598-017-18704-0.

(99) Narayanan, A.; Ridilla, M.; Yernool, D. A. Restrained Expression, a Method to Overproduce Toxic Membrane Proteins by Exploiting Operator–Repressor Interactions. *Protein Sci* **2011**, *20* (1), 51–61. https://doi.org/10.1002/pro.535.

(100) Bok, J. W.; Keller, N. P. Fast and Easy Method for Construction of Plasmid Vectors Using Modified Quick-Change Mutagenesis. *Methods Mol Biol* **2012**, *944*, 163–174. https://doi.org/10.1007/978-1-62703-122-6_11.

(101) Suzuki, T.; Yasui, K. Plasmid Artificial Modification: A Novel Method for Efficient DNA Transfer into Bacteria. *Methods Mol Biol* **2011**, *765*, 309–326. https://doi.org/10.1007/978-1-61779-197-0_18.

(102) Marschall, L.; Sagmeister, P.; Herwig, C. Tunable Recombinant Protein Expression in E. Coli: Enabler for Continuous Processing? *Appl Microbiol Biotechnol* **2016**, *100*, 5719–5728. https://doi.org/10.1007/s00253-016-7550-4.

(103) Schuster, L. A.; Reisch, C. R. Plasmids for Controlled and Tunable High-Level Expression in E. Coli. *Appl Environ Microbiol* **2022**, *88* (22), e00939-22. https://doi.org/10.1128/aem.00939-22.

(104) Rouches, M. V.; Xu, Y.; Cortes, L. B. G.; Lambert, G. A Plasmid System with Tunable Copy Number. *Nat Commun* **2022**, *13* (1), 3908. https://doi.org/10.1038/s41467-022-31422-0.

(105) Silva, F.; Queiroz, J. A.; Domingues, F. C. Evaluating Metabolic Stress and Plasmid Stability in Plasmid DNA Production by Escherichia Coli. *Biotechnol Adv* **2012**, *30* (3), 691–708. https://doi.org/10.1016/j.biotechadv.2011.12.005.

(106) Ding, D.; Green, A. G.; Wang, B.; Lite, T.-L. V.; Weinstein, E. N.; Marks, D. S.; Laub, M. T. Co-Evolution of Interacting Proteins through Non-Contacting and Non-Specific Mutations. *Nat Ecol Evol* **2022**, *6* (5), 590–603. https://doi.org/10.1038/s41559-022-01688-0.

(107) Kurata, T.; Saha, C. K.; Buttress, J. A.; Mets, T.; Brodiazhenko, T.; Turnbull, K. J.; Awoyomi, O. F.; Oliveira, S. R. A.; Jimmy, S.; Ernits, K.; Delannoy, M.; Persson, K.; Tenson, T.; Strahl, H.; Hauryliuk, V.; Atkinson, G. C. A Hyperpromiscuous Antitoxin Protein Domain for the Neutralization of Diverse

Toxin Domains. *Proceedings of the National Academy of Sciences* **2022**, *119* (6), e2102212119. https://doi.org/10.1073/pnas.2102212119.

(108) McGillick, J.; Ames, J. R.; Murphy, T.; Bourne, C. R. A YoeB Toxin Cleaves Both RNA and DNA. *Sci Rep* **2021**, *11*, 3592. https://doi.org/10.1038/s41598-021-82950-6.

(109) Collin, F.; Karkare, S.; Maxwell, A. Exploiting Bacterial DNA Gyrase as a Drug Target: Current State and Perspectives. *Appl Microbiol Biotechnol* **2011**, *92* (3), 479–497. https://doi.org/10.1007/s00253-011-3557-z.

(110) Kato, F.; Yamaguchi, Y.; Inouye, K.; Matsuo, K.; Ishida, Y.; Inouye, M. A Novel Gyrase Inhibitor from Toxin-Antitoxin System Expressed by Staphylococcus Aureus. *FEBS J* **2022**. https://doi.org/10.1111/febs.16634.

(111) Roberts, R. C.; Ström, A. R.; Helinski, D. R. The parDE Operon of the Broad-Host-Range Plasmid RK2 Specifies Growth Inhibition Associated with Plasmid Loss. *Journal of Molecular Biology* **1994**, *237* (1), 35–51. https://doi.org/10.1006/jmbi.1994.1207.

(112) Gupta, M.; Nayyar, N.; Chawla, M.; Sitaraman, R.; Bhatnagar, R.; Banerjee, N. The Chromosomal parDE2 Toxin–Antitoxin System of Mycobacterium Tuberculosis H37Rv: Genetic and Functional Characterization. *Front Microbiol* **2016**, *7*, 886. https://doi.org/10.3389/fmicb.2016.00886.

(113) Anindyajati; Artarini, A. A.; Riani, C.; Retnoningrum, D. S. Plasmid Copy Number Determination by Quantitative Polymerase Chain Reaction. *Sci Pharm* **2016**, *84* (1), 89–101. https://doi.org/10.3797/scipharm.ISP.2015.02.

(114) Skulj, M.; Okrslar, V.; Jalen, S.; Jevsevar, S.; Slanc, P.; Strukelj, B.; Menart, V. Improved Determination of Plasmid Copy Number Using Quantitative Real-Time PCR for Monitoring Fermentation Processes. *Microb Cell Fact* **2008**, *7*, 6. https://doi.org/10.1186/1475-2859-7-6.

(115) Robbins-Manke, J. L.; Zdraveski, Z. Z.; Marinus, M.; Essigmann, J. M. Analysis of Global Gene Expression and Double-Strand-Break Formation in DNA Adenine Methyltransferase- and Mismatch Repair-Deficient Escherichia Coli. *Journal of Bacteriology* **2005**, *187* (20), 7027–7037. https://doi.org/10.1128/jb.187.20.7027-7037.2005.

(116) Kamruzzaman, M.; Iredell, J. A ParDE-Family Toxin Antitoxin System in Major Resistance Plasmids of Enterobacteriaceae Confers Antibiotic and Heat Tolerance. *Sci Rep* **2019**, *9* (1), 9872. https://doi.org/10.1038/s41598-019-46318-1.

(117) Fernandez-Garcia, L.; Kim, J. -S.; Tomas, M.; Wood, T. K. Toxins of Toxin/Antitoxin Systems Are Inactivated Primarily through Promoter Mutations. *Journal of Applied Microbiology* **2019**, *127* (6), 1859–1868. https://doi.org/10.1111/jam.14414.

(118) Khlebnikov, A.; Risa, Ø.; Skaug, T.; Carrier, T. A.; Keasling, J. D. Regulatable Arabinose-Inducible Gene Expression System with Consistent Control in All Cells of a Culture. *Journal of Bacteriology* **2000**, *182* (24), 7029–7034. https://doi.org/10.1128/JB.182.24.7029-7034.2000.

(119) Crozier, L.; Marshall, J.; Holmes, A.; Wright, K. M.; Rossez, Y.; Merget, B.; Humphris, S.; Toth, I.; Jackson, R. W.; Holden, N. J. The Role of L-Arabinose Metabolism for Escherichia Coli O157:H7 in Edible Plants. *Microbiology (Reading)* **2021**, *167* (7), 001070. https://doi.org/10.1099/mic.0.001070.

(120) Friehs, K. Plasmid Copy Number and Plasmid Stability. In *New Trends and Developments in Biochemical Engineering*; Scheper, T., Ed.; Advances in Biochemical Engineering; Springer: Berlin, Heidelberg, 2004; pp 47–82. https://doi.org/10.1007/b12440.

(121) Dumon-Seignovert, L.; Cariot, G.; Vuillard, L. The Toxicity of Recombinant Proteins in Escherichia Coli: A Comparison of Overexpression in BL21(DE3), C41(DE3), and C43(DE3). *Protein Expression and Purification* **2004**, *37* (1), 203–206. https://doi.org/10.1016/j.pep.2004.04.025.

(122) Kingsbury, D. T.; Helinski, D. R. Temperature-Sensitive Mutants for the Replication of Plasmids in Escherichia Coli: Requirement for Deoxyribonucleic Acid Polymerase I in the Replication of the Plasmid ColE1. *J Bacteriol* **1973**, *114* (3), 1116–1124.

(123) Kingsbury, D. T.; Helinski, D. R. DNA Polymerase as a Requirement for the Maintenance of the Bacterial Plasmid Colicinogenic Factor E1. *Biochem Biophys Res Commun* **1970**, *41* (6), 1538–1544. https://doi.org/10.1016/0006-291x(70)90562-0.

(124) Thompson, E. H. Z.; Bailey, M. F.; van der Schans, E. J. C.; Joyce, C. M.; Millar, D. P. Determinants of DNA Mismatch Recognition within the Polymerase Domain of the Klenow Fragment. *Biochemistry* **2002**, *41* (3), 713–722. https://doi.org/10.1021/bi0114271.

(125) Astatke, M.; Ng, K.; Grindley, N. D. F.; Joyce, C. M. A Single Side Chain Prevents Escherichia Coli DNA Polymerase I (Klenow Fragment) from Incorporating Ribonucleotides. *Proceedings of the National Academy of Sciences* **1998**, *95* (7), 3402–3407. https://doi.org/10.1073/pnas.95.7.3402.

(126) Minnick, D. T.; Bebenek, K.; Osheroff, W. P.; Turner, R. M.; Astatke, M.; Liu, L.; Kunkel, T. A.; Joyce, C. M. Side Chains That Influence Fidelity at the Polymerase Active Site of *Escherichia Coli* DNA Polymerase I (Klenow Fragment)*. *Journal of Biological Chemistry* **1999**, *274* (5), 3067–3075. https://doi.org/10.1074/jbc.274.5.3067.

(127) Singh, K.; Modak, M. J. Presence of 18-Å Long Hydrogen Bond Track in the Active Site of Escherichia Coli DNA Polymerase I (Klenow Fragment): ITS REQUIREMENT IN THE STABILIZATION OF ENZYME-TEMPLATE-PRIMER COMPLEX *. *Journal of Biological Chemistry* **2003**, *278* (13), 11289–11302. https://doi.org/10.1074/jbc.M211496200.

(128) Pouresmaeil, M.; Azizi-Dargahlou, S. Factors Involved in Heterologous Expression of Proteins in E. Coli Host. *Arch Microbiol* **2023**, *205* (5), 212. https://doi.org/10.1007/s00203-023-03541-9.

(129) Fakruddin, Md.; Mohammad Mazumdar, R.; Bin Mannan, K. S.; Chowdhury, A.; Hossain, Md. N. Critical Factors Affecting the Success of Cloning, Expression, and Mass Production of Enzymes by Recombinant E. Coli. *ISRN Biotechnol* **2012**, *2013*, 590587. https://doi.org/10.5402/2013/590587.

(130) Gao, S.; Li, Q.; Zhang, S.; Sun, X.; Zhou, H.; Wang, Z.; Wu, J. A Novel Biosensing Platform for Detection of Glaucoma Biomarker GDF15 via an Integrated BLI-ELASA Strategy. *Biomaterials* **2023**, *294*, 121997. https://doi.org/10.1016/j.biomaterials.2023.121997.

(131) Gao, S.; Li, Q.; Zhang, S.; Sun, X.; Zheng, X.; Qian, H.; Wu, J. One-Step High-Throughput Detection of Low-Abundance Biomarker BDNF Using a Biolayer Interferometry-Based 3D Aptasensor. *Biosensors and Bioelectronics* **2022**, *215*, 114566. https://doi.org/10.1016/j.bios.2022.114566.

(132) Carvalho, S. B.; Dias, M. M.; Matheise, J.-P.; Knott, I.; Gomes-Alves, P.; Alves, P. M. Biolayer Interferometry Analysis for a Higher Throughput Quantification of In-Process Samples of a Rotavirus Vaccine. *Vaccines* **2022**, *10* (10), 1585. https://doi.org/10.3390/vaccines10101585.

(133) Hao, Y.; Yang, H. S.; Karbaschi, M.; Racine-Brzostek, S. E.; Li, P.; Zuk, R.; Yang, Y. J.; Klasse, P. J.; Shi, Y.; Zhao, Z. Measurements of SARS-CoV-2 Antibody Dissociation Rate Constant by Chaotrope-Free Biolayer Interferometry in Serum of COVID-19 Convalescent Patients. *Biosensors and Bioelectronics* **2022**, *209*, 114237. https://doi.org/10.1016/j.bios.2022.114237.

(134) Gao, S.; Cheng, Y.; Zhang, S.; Zheng, X.; Wu, J. A Biolayer Interferometry-Based, Aptamer–Antibody Receptor Pair Biosensor for Real-Time, Sensitive, and Specific Detection of the Disease Biomarker TNF-α. *Chemical Engineering Journal* **2022**, *433*, 133268. https://doi.org/10.1016/j.cej.2021.133268.

(135) Dubrow, A.; Zuniga, B.; Topo, E.; Cho, J.-H. Suppressing Nonspecific Binding in Biolayer Interferometry Experiments for Weak Ligand–Analyte Interactions. *ACS Omega* **2022**, *7* (11), 9206–9211. https://doi.org/10.1021/acsomega.1c05659.

(136) Bian, S.; Tao, Y.; Zhu, Z.; Zhu, P.; Wang, Q.; Wu, H.; Sawan, M. On-Site Biolayer Interferometry-Based Biosensing of Carbamazepine in Whole Blood of Epileptic Patients. *Biosensors* **2021**, *11* (12), 516. https://doi.org/10.3390/bios11120516.

(137) Williams, J. J.; Hergenrother, P. J. Artificial Activation of Toxin–Antitoxin Systems as an Antibacterial Strategy. *Trends in Microbiology* **2012**, *20* (6), 291–298. https://doi.org/10.1016/j.tim.2012.02.005.

(138) Równicki, M.; Pieńko, T.; Czarnecki, J.; Kolanowska, M.; Bartosik, D.; Trylska, J. Artificial Activation of Escherichia Coli mazEF and hipBA Toxin–Antitoxin Systems by Antisense Peptide Nucleic Acids as an Antibacterial Strategy. *Front. Microbiol.* **2018**, *9*. https://doi.org/10.3389/fmicb.2018.02870.

(139) Wojciechowska, M.; Równicki, M.; Mieczkowski, A.; Miszkiewicz, J.; Trylska, J. Antibacterial Peptide Nucleic Acids—Facts and Perspectives. *Molecules* **2020**, *25* (3), 559. https://doi.org/10.3390/molecules25030559.

(140) Good, L.; Awasthi, S. K.; Dryselius, R.; Larsson, O.; Nielsen, P. E. Bactericidal Antisense Effects of Peptide–PNA Conjugates. *Nat Biotechnol* **2001**, *19* (4), 360–364. https://doi.org/10.1038/86753.

(141) Lioy, V. S.; Rey, O.; Balsa, D.; Pellicer, T.; Alonso, J. C. A Toxin–Antitoxin Module as a Target for Antimicrobial Development. *Plasmid* **2010**, *63* (1), 31–39. https://doi.org/10.1016/j.plasmid.2009.09.005.

(142) Kingsbury, D. T.; Helinski, D. R. Temperature-Sensitive Mutants for the Replication of Plasmids in Escherichia Coli: Requirement for Deoxyribonucleic Acid Polymerase I in the Replication of the Plasmid ColE1. *J Bacteriol* **1973**, *114* (3), 1116–1124.

Acknowledgement

First of all, I would like to express the most solemn gratitude to my PI, Dr. Christina Bourne. In the five years of doctoral life, she not only provided endless help and advice in academics and experiments, but also cared about me very much in life, that is why I like sharing my life with her. She will never blame you, even if I carelessly designed the wrong primer and broke the experimental instrument. On the contrary, when I was trapped in the experiment dilemma, she always gave encouragement and affirmation. Based on these, I am proud to join her laboratory. Of course, I would also like to thank Dr. Phil Bourne, for the equipment, assistance, and suggestions from PPCC, and my committee members, Dr. Ann West, Dr. Si Wu (former), Dr. Rakhi Rajan and Dr. John Masly, for the time they spent and advice they provided for the annual advisory meetings, Preliminary and General Exams.

Then I want to thank all Bourne lab members: Dr. Keven Snead for the helps toward experiments; Michelle Holt and Jeff Tu for their company and help as peers; Twahirwa Sam, Joel Langford and Walter Galie for joining Bourne lab to bring a “noisy” atmosphere; and all undergraduates for their trust.

Lastly, I must thank my wife, Yanting Guo, and our doggie, Beta, for a life full of love and happiness. I cannot image how fast these five years have passed. Without the company, support, and urge sometimes, from Yanting, I don’t believe I can do it now.

Appendix A

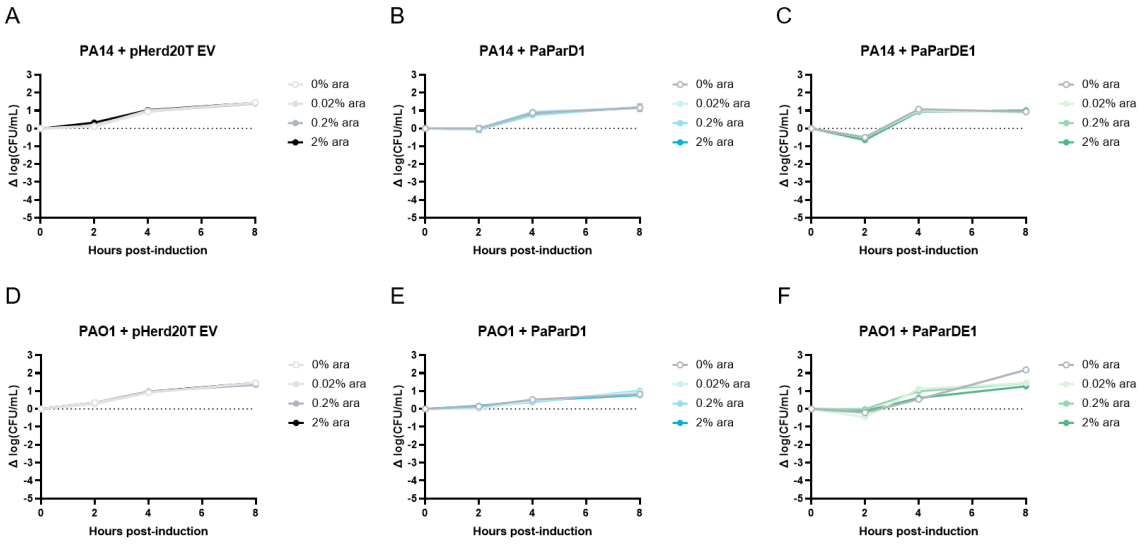

Figure S2.1. Impact of Empty Vector, PaParD1 antitoxin or PaParDE1 toxin-antitoxin expression on *P. aeruginosa* cell viability. The expression of pHerd20T empty vector (EV) (**A** and **D**) or PaParD1 antitoxin alone (**B** and **E**), or the co-expression of PaParDE1 toxin-antitoxin (**C** and **F**) was induced in *P. aeruginosa* PA14 (**A** to **C**) and PAO1 (**D** to **F**) cells using speficied concentrations of arabinose (ara) in M9 minimal medium. Each data point is presented with the standard error of the mean (SEM), representing at least two independent experiments.

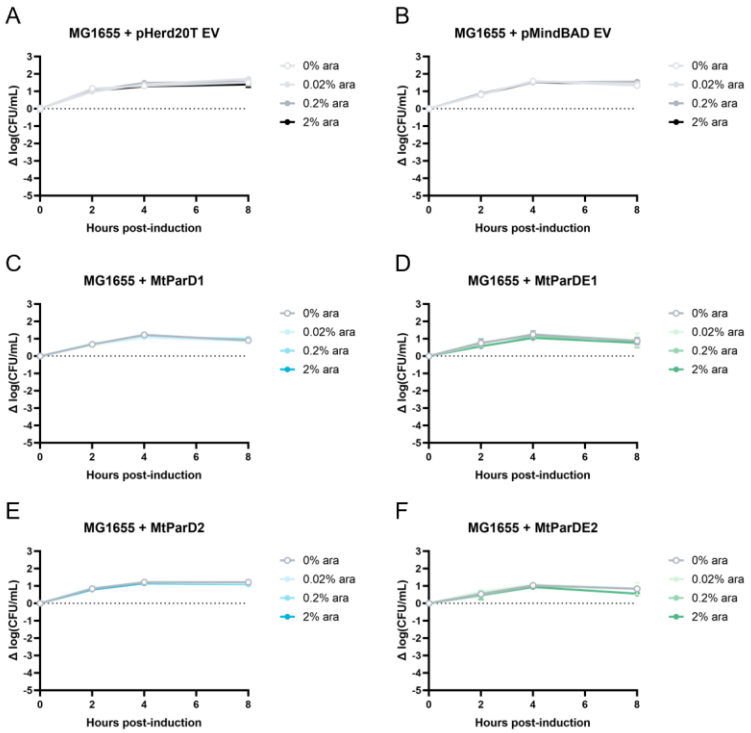

Figure S2.2. Impact of Empty Vector, MtParD antitoxin or MtParDE toxin-antitoxin expression on *E. coli* cell viability. The expression of pHerd20T (**A**) or pMind (**B**) empty vector (EV), MtParD1 (**C**) or MtParD2 (**E**) antitoxin, or the co-expression of MtParDE1 (**D**) or MtParDE2 (**F**) toxin-antitoxin was induced in *E. coli* MG1655 cells using specified concentrations of arabinose (ara) in LB media. Each data point is presented with the standard error of the mean (SEM), representing at least two independent experiments.

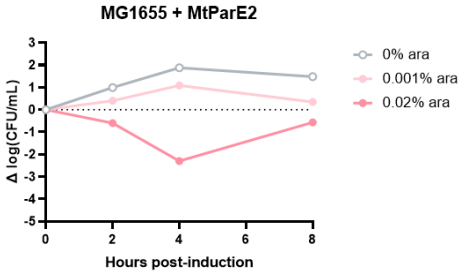

Figure S2.3. Impact of MtParE2 toxin expression on *E. coli* cell viability. The expression of toxin protein MtParE2 was induced in *E. coli* MG1655 cells using specified concentrations of arabinose (ara) in LB media. Each data point is presented with the standard error of the mean (SEM), representing at least two independent experiments.

PA14 + PaParE1

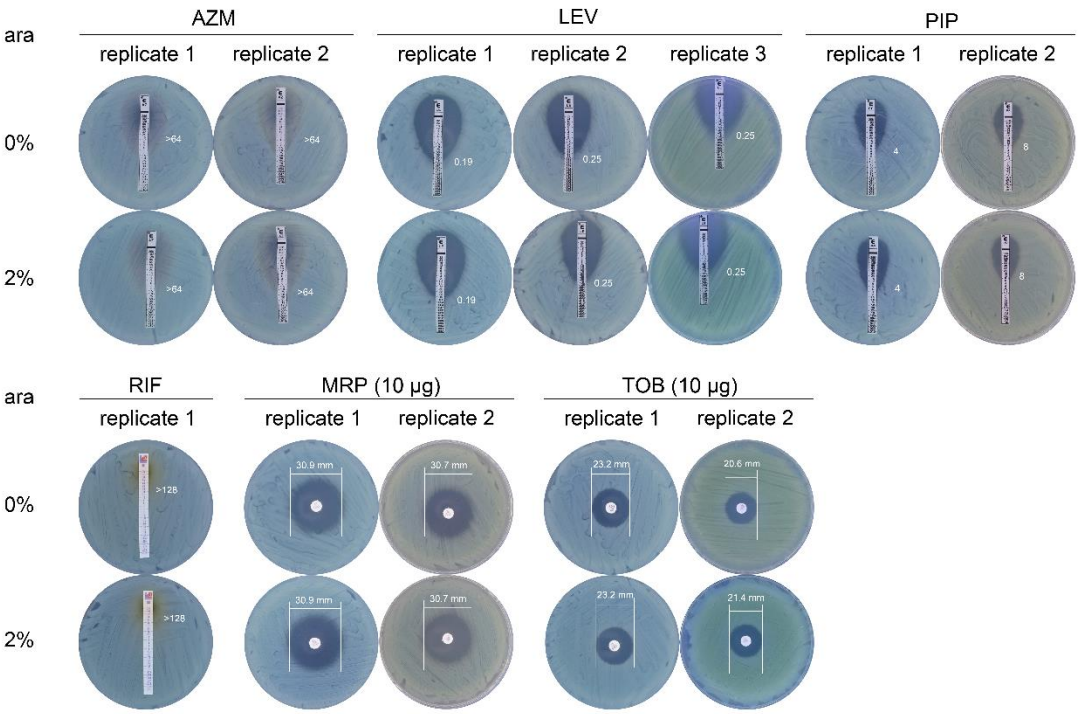

PAO1 + PaParE1

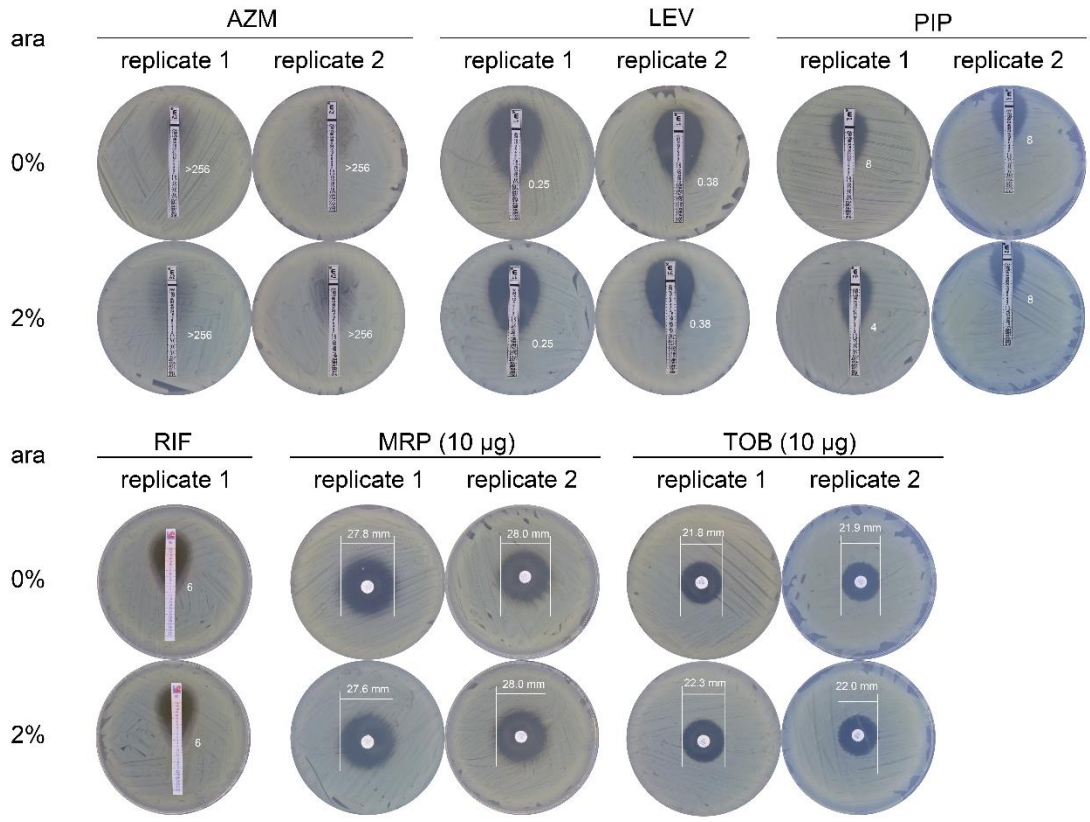

Figure S2.4. Impact of PaParE toxin expression on *P. aeruginosa* cell antibiotic susceptibility. Cell cultures were spread on test media plates after 8 h of PaParE expression at indicated induction strengths and then E-strips or discs of specific antibiotics were placed on the plates. Antibiotic susceptibilities were evaluated by assessing the alteration in the size of the clear zone or by determining the MIC change on-scale. AZM: azithromycin; TOB: tobramycin; LEV: levofloxacin; PIP: piperacillin; MRP: meropenem.

MG1655 + MtParE1

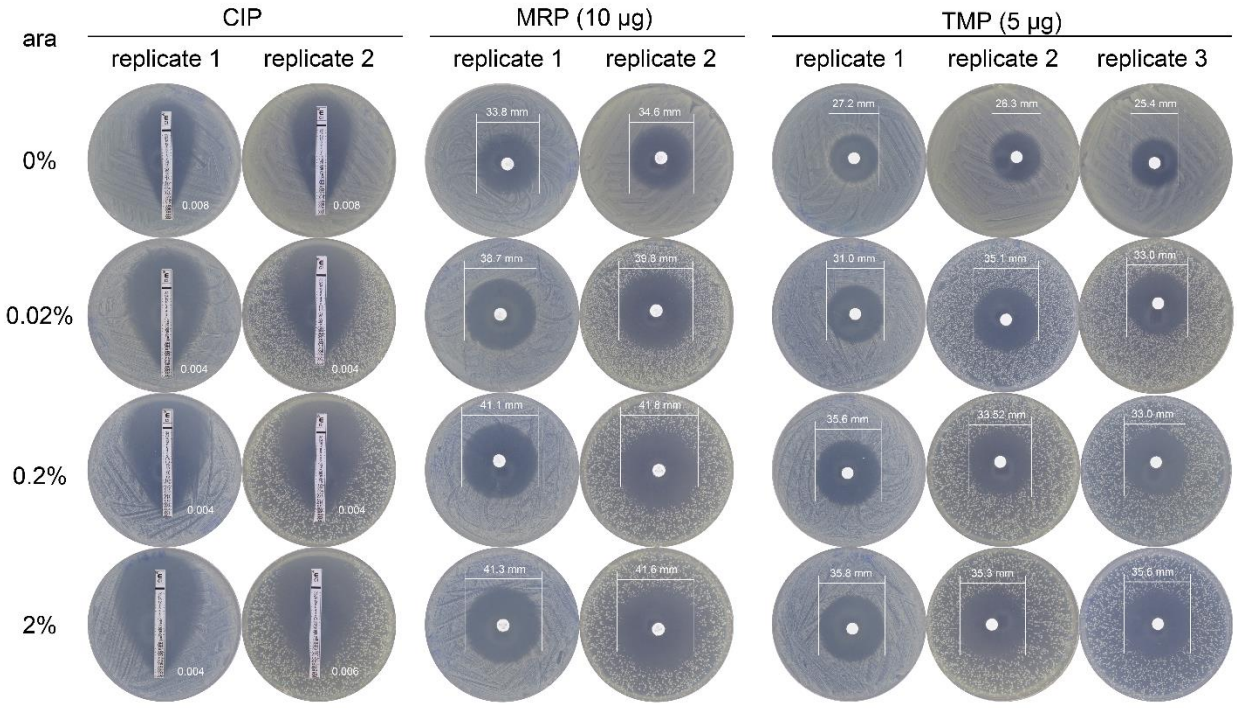

MG1655 + MtParE2

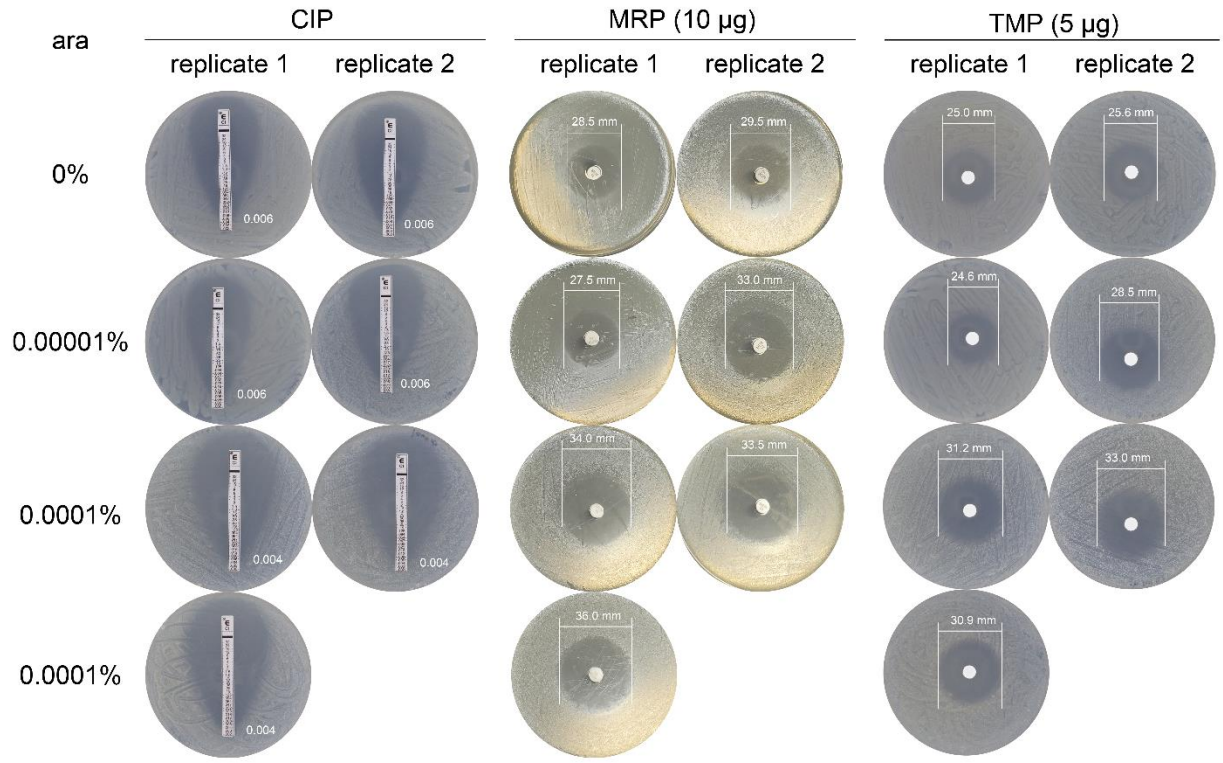

Figure S2.5. Impact of MtParE toxin expression on *E. coli* cell antibiotic susceptibility. Normalized cultures of *E. coli* MG1655 cells expressing MtParE1 or MtParE2 were smeared on LB agar plates following 8 h of MtParE expression at indicated arabinose (ara) concentrations and then discs or E-test strips of specified antibiotics were placed on the plates. Antibiotic susceptibilities were evaluated by determining the diameter change of the inhibition zones or MIC value change on strips. CIP: ciprofloxacin; MRP: meropenem; TMP: trimethoprim.

Appendix B

Table S3.1.

Bacterial strains and plasmids used in this study

Strains or plasmids	Description	Source of reference
Strains		
E. coli K-12		From our laboratory
MG1655	F- lambda- *ilvG*- *rfb*-50 *rph*-1	MG1655 strain was a gift from Tyrrell Conway (Oklahoma State University)
TOP10	F- *mcrA* Δ(*mrr-hsd*RMS-*mcr*BC) Φ80*lac*ZΔM15 Δ *lac*X74 *rec*A1 *ara*D139 Δ(*araleu*)7697 *gal*U *gal*K *rps*L (StrR) *end*A1 *nup*G	Invitrogen (Cat# C404010)
Plasmids		
pMind	ColE1/pMB1/pBR322/pUC origin of replication, tetRO promoter, Neo^r Kam^r	pMind was a gift from Brian Robertson (Addgene plasmid # 24730; http://n2t.net/addgene:24730; RRID:Addgene_24730)
pHerd20T	ColE1/pMB1/pBR322/pUC origin of replication, donor for *araC*-P_{BAD} fragment, pBAD promoter, Amp^r	pHerd20T was a gift from Hongwei Yu (Marshall University)
pRK2::*araE*	Constitutive promoter expressing AraE on RK2 origin	pRK2-AraE was a gift from Brian Pfleger (Addgene plasmid # 110141 ; http://n2t.net/addgene:110141 ; RRID:Addgene_110141)
pHerd20T::*mCherry*	pHerd20T carrying the *mCherry* gene in the MCS	From our laboratory
pMind::*mtparE1*	pMind carrying the *mtparE1* gene in the MCS	This study
pMind::*Strep-mtparE2*	pMind carrying the *Strep*-tagged *mtparE2* gene in the MCS	This study

pMind::*mtparD1E1*	pMind carrying the *mtparD1E1* gene in the MCS	This study
pMind::*mtparD2E2*	pMind carrying the *mtparD2E2* gene in the MCS	This study
pMindBAD::*mtparE1*	pMind::*mtparE1* tetRO promoter replaced with a 1.216-kb fragment of *araC*-P_{BAD} from pHerd20T	This study
pMindBAD::*Strep-mtparE2*	pMind::*Strep-mtparE2* tetRO promoter replaced with a 1.216-kb fragment of *araC*-P_{BAD} from pHerd20T	This study

Table S3.2.

Oligonucleotide primers used for PCR cloning, sequencing, qPCR and RT-qPCR

Primer	Purpose	Sequence (5'-3') [a]
pMind_FWD	PCR	GATATCCTTAATTAAGTATGCATCG
pMind_REV	PCR	GGATCCTGTCAGGATTCC
parE1_FWD	PCR	gtggaatcctgacaggatccGTGAGTAGCCGATACCTTC
parE1_REV	PCR	catacttaattaaggatatcTCAGAGGTTCCGGTCGAC
parD1E1_FWD	PCR	gtggaatcctgacaggatccGTGAGTAGCCGATACCTTC
parD1E1_REV	PCR	catacttaattaaggatatcTCAGAGGTTCCGGTCGAC
parD2E2_FWD	PCR	gtggaatcctgacaggatccGTGGTGGTCAACCGGGCA
parD2E2_REV	PCR	catacttaattaaggatatcTCACTCGAAGGTGCGGCC
parE2+Strep_FWD	PCR	gcagtttgaaaaaATGACGCGCAGGCTGCGC
parE2+Strep_REV	PCR	ggatggctccacatGGATCCTGTCAGGATTCCACGATGAG
araC-pBAD_FWD	PCR	tacctctagaTTATGACAACTTGACGGC
araC-pBAD_REV	PCR	tccttccacgATTATTTCTAGCCCAAAAAAAC
pMind+araC-pBAD_FWD	PCR	tagaaataatCGTGGAAGGAGGAGAGGATCCATG
pMind+araC-pBAD_REV	PCR	gttgtcataaTCTAGAGGTACCGAGCTC
gapA-qPCR_FWD	qPCR and RT-qPCR	TATGACTGGTCCGTCTAAAGACAA
gapA-qPCR_REV	qPCR and RT-qPCR	GGTTTTCTGAGTAGCGGTAGTAGC
ori-qPCR_FWD	qPCR	AGGTAACTGGCTTCAGCAGAG
ori-qPCR_REV	qPCR	TGCGCCTTATCCGGTAACTATC
parE1-qPCR_FWD	qPCR	GCAGGCACATCTGGAAGAGA
parE1-qPCR_REV	qPCR	GCCAGTCACCCGATAGAACAA
parE2-qPCR_FWD	qPCR	ACGACCTATTCGAGGCGTTT
parE2-qPCR_REV	qPCR	CGTCCGATAGGCAACGTAGT
RNA-I-qPCR_FWD	RT-qPCR	AACAAAAAAACCACCGCTACCA
RNA-I-qPCR_REV	RT-qPCR	ACAGTATTTGGTATCTGCGCTCT
RNA-II-qPCR_FWD	RT-qPCR	ACTGAGATACCTACAGCGTGAG
RNA-II-qPCR_REV	RT-qPCR	CCCTGACGAGCATCACAAA
araE-qPCR_FWD	RT-qPCR	GCGGTCGCAGGATTGTTATTTG
araE-qPCR_REV	RT-qPCR	CCCGCCATCAGGCTGTATTTA
pMindSeq_FWD	Sequencing	GGTGAGTCATAGTTGCACTT

M13_REV	Sequencing	CAGGAAACAGCTATGAC
pBAD_FWD	Sequencing	ATGCCATAGCATTTTTATCC

[a] The overlap used for gene assembly is in lower case.

Table S3.3.

Bacterial whole genome sequencing results compared to the published *E. coli* K-12 MG1655 sequences

Potential mutations	**R002**	**R2**	**U00096.1**	**U00096.2 and U00096.3**	**ATCC 700926**	**ATCC 47076**
23S ribosomal RNA (*rrlD*)	…UCCC AAGGGU AUGGCU GUUC…	…UCCC AAGGGU AUGGCU GUUC…	…UCCCC AAGGGU AUGCUG UUC…	…UCCC AAGGG**U** **GAU**GCU GUUC…	…UCCC AAGGGU AUGGCU GUUC…	…UCCC AAGGGU AUGGCU GUUC…
DNA polymerase I (Pol I)	**N845S**	**N845S**	N845	N845	N845	N845
Long-chain fatty acid outer membrane channel/bacteriophage T2 receptor (FadL)	S383	**Frameshifted from S383**	S383	S383	S383	S383
RNase P protein component	V93	**Frameshifted from V93**	V93	V93	V93	V93
Diguanylate cyclase (DgcJ)	**IS1 family protein InsB and represser TnpA were inserted within DgcJ**	**IS1 family protein InsB and represser TnpA were inserted within DgcJ**	Intact DgcJ	Intact DgcJ	**IS1 family protein InsB and represser TnpA were inserted within DgcJ**	Intact DgcJ
Repeat sequences between Sel1 repeat-containing protein YjcO	**2 repeats**	**2 repeats**	3 repeats	3 repeats	3 repeats	**2 repeats**

and glutamate/aspa rate : H(+) symporter						
Repeat sequences between uncharacterize d YcdU and tRNA-Ser	**3 repeats**	**3 repeats**	2 repeats	2 repeats	2 repeats	**3 repeats**

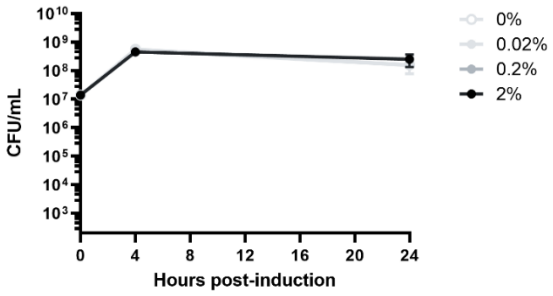

Figure S3.1. Impact of pMind Empty Vector on *E. coli* cell viability. *E. coli* MG1655 cells were transformed with pMind "empty" vector lacking the inserted ParE-encoding gene. Cell growths were measured with the addition of 0% to 2% arabinose. Cell viability was assessed by quantifying CFU/mL at specified time intervals (limit of detection of 200 CFU/mL). The standard error of the mean (SEM) was calculated from at least three independent experiments.

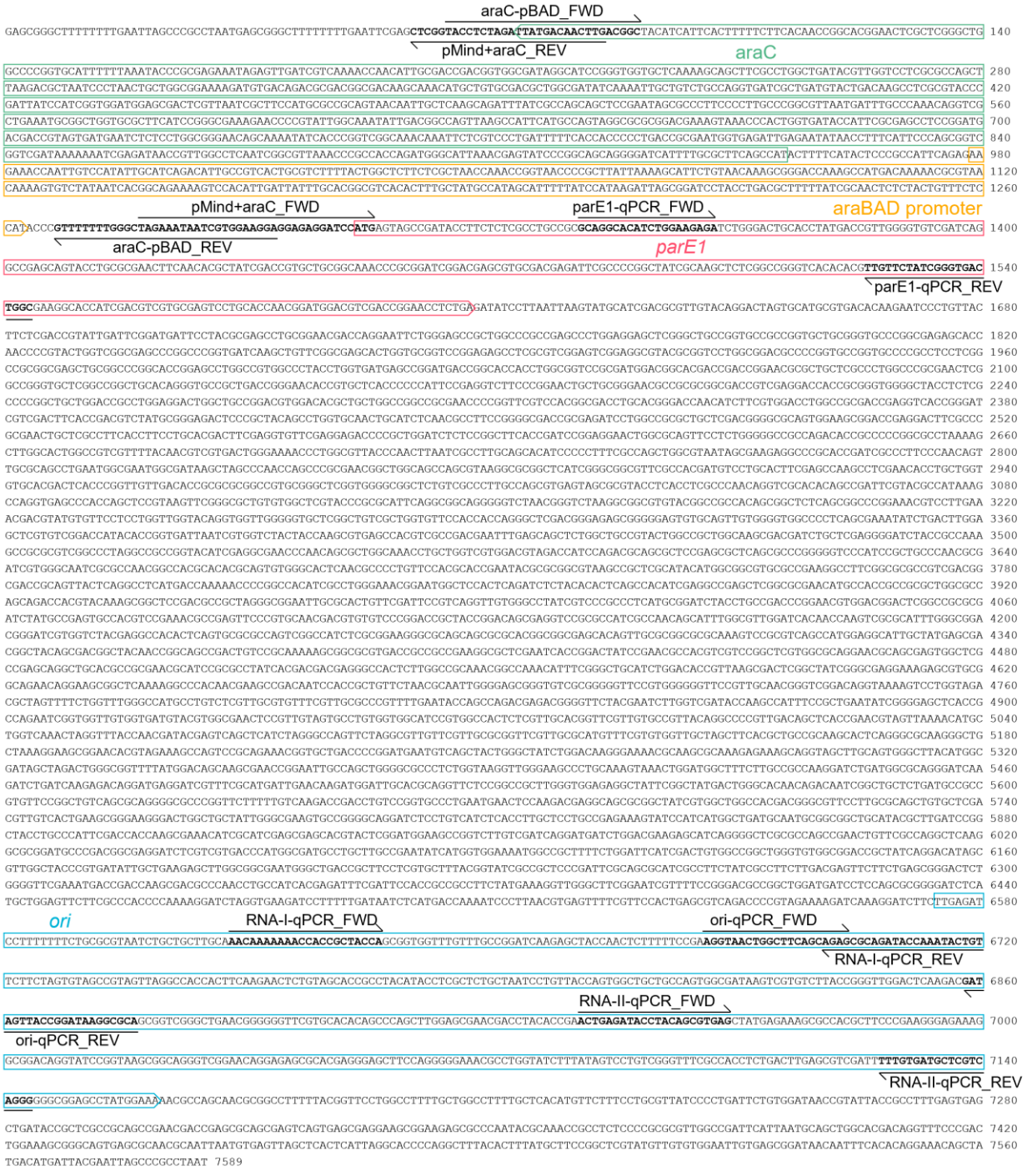

Figure S3.2. Complete DNA sequence of the pMindBAD::*mtparE1* plasmid with gene and primer annotations. Gene sequences are sourced from SnapGene Viewer software 7.0.3.

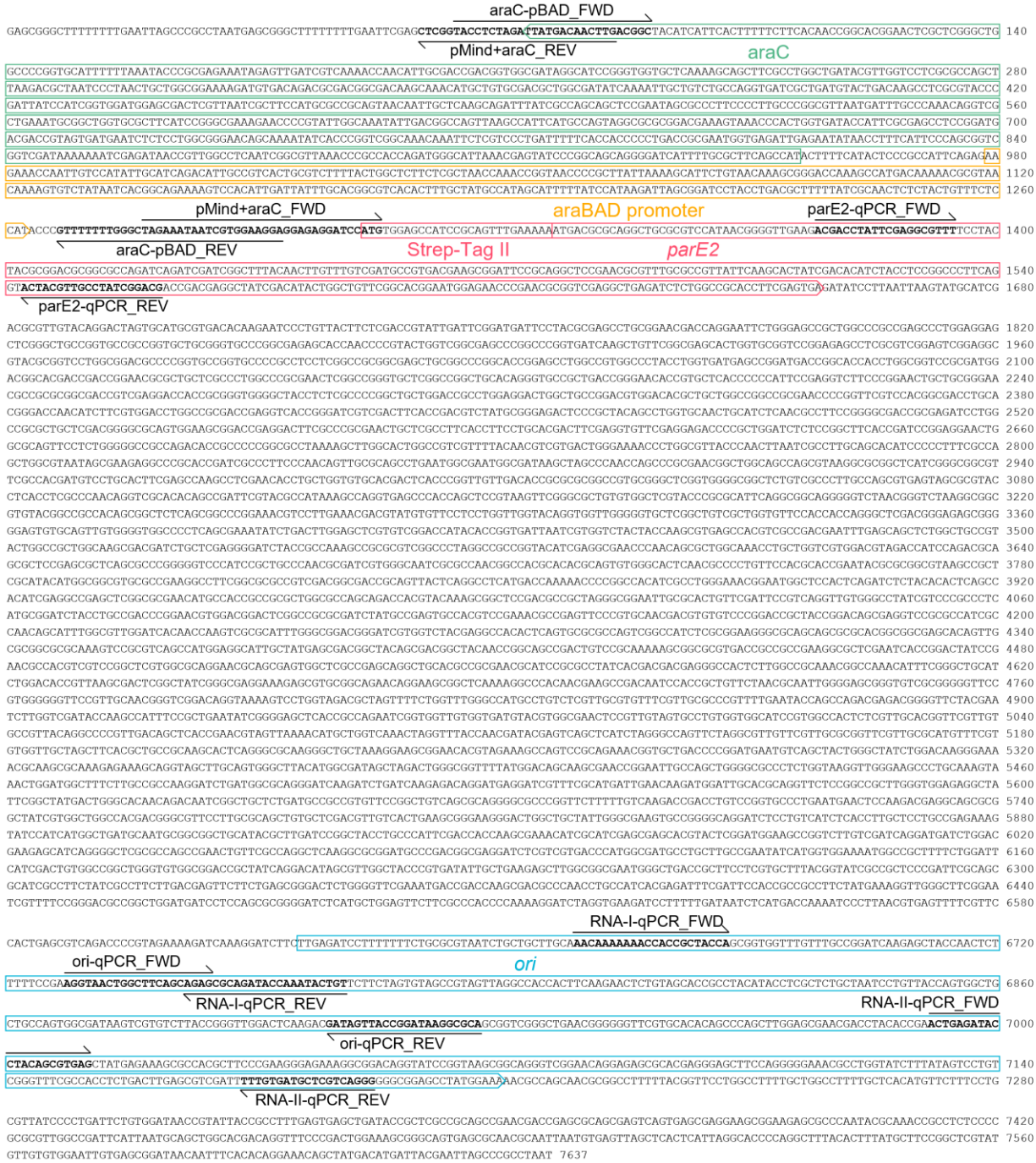

Figure S3.3. Complete DNA sequence of the pMindBAD::*Strep-mtparE2* plasmid with gene and primer annotations. Gene sequences are sourced from SnapGene software 7.0.3.

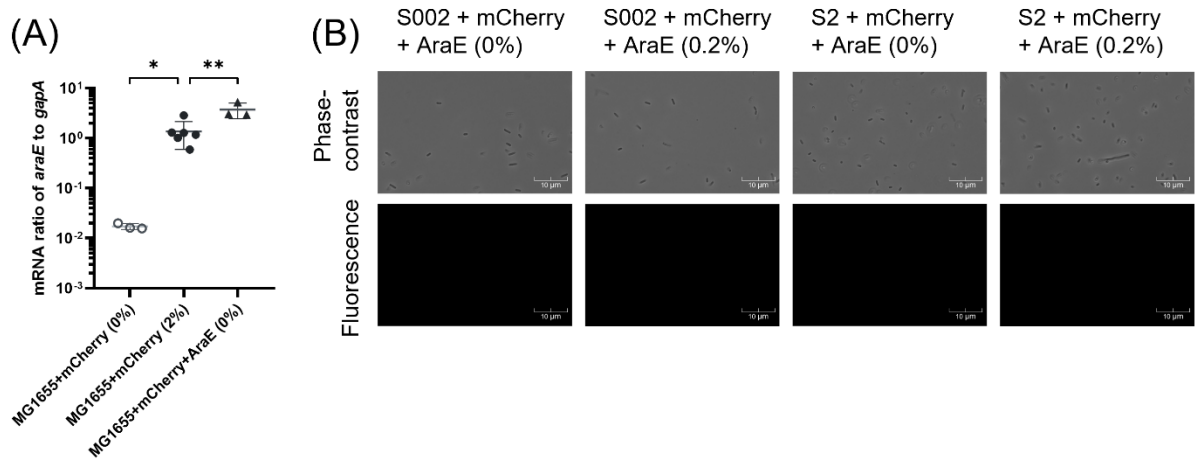

Figure S3.4. Supplementary expression of AraE transporter didn't rescue the lack of expression of fluorescent protein mCherry in cells previously exposed to ParE1 protein expression. (**A**) The pHerd20T reporter plasmid, carrying an arabinose-inducible fluorescent protein mCherry gene, was transformed into the "starting" *E. coli* MG1655 cells, or co-transformed with the pRK2 plasmid constitutively expressing arabinose transporter AraE into the "starting" *E. coli* MG1655 cells. Overnight cultures were induced for mCherry expression by the addition of 0% or 2% arabinose for 4-5 hr. Cells were harvested by centrifugation and RT-qPCR was employed to determine the mRNA ratio of the arabinose transporter *araE* to chromosomal *gapA* in these cells post incubation with 0% or 2% arabinose. Each measurement with standard deviation (SD) represents at least one independent experiment with each experiment containing at least 3 technical replicates. Unpaired two-tailed Student's *t*-test was performed: *, $P < 0.05$; **, $P < 0.01$. (**B**) The pHerd20T reporter plasmid, carrying an arabinose-inducible fluorescent protein mCherry gene, was co-transformed with the pRK2 plasmid constitutively expressing arabinose transporter AraE into the plasmid-cured surviving cells S002 and S2. Overnight cultures of each strain were divided into two, with one culture induced for mCherry expression by the addition of 2% arabinose for 4-5 hr, and the other one serving as a control with the addition of sterile distilled water. Fluorescence microscopy was utilized to visualize mCherry expression, with a representative image presented for each sample.

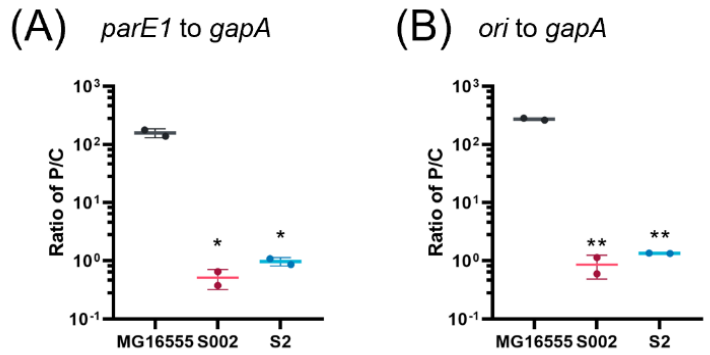

Figure S3.5. Quantification of plasmid copy number in surviving cells. The PCN represented by the ratio of P/C was determined by qPCR for the surviving cells S002 and S2 as well as pre-induction MG1655 cells harboring ParE1-concoding plasmid. The gapA-qPCR primer set was used for the amplification of chromosome, the parE1-qPCR (A) or ori-qPCR (B) primer set was used for the amplification of plasmid. Each measurement with standard deviation (SD) represents 2 technical replicates. The ratios of P/C of the surviving cells were compared to the ratio of P/C of the pre-induction cells and unpaired two-tailed Student's *t*-test was performed: *, $P < 0.05$, **, $P < 0.01$.

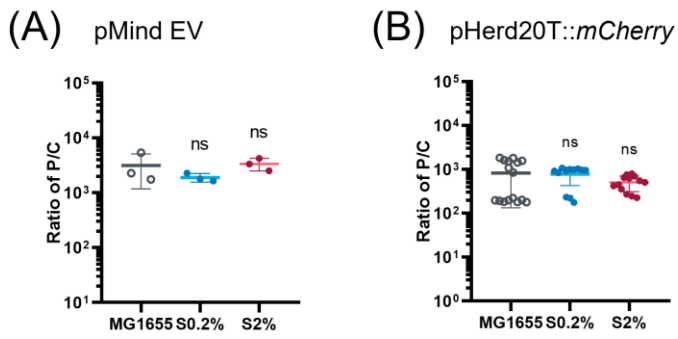

Figure S3.6. Reduction in PCN is not evident for cells that have not experienced toxic protein expression. The pMind "empty" vector without insertion of ParE gene (A) or the pHerd20T plasmid carrying the arabinose-inducible fluorescent protein mCherry gene (B) was transformed into the "starting" MG1655 *E. coli* cells. Following a 24-hr induction with 0.2% or 2% arabinose, cell cultures were passaged at a 1:20 dilution in fresh LB media containing the same arabinose concentration. After two 24-hr passages with arabinose inductions, at least one colony from each induction level (*e.g.*, S0.2% denotes cells survived two 24-hr passages of 0.2% induction) were isolated. The PCNs of these cells were determined by qPCR analysis. The gapA-qPCR primer set was used for the amplification of chromosome, the ori-qPCR primer set was used for the amplification of plasmid. Each measurement with SD represents 1 independent experiment, with each experiment containing three technical replicates. The ratios of P/C of surviving cells were compared to that of the pre-induction MG1655 cells and unpaired two-tailed Student's *t*-test was performed: ns, non-significant.

```
# Length: 114
# Identity:      23/114 (20.2%)
# Similarity:    42/114 (36.8%)
# Gaps:          24/114 (21.1%)
# Score: 24.5
#
#
#=======================================

parE1              1 MSSRYLLSPAAQAHLEEIWDCTYDRWGVDQAEQYLRELQHA-IDRAAANP     49
                     |:.|..:...:..|.|.:.     :..|.|...:..|.:. :|  |...
parE2              1 MTRRLRVHNGVEDDLFEAFS-----YYADAAPDQIDRLYNLFVD--AVTK     43

parE1             50 RIGRACDEIRPGYRK-----LSAGSHTLFYRVTGEGTIDVVRVLHQRMD-     93
                     ||.:|.:...|.::.     |....:.:||.|.| .||::.|.|...:
parE2             44 RIPQAPNAFAPLFKHYRHIYLRPFRYYVAYRTTDE-AIDILAVRHGMENP     92

parE1             94 --VDRNL-------     98
                        |:..:
parE2             93 NAVEAEISGRTFE*    106


#---------------------------------------
#---------------------------------------
```

Figure S3.7. Global Alignment of protein sequences of ParE1 and ParE2 toxins. Protein sequences are aligned using Needle (EMBOSS).

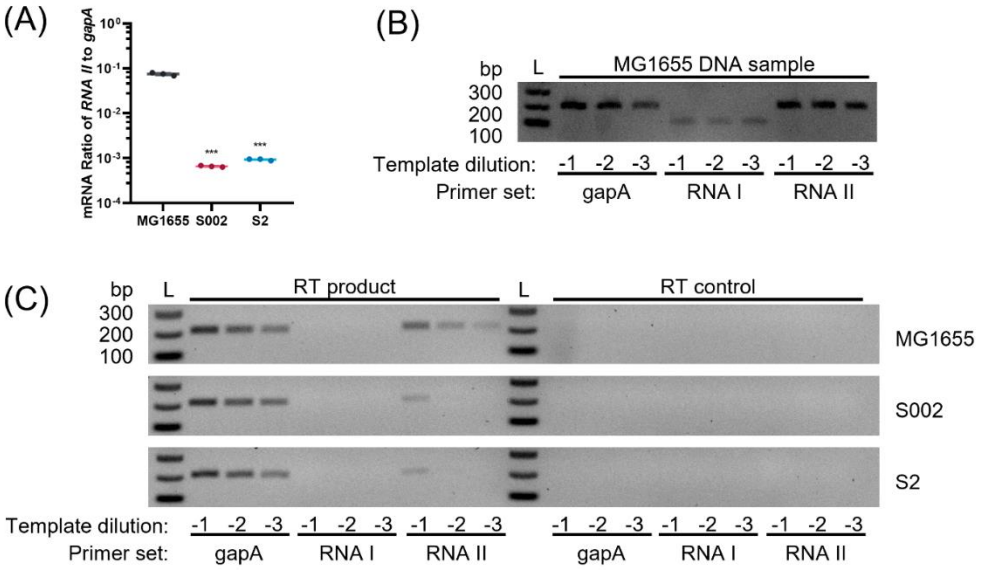

Figure S3.8. Analysis of RNA I and RNA II ratios in surviving cells in relation to plasmid replication regulation. The surviving cells S002 and S2 as well as the pre-induction MG1655 cells harboring pMindBAD::*mtparE1* plasmid were grown in LB media overnight without the addition of arabinose. (**A**) Cells were harvested by centrifugation and RT-qPCR was employed to determine the mRNA ratio of RNA II to chromosomal GapA. The gapA-qPCR primer set was used for the amplification of *gapA* cDNA, the RNA-II-qPCR primer set was used for the amplification of RNA II cDNA. Each measurement with standard deviation (SD) represents one experiment with 3 technical replicates. Unpaired two-tailed Student's *t*-test was performed: ***, $P < 0.001$. (**B**) The pre-induction MG1655 cells harboring pMindBAD::*mtparE1* were harvested by centrifugation and PCR was employed to amplify *gapA*, RNA I and RNA II fragments with serial dilutions of the DNA samples. The gapA-qPCR primer set was used for the amplification of *gapA* DNA, the RNA-I-qPCR and RNA-II-qPCR primer sets were used for the amplification of RNA I and RNA II complementary DNA in *ori*. PCR products were checked by 2% agarose gel electrophoresis. (**C**) PCR was employed to amplify *gapA*, RNA I and RNA II fragments with serial dilutions of the reverse transcription (RT) products from (A). The gapA-qPCR primer set was used for the amplification of *gapA* cDNA, the RNA-I-qPCR and RNA-II-qPCR primer sets were used for the amplification of RNA I and RNA II cDNA. The reverse transcriptase in RT reaction was replaced with an equal amount of water in RT control reaction.

Appendix C

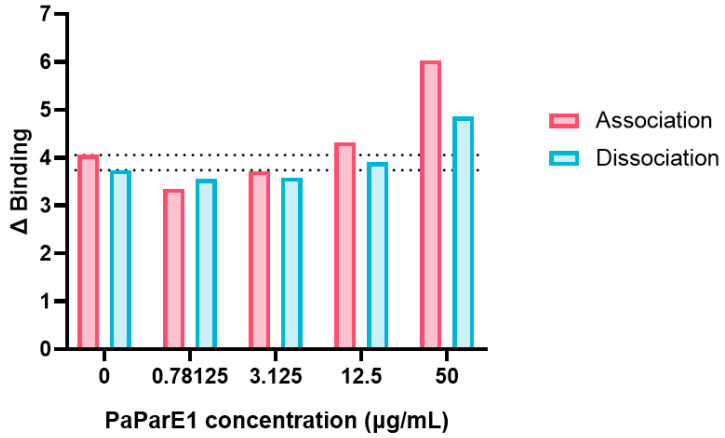

Figure S4.1. Total binding signals against PaParE1 protein concentrations. This figure presents graphs showing the total binding signal of the sample (Δ binding signal, including the specific binding signal of PaParE1 protein and the binding signal of non-specific binding (NSB) molecules) from the 3-dip loading and washing steps against the concentration of PaParE1 protein in the running buffer with 20% EV lysate, ranging from 0 to 50 µg/mL, using HIS1K biosensor. The binding signal of the sample containing PaParE1 protein below 12.5 µg/mL was lower than the binding signal of NSB (0 µg/mL). Dash lines indicates the Δ binding signals of 0 µg/mL from loading and washing steps, respectively.

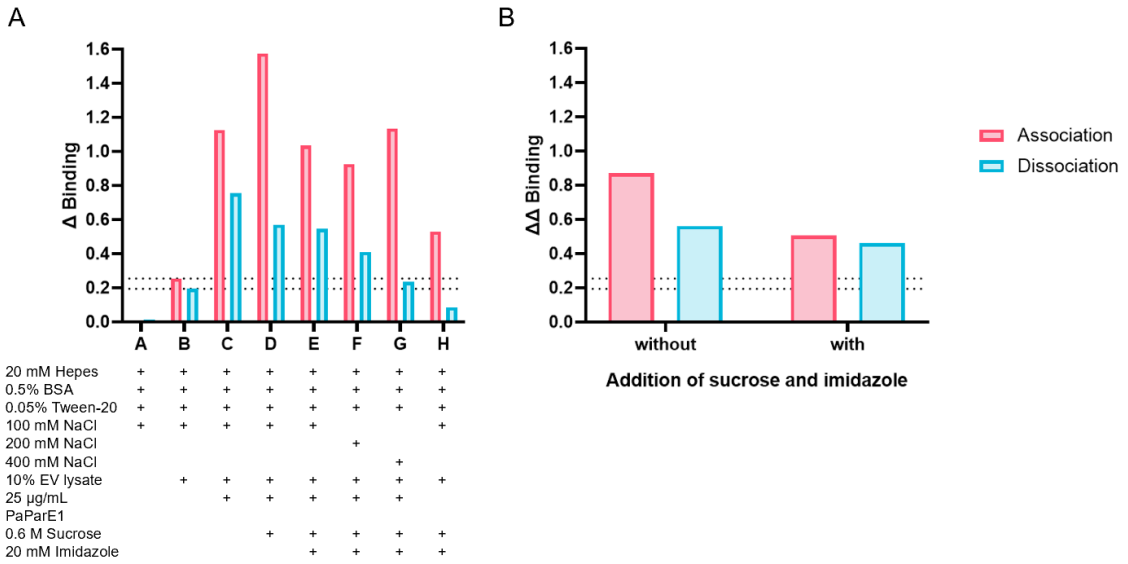

Figure S4.2. Optimization work to reduce non-specific binding with HIS1K biosensor. (**A**) Different combinations of 100-400 mM NaCl, 0.6 M sucrose and 20 mM imidazole were incorporated in the running buffer to assess the impacts on reducing non-specific binding (NSB) with the HIS1K biosensor. A to B is the order of biosensor tips in one column. (**B**) The Δ binding signal of biosensor tip B was subtracted from the Δ binding signal of biosensor tip C, generating the specific binding signal (ΔΔ binding) of PaParE1 protein in the absence of sucrose and imidazole. The Δ binding signal of biosensor tip H was subtracted from the Δ binding signal of biosensor tip E, generating the specific binding signal (ΔΔ binding) of PaParE1 protein in the presence of 0.6 M sucrose and 20 mM imidazole. The additions of 0.6 M sucrose and 20 mM imidazole did reduce NSB but also reduce the specific binding signal of PaParE1 protein. Dash lines indicates the Δ binding signals of tip B from loading and washing steps, respectively.